

https://dspace.org/

Corrosion of tungsten carbide exposed to organic acid environments

Basi, Qinisile

2022

https://hdl.handle.net/10539/35735

Downloaded from a DSpace repository. https://dspace.org/

MSc Dissertation:

Corrosion of Tungsten Carbide Exposed to Organic Acid Environments

---



WITS
UNIVERSITY

Prepared by:

Qinisile Basi (1225499)

Submitted to:

School of Chemical and Metallurgical Engineering, Faculty of Engineering and the Built Environment, University of the Witwatersrand, Johannesburg, South Africa

Supervisor: Prof. Josias Van der Merwe

October, 2022

Corrosion of Tungsten Carbide Exposed to Organic Acid Environments

Qinisile Monica Basi

A dissertation submitted to the faculty of Engineering and the Built Environment, University of the Witwatersrand, Johannesburg, in fulfilment of the requirements for the degree of Masters of Science in Engineering.

Johannesburg, October 2022

DECLARATION

I (Qinisile Monica Basi) declare that the dissertation is my own unaided work except where references were made and were properly acknowledged. It is being submitted for the degree of Master of Science in Engineering in the University of the Witwatersrand, Johannesburg. It has not been submitted previously at this or any other university for any degree or examination.

Qinisile Monica Basi

At Date:

Abstract

Corrosion plays a major role in decreasing a tool's lifespan during abrasive applications. The main focus of this study was to investigate the effect of the binder compositions on the wear, corrosion and tribocorrosion resistance of the WC-Co by varying the binder contents. The study involved a characterization of microstructures, grain size, hardness, and chemical composition by using energy X-ray dispersion in the SEM. The corrosion and tribo-corrosion behaviour of the WC-Co was investigated using an electrochemical and cyclic potentiodynamic polarization test in 3.5% NaCl at pH 2, 3 and 5 of acetic and sulphuric acid solutions, respectively. Electrochemical corrosion resistance was determined by performing the OCP for 1 hour followed by a potentiodynamic scan at a scan rate of 0.17 V/s for the samples exposed to both acidic salt solutions. Furthermore, the tribo-corrosion characteristics were investigated by assessing the electrochemistry while samples were exposed to a ball-on-disc test.

The density of the WC-Co alloys was between 13.93 to 14.45 g/cm3 with microhardness values ranging from 1400 to 1730. The alloys had shown a fine microstructure, 6.4%Co-3.2%Ni-2.0%Cr-4.8%V had more fine-grained structure with high $HV_{0.3}$ value of 1730. During the cyclic polarization test, the additions of chromium and nickel had shown to have an effect in stabilizing the cobalt binder phase at pH 2 and 5. The grain size had little influence on the corrosion behaviour of the alloys. Positive hysteresis loop was observed at higher pH levels, where it was dictated that the presence of chloride ions in acid might accelerate the growth of pits during the cyclic potentiodynamic polarization test. Negative hysteresis loop was also observed at lower pH levels for an alloy with <1%Co as the reverse scan had shown a decreasing current density. During the tribocorrosion test, it was found that the wear conditions, alloy, and acid electrolyte controlled the wear-corrosion interaction. While some alloys had shown dominant corrosion behaviour, the hardmetals did not show any wear. The varied pH conditions had a great influence on the wear rates of the alloys which in turn accelerated the corrosion attack with increasing acid strength.

Acknowledgements

Firstly, I would like to thank My **God and Saviour**, for the strength, empowerment and wisdom.

I wish to thank the following people who have contributed in the completion of this project:

Professor J. Van der Merwe: For the best supervision, constructive criticism and guidance. Thank you for the support throughout this journey.

Mr Donald Mahole: For the best advice, helping with corrosion experiments, moral support and for helping in difficult situations.

Ms Letta and Mr Naftali: For assisting me with AAS analysis.

Mr Bruce Mothibeli: For assisting me with access and for opening the corrosion lab gate for me.

Mr Shadrack: For assisting with grinding and polishing machine.

Ms Petra Dinham: For assisting with the SEM/EDS analysis.

Mr Phathu and Mr Hopewell Gumede: For assisting me with the cutting and drilling of my samples.

I would like to thank all the **staff members** of the School of Chemical and Metallurgical Engineering at Wits University for the support during this study.

Ms Thuli Mkhaliphi: For assisting me with my proposal and providing positive feedback.

I would like to acknowledge the financial support for funding this project received from The DST/NRF Centre of Excellence in Strong Materials. I am truly grateful for the opportunity.

I would like to express my sincere gratitude to my family (Basi) for the prayers, love and support I received throughout my studies. Thanks to my mother **Duduzile Basi** and my brother **Thulani Basi** as well as my sister **Mrs Thembekile Dlamini** for the support and for believing in me. I would like to thank my special friend (**Linda Madlala**) for being my biggest cheerleader. Thanks to my friends for the financial and moral support, encouragement and for believing in me.

Dedications

In loving memory of my father

Sthenjwa Solomon Basi.

He has always been there for me in spirit. He taught me life and equipped with wisdom that has helped me to be where I am today. He taught me independence, courage, confidence and to be a hardworker.

Rest in eternal peace Hlozini, May God protect you.

Table of Contents

Acknowledgements v

List of Figures x

List of Tables xii

1. Introduction 1

1.1. Background 1

1.2. Problem Statement 2

1.3. Objectives 2

1.4. Hypothesis 3

1.5. General Layout 3

2. Literature Review 4

2.1. Woodcutting Tools 4

2.2. Woodcutting Tool Wear 5

2.2.1. Properties of Wood during Woodcutting 5

2.2.2. Tool Wear Mechanism 6

2.3. Tungsten Carbides 7

2.3.1. Hardmetals 7

2.3.2. WC-Co Manufacture 8

2.3.3. Applications of WC-Co 9

2.3.4. Limitations 10

2.3.5. Grain Growth Inhibitors 10

2.4. Corrosion 11

2.4.1. Introduction to the Corrosion of WC-Co Hardmetals 11

2.4.2. The Mechanism of Corrosion 12

2.4.3. The Effect of the Binder Content on the Corrosion 14

2.4.4. The Influence of Various Parameters on Corrosion 16

2.4.5. Effect of organic acid on WC-Co 16

2.5. Wear 17
2.5.1. Wear mechanism of WC-Co 18
2.5.2. Effect of the Lubricant 20
2.6. Tribocorrosion of WC-Co 21
2.7. Effect of WC grain size on corrosion 22
3. Experimental Methods 23
3.1. Materials 23
3.1.1. Sample characterization 23
3.1.2. Sample Preparation 23
3.1.3. Material Characterization 24
3.2. Methods 24
3.2.1. Density Measurement 24
3.2.2. Microhardness Test 25
3.2.3. Grain size Measurement 26
3.2.4. Wear Test 26
3.3. Corrosion Tests 26
3.3.1. Open Circuit Potential (OCP) and Cyclic Potentiodynamic Polarization Measurements 27
3.3.2. Determining the Corrosion Rate 27
3.4. Tribocorrosion Tests 29
4. Results 30
4.1. Material Characterisation 30
4.1.1. Optical Microscopy 30
4.1.2. Scanning Electron Microscope (SEM) 31
4.2. Wear tests 33
4.2.1. Wear rates under dry conditions 33
4.2.2. Microstructural analysis 36

4.3. Corrosion tests 37
4.3.1. Open Circuit Potential Values 38
4.3.2. Cyclic Polarization Curves 40
4.4. Tribocorrosion tests 53
4.4.1. Open Circuit Circuit 54
4.4.2. Polarization Curves 60
4.4.3. Comparison of the wear rates under varied pH conditions 69
4.4.4. Microstructural Analysis 71
5. Discussion 76
5.1. Corrosion response of the WC-Co alloys 76
5.2. Wear response of the WC-Co alloys 78
5.3. Tribocorrosion response of the WC-Co alloy 80
6. Conclusions 83
References 85
Appendix 95
EDS analysis 95

List of Figures

Figure 2.1: Manufacturing of WC-Co (Stefaniak, et al., 2007) 9
Figure 2.2: Pourbaix diagram for the cobalt-water system at 25℃ (Garcia, et al., 2008). 13
Figure 2.3: Tribosystem (Massola, et al., 2016). 18
Figure 2.4: The Stribeck curve (Chong & Cruz, 2014) 21
Figure 3.1: Polarisation curve of sample 6.5%Co-1.8%Ni-0.8%Cr exposed to 3.5%NaCl acetic acid solution at pH 2. 28
Figure 3.2: Tribocorrosion schematic diagram (Barao, et al., 2013). 29
Figure 4.1: Optical micrographs of the WC alloys: a) 0.08%Co-8.0%Ni, b) 6.5%Co-1.8%Ni-0.8%Cu, c) 6.4%Co-3.2%Ni-1.9%Cr-4.8%V, d) 10.1%Co-4.6%Ni-0.7%Cr-0.4%Cu and e) 11.1%Co-4.6%Ni-1.5%Cr-0.2%V 31
Figure 4.2: SEM micrographs of the WC alloys: a) 0.08%Co-8.0%Ni, b) 6.5%Co-1.8%Ni-0.8%Cu, c) 6.4%Co-3.2%Ni-1.9%Cr-4.8%V, d) 10.1%Co-4.6%Ni-0.7%Cr-0.4%Cu and e) 11.1%Co-4.6%Ni-1.5%Cr-0.2%V 32
Figure 4.3: Wear rates of the WC-Co alloys under dry conditions 34
Figure 4.4: Relationship between the coefficient of friction and sliding distance. 35
Figure 4.5: Contact pressure vs wear 35
Figure 4.6: Wear micrographs: a) 0.08%Co-8.0%Ni, b) 6.5%Co-1.8%Ni-0.8%Cu, c) 11.1%Co-4.6%Ni-1.5%Cr-0.2%V, d) 10.1%Co-4.6%Ni-0.7%Cr-0.4%Cu and e) 6.4%Co-3.2%Ni-1.9%Cr-4.8%V. 37
Figure 4.7: OCP of acetic and sulphuric acid electrolytes at pH 2. 38
Figure 4.8: OCP of acetic and sulphuric acid electrolytes at pH 3. 39
Figure 4.9: OCP of acetic and sulphuric acid electrolytes at pH 5. 40
Figure 4.10: Cyclic polarization curve of acetic acid electrolyte at pH 2. 41
Figure 4.11: Polarization curve of sulphuric acid electrolyte at pH 2. 42
Figure 4.12: Corrosion rates against cobalt content at pH 2. 44
Figure 4.13: Polarization curves of the Acetic acid at pH 3. 45
Figure 4.14: Polarization curves of Sulphuric acid at pH 3. 46
Figure 4.15: Corrosion rates of acetic and sulphuric acid at pH 3. 48
Figure 4.16: Polarization curves of Acetic acid at pH 5. 49
Figure 4.17: Polarization curves of Sulphuric acid at pH 5. 50
Figure 4.18: Corrosion rates of acetic and sulphuric acid at pH 5. 51
Figure 4.19: OCP scans of the WC-Co alloys in acetic acid electrolyte at pH 2. 55

Figure 4.20: OCP scans of WC-Co alloys in sulphuric acid electrolyte at pH 2. 56
Figure 4.21: OCP scans of WC-Co alloys in acetic acid electrolytes at pH 3. 57
Figure 4.22: OCP scans of the WC-Co alloys in sulphuric acid electrolytes at pH 3. 58
Figure 4.23: OCP scan of WC-Co alloys in acetic acid at pH 5. 59
Figure 4.24: OCP scans of the WC-Co alloys in sulphuric acid electrolyte at pH 5. 60
Figure 4.25: Polarization curves of WC-Co alloys in acetic acid electrolyte at pH 2. 61
Figure 4.26: Tribocorrosion rates of the hardmetals in acetic and sulphuric acid at pH 2. 62
Figure 4.27: Polarization curves for WC-Co in sulphuric acid electrolytes at pH 3. 63
Figure 4.28: Tribocorrosion rates of hardmetals in acetic and sulphuric acid at pH 3. 64
Figure 4.29: Polarization curves of the WC-Co alloys in acetic acid electrolyte at pH 5. 65
Figure 4.30: Tribocorrosion rates of hardmetals in acetic and sulphuric acid at pH 5. 66
Figure 4.31: Comparisons of the WC-Co hardmetals wear rates under dry and pH 5 conditions. 71
Figure 4.32: Worn surfaces at pH 2. (i) when exposed to acetic acid: a) 6.5%Co-1.8%Ni-0.8%Cu and b) 6.4%Co-3.2%Ni-1.9%Cr-4.8%V and (ii) when exposed to sulphuric acid: c) 0.08%Co-8.0%Ni and d) 6.5%Co-1.8%Ni-0.8%Cu. 72
Figure 4.33: Worn surfaces at pH 3 when exposed to acetic acid: a) 0.08%Co-8.0%Ni, (b) 6.5%Co-1.8%Ni-0.8%Cu and (c) 10.1%Co-4.6%Ni-0.7%Cr-0.4%Cu and when exposed to sulphuric acid: d) 0.08%Co-8.0%Ni, e) 6.5%Co-1.8%Ni-0.8%Cu and f) 6.4%Co-3.2%Ni-1.9%Cr-4.8%V 73
Figure 4.34: Worn surfaces Acetic acid pH 5: a) 11.1%Co-4.6%Ni-1.5%Cr-0.2%V, b) 6.4%Co-3.2%Ni-1.9%Cr-4.8%V, c) 6.5%Co-1.8%Ni-0.8%Cu and d) 10.1%Co-4.6%Ni-0.7%Cr-0.4%Cu. 74
Figure 4.35: Worn surfaces in Sulphuric acid pH 5: a) 0.08%Co-8.0%Ni, b) 6.4%Co-3.2%Ni-1.9%Cr-4.8%V, c) 10.1%Co-4.6%Ni-0.7%Cr-0.4%Cu, d) 11.1%Co-4.6%Ni-1.5%Cr-0.2%V and e) 6.5%Co-1.8%Ni-0.8%Cu. 75
Figure 5.1: Averaged corrosion values under varied pH conditions. 78
Figure 5.2: Averaged tribocorrosion rates under varied pH conditions. 81
Figure 5.3: Disk volume loss under varied pH condition. 82

List of Tables

Table 3.1: Compositions for all samples from the EDS analysis 23
Table 3.2: Activities to prepare the samples for material characterization (Elssner, et al., 1999) 24
Table 3.3: The density results of the WC-Co samples.....24
Table 3.4: The microhardness results of the WC-Co samples.....25
Table 3.5: Grain size results of the WC-Co samples. 26
Table 3.6: These are different electrolytes that were used for corrosion tests at room temperature. 28
Table 4.1: Raw wear rate data.....33
Table 4.2: Raw data for acetic and sulphuric acid at pH 2 44
Table 4.3: Raw data of acetic and sulphuric acid corrosion rates at pH 3 48
Table 4.4: Raw data for acetic and sulphuric acid at pH 5 51
Table 4.5: AAS analysis for corrosion tests solutions. 53
Table 4.6: Raw data for acetic and sulphuric acid at pH 2 62
Table 4.7: Raw data for acetic and sulphuric acid at pH 3 64
Table 4.8: Raw data for acetic and sulphuric acid at pH 5 66
Table 4.9: AAS analysis for tribocorrosion tests solutions.....68
Table 4.10: Corrosive and dry wear rates information for the WC-Co alloys.....70

1. Introduction

1.1. Background

Cemented tungsten carbide (WC-Co) has been a material of choice in mining, rock drilling, underground drilling, and tunnelling because of the outstanding blend of wear and corrosion resistance properties (Katiyar, 2020). It has a high hardness and low fracture toughness (Allen & Wentzel, 1995). Tungsten carbide can be utilized as a coating material for protection against wear and high temperature oxidation because of high hardness and thermal stability (Thanjekwayo, 2009); (Human & Exner, 1996) & (Palomar, et al., 2009).

These WC-Co materials were introduced to the woodcutting industry because of their high wear resistance and hardness which gives a tool an increased lifetime (Ramasamy & Ratnasingam, 2010) & (Sacks, 2002). WC-Co cutting tools have high wear resistance which makes it possible to employ higher cutting speeds compared to when using High Speed Steel (HSS) cutting tools. The cutting speeds are at least ten times higher than when using HSS cutting tools, thereby increasing production rates (Bailey, et al., 1983) & (AZoM, 2002). However, these cutting tools are susceptible to corrosion which reduces the tool life. Furthermore, alloying tungsten carbide with elements such as titanium and tantalum make the metal an essential cutting tool which makes it economically viable in the industry because of its improved hardness (Upadhyaya, 1997). These elements tend to be employed because of their high electron affinity for carbon which promotes the formation of stable carbides.

Corrosion plays a major role in decreasing the tool life during abrasive applications in the presence of wood extracts. Research has shown that the organic extractants can decrease the performance of the tool by influencing the mechanical properties of WC-Co. This decrease in performance is evaluated to be caused by the corrosive nature of organic extractants present in wood which in turn accelerate the wear rate of the cutting tool (Pugsley, et al., 2001). Previously, studies have been conducted on the improvements of the WC-Co's strength and it has been found that in order for improvements to be made corrosion kinetics and thermodynamics must be understood when the material is used in corrosive environments (Sutthiruangwong & Mori, 2003). Kosters, et al., (2005) reported that chromium in the binder of WC-Co increases corrosion resistance by stabilizing the cobalt-based passive oxide layer.

Tribocorrosion is a process whereby the corrosion and wear effects are combined on the degradation of a material. During this test it is important to consider the synergistic behaviour of the tribocorrosion as the study have shown that a metal binder that is optimum in one degradation process is not optimum when both corrosion and wear are in place. For example, nickel performs best for corrosion alone but performs poorly in tribocorrosion conditions, this is assumed to be caused by the passive layer which takes time to form and is mechanically weak causing it to be removable when a certain load is applied. However, there has been limited research on the effect of WC grain sizes on the wear, tribocorrosion and corrosion of this hard metal when it is exposed to organic acid environments (Wood, et al., 2017).

1.2. Problem Statement

Cemented tungsten carbides are heterogeneous materials. They suffer from galvanic corrosion in the presence of aggressive corrosive media which preferentially attacks the cobalt binder material while the tungsten carbide itself remains immune. This material has been used in the wood and timber industry as a woodcutting tool. The degradation of woodcutting tool is not always well understood or defined. The number of parameters related to the machining of different wood materials obstructs the prediction of the evolution of wear, corrosion and tribocorrosion of tools. These parameters include but are not limited to temperature, wood pH and wood abrasives. It is a challenge to determine the magnitude of each mechanism so that improvements of the woodcutting tools can be made (Gauvent, et al., 2006) & (Darmawan, et al., 2012). Much of the research that has been conducted broadly investigates the corrosion behaviour of WC-Co as a cutting tool, but strong acid and alkali solutions are typically used. However, there is little information when the cutting tool is exposed to organic acid solutions, such as acetic acid. In addition, research proved that wood moisture and multi-component nature of wood play an important role in the kinetics of the tool's degradation (Ramasamy & Ratnasingam, 2010) & (Sutthiruangwong & Mori, 2003).

This study will focus on the effect of the binder compositions on the wear, corrosion and tribocorrosion resistance of the WC-Co by varying the binder contents. The WC-Co will be exposed to the organic acid environments.

1.3. Objectives

This study aims to investigate and understand the effect of binder contents on the corrosion resistance and tribocorrosion resistance of WC-Co in organic acid environments.

The objectives of this study are as follows:

- Determine the influence of Cr and Ni additions on the microstructure of WC-Co.
- Investigate the effects of different binder compositions on corrosion resistance of WC-Co in different media.
- Study the combined action of wear-corrosion (tribocorrosion) of the developed WC-Co with binders.

1.4. Hypothesis

There are two hypotheses that were mapped out for this study. The first hypothesis will be constructed on the theory that the presence of chromium in the binder increases the corrosion resistance by stabilizing the cobalt-based passive oxide layer alongside with nickel. The second hypothesis will be based on the theory that the presence of nickel is not optimal for tribocorrosion. Wood, et al., (2017), assumed that this can be caused by the passive layer which takes time to form, and is mechanically weak which makes it susceptible to the removal due to the applied load.

1.5. General Layout

This dissertation is comprised of six chapters. This chapter has provided the background of the study. The next chapter, chapter 2 provides the literature review, an overview description of the tungsten carbide as a hardmetal as well as its corrosion behaviour when exposed to organic acid environments. Chapter 3 comprises provides a detailed experimental procedure, equipment and software used in this work. Chapter 4 includes the results and short discussion, and Chapter 5 provides a full discussion. Chapter 6 provides conclusions and recommendations that could be considered for future research.

2. Literature Review

2.1. Woodcutting Tools

The wood industry has poor knowledge of the degradation of the tools in contact with wood and the woodcutting processes are very difficult to explain and describe. Therefore, good understanding of the material behaviour during machining is required for economical and productive reasons (Gauvent, et al., 2006); (Cristovao, 2013) & (Eyma, et al., 2004). There are many factors that influence the woodcutting processes such as wood properties, cutting tool geometry and cutting parameters. The woodcutting tools during the interaction with wood are subjected to severe loads and transverse vibrations, hence, different wear characteristics and mechanisms are produced. It is generally accepted that different wear mechanisms occur during woodcutting; and the dominant wear mechanism may be different under different cutting conditions (Cristovao, 2013); (Naylor & Hackney, 2013) & (Sacks, 2002).

High carbon steels (about 1.0%C) or high-speed steels (T or M series) were the most used cutting tool materials in the wood industry before the introduction of WC-Co. The tool life and performance had usually been good because of the excellent wear characteristics. The enhancement of the tool life and performance was obtained by the use of WC-Co cutting tools, this material has the wear resistance that is superior to that of steels and is used extensively in the machining of high strength ferrous and non-ferrous alloys. However, researchers suggested that when WC-Co is used in wood products with high moisture contents it shows a rapid degradation and high wear rates compared to the aforementioned steels under same conditions (Bailey, et al., 1983) & (Naylor & Hackney, 2013).

Studies have shown that wood moisture and multi-component nature play an important role in the kinetics of the tool's degradation. Moreover, further understanding of corrosion kinetics and thermodynamics is essential for the development of the cemented carbide cutting tool when used in corrosive environments. However, there is limited information on the behaviour of cutting tools when machining different wood materials under different conditions (Ramasamy & Ratnasingam, 2010) & (Sutthiruangwong & Mori, 2003).

2.2. Woodcutting Tool Wear

The cutting process is impenetrable with many influencing factors which include material properties, cutting tool geometry and cutting parameters (Cristovao, 2013). Hence, basic understanding of wood machining properties that the industry employs to assess the cutting tool wear comprise of cutting tool wear, cutting forces, power consumption and tensioning of cutting tools. This will give the possibility of enhancing product quality, increasing production efficiency, or otherwise improving the machining process (Cristovao, 2013) & (Sacks, 2002).

Research on woodcutting tool wear done up until the present time is centred on the cutting tool itself, the type of wood, tool performance and cutting conditions. The following sections will give a review of the woodcutting tool wear trends.

2.2.1. Properties of Wood during Woodcutting

Wood is promptly available heterogeneous material with plenty of varieties. This material is used in the furniture, packing, building constructions, flooring and panelling, window frames (Bendikiene & Keturakis, 2017). Wood consists of organic constituents such as cellulose, hemicellulose, lignin and extractives (Ramage, et al., 2017). Furthermore, it also consists of small substances such as gums, fats, resins, sugars, oils, starches, alkaloids and tannis (Darmawan, et al., 2011) & (Darmawan, et al., 2012). However, these substances occur in small amounts, they play a big role in wood properties. It has been reported that a number of organic acids were found that they exist in wood which include tannic acid, acetic acid, citric acid and formic acid (Sacks, 2002) & (Gibson & Watt, 2010). Moreover, mild acids such as acetic acid have little effect on strength, in contrast strong acids, such as sulphuric acid; cause substantial strength losses (Winandy & Rowell, 1984).

The physical and mechanical properties of wood are determined by moisture content as well as temperature (Chiniforush, et al., 2019) & (Winandy & Rowell, 1984). Studies have shown that if the temperature increases to a point where the pH of the environment changes, this can lessen the strength properties of wood. Furthermore, it has been found that these effects are further aggravated by time and moisture (Winandy & Rowell, 1984).

Hardwoods are known to emit more acetic acid than softwoods. Additionally, the acetic acid source is due to the hydrolysis of acetyl group esters in the hemicellulose, which is one-third of the total carbohydrate in the wood (Gibson & Watt, 2010). From literature, hardwoods are

found to be usually more susceptible to degradation by either acids or alkalis than softwoods are. This effect is assumed to be due to hardwood's lower lignin content and higher proportion of pentosan hemicelluloses (Winandy & Rowell, 1984).

2.2.2. Tool Wear Mechanism

Research had shown that the tool wear and blunting of cutting edges can occur by either one of two ways. It can occur by large scale fracturing of the tool edge, and it is generally caused by the poor tool design or operating processes. Lastly, this is a not easy to avoid type of wear that takes place on a smaller scale where particles are removed by abrasion (Sacks, 2002) & (Sheikh-Ahmad & Bailey, 1999).

The performance of the cutting tools differs as they are used. The range in performance of the cutting tools can be monitored by observing the change in the edge geometry of the cutting tool, change in the forces acting during cutting and change in power consumption (Cristovao, 2013). Therefore, a study on the interconnection of the tool, wood and machining environment is essential in the measurement of tool wear and blunting of cutting edge with an aim of identifying the predominant wear (Sacks, 2002). Further and more accurate study can be conducted, once the relationship between the tool, wood and machining environment is known, that will focus on the impact of changing the cutting parameters (Sacks, 2002).

Researchers proposed various parameters such as nose width, edge recession in rake face, edge recession in clearance, edge radius, etc to evaluate tool wear and blunting of cutting edges (Cristovao, 2013). However, there is still a misunderstanding to which wear parameter is the most representative of the state of bluntness of the tool (Sheikh-Ahmad & McKenzie, 1997) & (Cristovao, 2013).

2.2.2.1. Natural Wood

Studies had shown that the amount and chemical nature of the extractives found in natural wood are the most contributing factors to the tool wear (Sacks, 2002). The chemicals that are mostly found in natural wood are tannic and acetic acid. These types of acids can lead to corrosion, and this is dependent on the moisture content and they eventually lead to the degradation of the cutting tool. Green wood is one of the natural woods that have been investigated extensively by many researchers. It was found to be the natural wood that

contains high moisture content and is more aggressive to the WC-Co as compared to the HHS.

Bailey, et al., (1983) conducted a similar investigation using different types of cemented tungsten carbide tools to machine oak. The wear mechanism that was observed involved the leaching of the binder (cobalt) through a chemical reaction that lead to the mechanical loss of tungsten carbide grains as the strength of the hardmetal deteriorated due to the removal of the binder (Bailey, et al., 1983).

Mohan, et al., (1981) investigated the susceptibility of cemented tungsten carbide woodcutting tool to corrosive wear when machining green wood. It was observed that a major part of the tool wear was due to corrosion. It was also found that the electrochemical action that was used to measure the corrosion susceptibility of the material can be influenced by changing the tool binder material and the amount of the tool binder material composition as well as the carbide grain size (Mohan & Klamecki, 1981). Another study was conducted on the wood products that contained high and low moisture contents which were green and cured wood, respectively. It was observed that the wear rate of the hardmetal was greater when it was exposed to high moisture content as compared to low moisture content (Ramasamy & Ratnasingam, 2010).

2.3. Tungsten Carbides

2.3.1. Hardmetals

Hardmetals are composite materials with one or more hard but relatively brittle components (tungsten carbide, titanium carbide, tantalum carbide) and a ductile binder (cobalt, nickel, iron) that gives a certain degree of toughness to the material without impairing the high hardness of the carbide components. The WC-Co are usually referred to as hardmetals. This distinctive combination of hardness and toughness makes them exceptional as tool materials in the industry (Ettmayer, 1989) & (Lassner & Schubert, 1999). Commercial hardmetals of the type [(WC-M); where M = Fe, Ni or Co] or their mixtures which are prepared in different ratios of binders, they normally give desired properties for a particular application such as electrolytic properties and corrosion resistance (Scholl, et al, 1992). The cemented carbides are of great importance in the manufacturing industry and are widely used for cutting, drilling, and grinding tools (Zhang & Chen, 2017).

2.3.2. WC-Co Manufacture

Cemented carbides are obtained by liquid phase sintering of a well-mixed and compacted powder mixture of alloyed or unalloyed carbides of the transition metals such as (WC, TiC, TaC) with cobalt (Ettmayer, 1989). The powders of the tungsten carbide and cobalt are milled to achieve the desired grain size, there are then mixed and compacted. After compaction, the hardmetal is sintered via liquid phase sintering under controlled sintering atmosphere, where densification takes place inorder to obtain a pore-free microstructure and final dimensions of the component (Fang & Eso, 2005) & (Garcia & Strelsky, 2010).

Cobalt is used as a primary binder because it has improved wettability with WC at high temperatures as well as its excellent mechanical properties (AZoM, 2002) & (Garcia & Strelsky, 2010).

The manufacturing processes are linked, which means that any changes that will occur in any manufacturing step in the production chain will have an impact on the following process and the quality of the final product (García, et al., 2019). Figure 2.1 below illustrates the summary of the manufacturing of WC-Co.

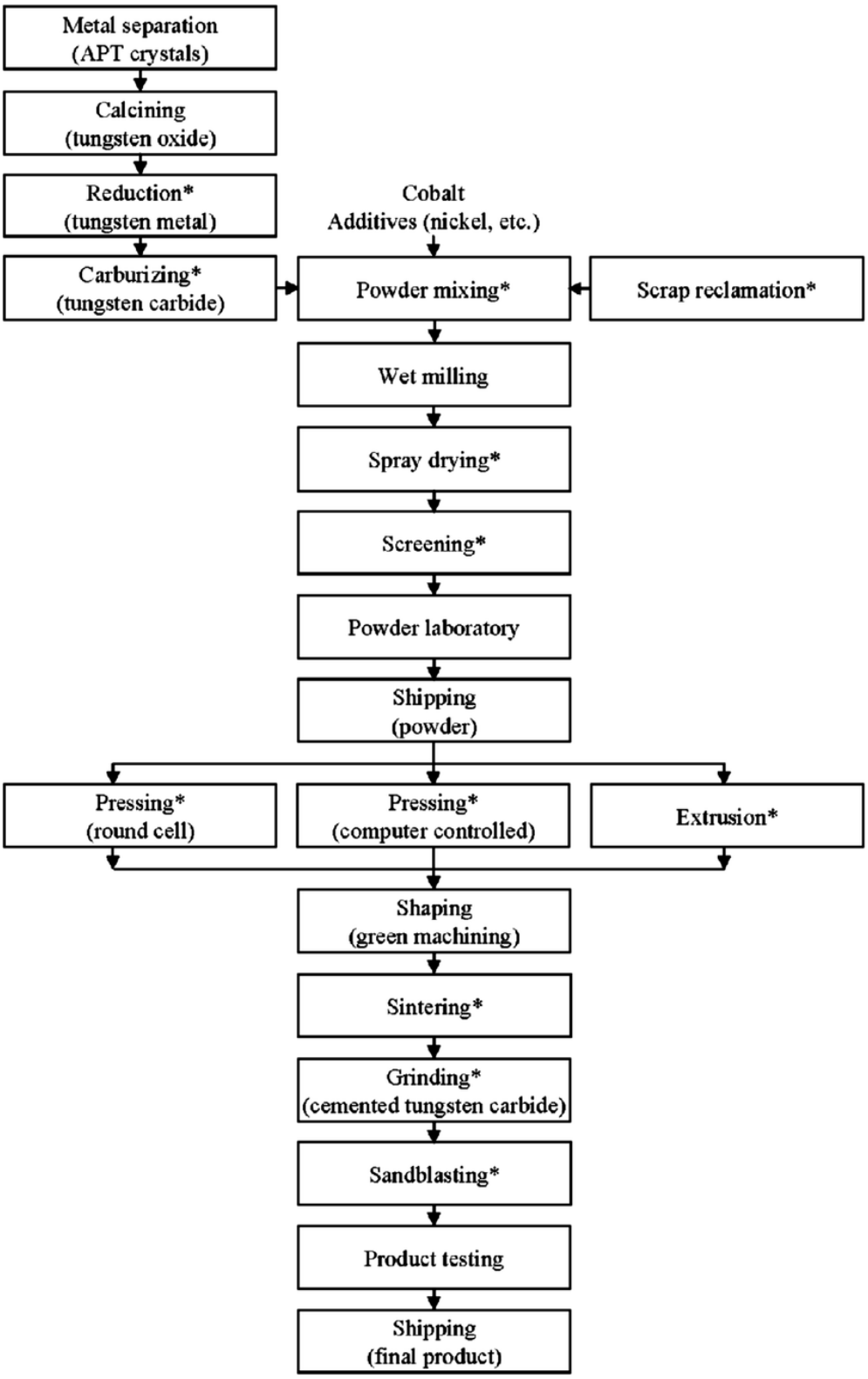


Figure 2.1: Manufacturing of WC-Co (Stefaniak, et al., 2007)

2.3.3. Applications of WC-Co

The tungsten carbide phase provides the alloy with exceptional hardness as well as superior wear resistance whilst the binder gives the composite material with strength and toughness

(Sun, et al., 2020). The logic behind the metal-matrix composite such as WC-Co is to form a material with the most prevailing mechanical properties such as high hardness and toughness as well as wear resistance (Sockel & Pugsley, 2004) & (Fangab & Llanesb, 2020). These properties makes the composite material to be more suitable for a wide range of applications in the industry, that is, as cutting tools and wear parts for machining of components in the automotive and aerospace industry; as drill bits or road headers in the rock and mining industry or sharp cutting teeth for the wood industry (Garcia & Strelsky, 2010). Tungsten carbide is used as a coating material because of its high hardness, corrosion resistance and wear resistance (Palomar, et al., 2009).

2.3.4. Limitations

Certain applications demand the WC-Co materials to remain in service for some years. These materials are exposed to corrosion and oxidation, as corrosion plays a major role in damaging the cemented tungsten carbide components making them more susceptible to wear, thus decreasing the tool life (Imasato, et al., 1995) & (Zhang, et al., 2019). Therefore, for longer service life and prevention of premature failure, the corrosion properties play a major in influencing the overall performance of the tool. However, corrosion resistance is not a primary requirement for the composite materials, nonetheless, it is still a very important requirement for industrial uses (Tarragó, et al., 2016) & (Thanjekwayo, 2009). Since the binder phase cobalt is susceptible to the corrosive media, it has been observed that the reduction on the cobalt content or substitution of cobalt by another element has a major effect on the corrosion resistance (Kim, et al, 2005).

2.3.5. Grain Growth Inhibitors

Grain growth inhibitors are used to produce finer carbide grain size microstructure which increases hardness, thus, wear resistance of the hardmetals (Sacks, 2002). Cubic carbides such as Cr_3C_2, TaC, NbC or VC are added to WC-Co hardmetal mixtures to inhibit the growth of the tungsten carbide grains during sintering and they have been found to be the most effective grain growth inhibitors (Stanciu, et al., 2017). Furthermore, the alloying elements such as Cr_3C_2 and VC have proved to be excellent grain growth inhibitors when alloyed into the binder as they improve corrosion resistance and fracture toughness of the hardmetal (Wood, et al., 2017).

In order for the grain growth inhibitor to be effective it is dependent on factors such as the inhibitor concentration and the sintering temperature. The latter plays a role in producing the final microstructure due to the solid state and liquid phase sintering effects. In addition, it has been observed that the carbon concentration in the cobalt binder have a visible effect on the WC grain growth (Morton, et al., 2005).

2.4. Corrosion

Corrosion is the deterioration of a material due to the chemical reaction with the environment; it is regarded as a reverse extractive metallurgy which is dependent on temperature and concentration of the environment (Kruger & Begum, 2016).

Corrosion resistance of the WC-Co is dependent on the binder composition, binder content and the size of the carbide grains (Sutthiruangwong & Mori, 2003) & (Kříž & Bricín, 2017). Since the cobalt binder phase is mostly affected by corrosion, it follows that making improvements of the corrosion resistance of the binder by adding other metallic alloy compositions will have a major influence on the overall corrosion resistance (Human & Exner, 1997) & (Wentzel & Allen, 1996). Therefore, the understanding of corrosion kinetics and thermodynamics is necessary for the improvement of the cemented carbides in such environments (Sutthiruangwong & Mori, 2003).

2.4.1. Introduction to the Corrosion of WC-Co Hardmetals

Tungsten carbide hardmetals have replaced the high speed and high carbon steels materials as woodcutting tools (Bailey, et al., 1983). However, the tungsten carbide hardmetals suffer corrosive wear and the high-speed steels are regarded as better corrosive resistant alternatives even though they are also sensitive to wood with high moisture (Naylor & Hackney, 2013). It has been observed that corrosion progresses by oxidation leaving only the tungsten carbide skeleton which is broken down by mechanical action (Sutthiruangwong & Mori, 2003); (Jacobson, 2018) & (Human & Exner, 1997). Therefore, this critically limits their use in extreme conditions as it decreases the hardmetal service performance (Guo, et al., 2020) & (Kellner, et al., 2009). Generally, WC-Co does not passivate (Kosters, et al., 2005). Studies have shown that tungsten (W) and cobalt (Co) show opposite behaviours when considering the influence of the environment acidity; W have shown to be more stable than Co when it is exposed to acidic environment and Co have shown to be more stable than W when it is exposed to alkaline environments (Santos, et al., 2020) & (Kellner, et al., 2009). In

applications where corrosion or oxidation resistance is required, the WC-Ni has shown to have better properties than the WC-Co hardmetals but fully or partially replacing the cobalt binder can compromise the mechanical properties of the hardmetal (Santos, et al., 2020).

2.4.2. The Mechanism of Corrosion

Most studies have shown that the corrosion response of tungsten carbide hardmetals has been conducted using the weight loss measurement from immersion tests with electrochemical procedures when it is exposed to various aqueous solutions (Sacks, 2002). Sutthiruangwong et al., (2003) reported that the hardmetals suffer galvanic corrosion (Sutthiruangwong & Mori, 2003). Furthermore, it has been studied that there are different electrode potentials found in these hardmetals where the hard WC grains acts as cathode and the soft binder phase acts as anode which leads to the formation of the micro galvanic couples between these phases in many aqueous environments causing corrosion (Katiyar, 2020). Studies have stated that this happens due to the large surface area covered by ceramic particles as a result corrosion is enhanced in the anodic sites of the hardmetal (Tarragó, et al., 2016). Although these tests have been conducted years ago on the different hardmetals, there lies a question on the exact mechanisms of corrosion and microstructural influence on the binder properties.

2.4.2.1. Galvanic Corrosion

Galvanic corrosion is known to take place whenever dissimilar metals come in contact in the presence of a corrosive electrolyte. This type of corrosion is driven by an electrode potential difference between two metals and each of the metals acts as either the anode or cathode (Kosaba, et al., 2021) & (Jones, 1996). This corrosion behaviour can be inhibited by substituting a cathodic material with one higher in the galvanic series than the binder (Gant & et al., 2004).

2.4.2.2. Corrosion of Cobalt

Cobalt has two main oxidation states which include Co^{2+} and Co^{3+}. The Co^{3+} ion is unstable and easily reduces to Co^{2+} because of that, the Co^{3+} can be overlooked for the consideration of the corrosion behaviour in acidic solutions. These equations show the potential-voltage versus the saturated calomel electrode (SCE) of cobalt.

$Co = Co^{2+} + 2e^-$, $\quad E^0 = -518$ mV vs SCE
$Co^{2+} = Co^{3+} + e^-$, $\quad E^0 = 1567$ mV vs SCE

The Pourbaix diagram for cobalt shown in figure 2.2, cobalt is shown that it actively corrodes in acidic media and oxide formation occurs at pH levels around 7 in oxygenated environments (Human, et al., 1998) & (Sacks, 2002).

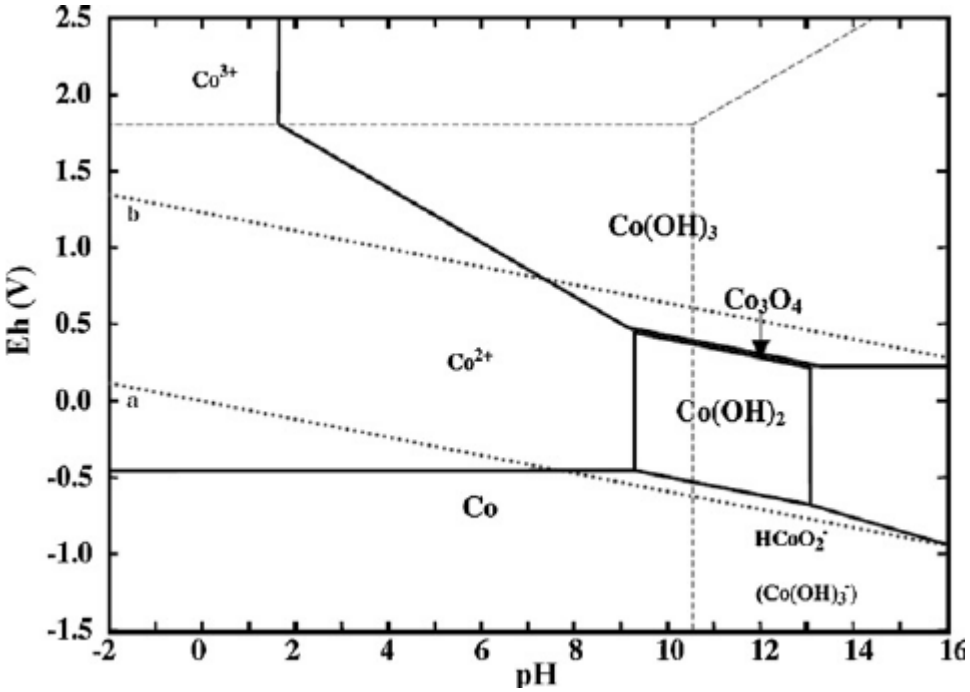


Figure 2.2: Pourbaix diagram for the cobalt-water system at 25°C (Garcia, et al., 2008).

2.4.2.3. Corrosion of Tungsten Carbide

Tungsten carbide (WC) is chemically more stable than cobalt when exposed to acidic environments. However, WC when it is exposed to alkaline solution it tends to behave differently as it becomes less stable when compared to cobalt (Human & Exner, 1996); (Kellner, et al., 2009) & (Potgieter, et al., 2011).

There has been a theory on the formation of an oxide WO_3 at the surface when it is exposed to sulphuric acid (Thanjekwayo, 2009); (Human & Exner, 1997) & (Bozzini, et al., 2004). This is demonstrated in the following equation:

$$WC + 5H_2O = WO_3 + CO + 10H^+ + 10e^-$$

In acidic and neutral environments, the pure WC-Co alloys show pseudopassivity (Thanjekwayo, 2009). Sutthiruangwong et al., (2003) investigated the cause of pseudopassivity and found that in WC-Co with high tungsten (W) content in the binder form the corrosion products such as WO_3 at the surface of the binder. Therefore, this decreases the

dissolution of rate by inhibiting further dissolution of the binder (Sutthiruangwong & Mori, 2003) & (Kosters, et al., 2005).

2.4.3. The Effect of the Binder Content on the Corrosion

Studies on the influence of binder compositions and binder content on WC-Co have been conducted; however, there are still debates of the literature on whether to increase or reduce the binder contents for a particular application. Gant et al., (2004) mentioned that the exact binder content will be dictated by the particular corrosive media encountered by an alloy. Furthermore, they suggested the material loss can be reduced by reducing the volume fraction of the binder. Sutthiruangwong et al., (2003) studied the corrosion properties of the cobalt-based cemented carbides in acidic solutions (Sutthiruangwong & Mori, 2003). It was observed that the reduction of the cobalt binder content it results to better corrosion resistance. However, Human et al., (1996) studied the electrochemical behaviour of the tungsten carbide hardmetals, where they were discussing the effect of the binder content ranging from 6 to 15 wt% and the WC grain size ranging between 1 to 5 μm. The material was exposed to sulphuric acid. It was observed that there was no significant change in the corrosion rate of the binder phase with varying binder content (Human & Exner, 1996).

Partial or total substitution of cobalt has been a subject of interest since few decades ago. The substitution of cobalt has been an aim and it was promoted because cobalt is a hazardous substance to human health. Nickel and its alloys as well as iron have been used and proved to be alternative binders to cobalt for increasing corrosion resistance. Both iron and nickel have been studied as candidates, since they are closest transition metals to cobalt in the periodic table and by consequence; they have similar affinity with carbon and tungsten (Sandoval, et al., 2019) & (Roulon, et al., 2020). However, fully replacing cobalt with nickel may be detrimental to the mechanical properties of cemented tungsten carbide. It can compromise the hardness, wear resistance and strength of this hardmetal (Zhang, et al., 2019).

Another study was conducted on the improvements of WC-Co, and it was also found that the addition of chromium into the binder phase improves the corrosion resistance of WC-Co in acidic solutions; however, it is detrimental to its mechanical properties (Zhang, et al., 2019). Cobalt can also be partly replaced by nickel-chromium, nickel-chromium-molybdenum (Human & Exner, 1996) & (Fazili, et al., 2020). The effect of each binder is outlined below.

2.4.3.1. Nickel

Various studies have been conducted on the effect of nickel as an alternative binder. Tomlinson et al., (1988), Scholl et al., (1992) and Wentzel et al., (1996) investigated the effect of nickel when it is exposed to acidic environments. It was reported that nickel is more corrosion resistant compared to cobalt (Tomlinson & Linzell, 1988); (Scholl, et al., 1992) & (Wentzel & Allen, 1996). Studies have observed that tungsten carbide-nickel in acidic environment is much better than tungsten carbide-cobalt (Tracey, 1992). However, mechanical properties such as hardness and strength are lower than that of cobalt when it is fully substituted. Furthermore, the substitution of cobalt with nickel, in whole or part, has been studied to strengthen the binder phase, as well as reducing the costs associated with the limited supply and the high market price of cobalt powder (Li, et al., 2020).

2.4.3.2. Iron

Studies have shown that iron has been identified as the promising candidate to substitute cobalt. It is induced by its ability to suppress the WC grain growth resulting from high affinity for carbon during thermal cycle required to sinter the alloys, together with its non-toxicity and low price (Zhao, et al., 2019). However, it has not gained much attention in the industry; it could be that the binder has the tendency to form martensite during cooling cycle (Ettmayer, 1989). Moreover, it was observed that it has not been attractive from aesthetic point of view because of possible rusting and also the hardness and strength of tungsten carbide-iron appears to be inferior to that of tungsten carbide-cobalt (Tracey, 1992) & (Zhao, et al., 2019).

2.4.3.3. Other binder compositions

Various studies have been conducted on the addition of chromium/chromium carbide into the binder phase. According to (Allen & Wentzel, 1995) & (Li, et al., 2020), chromium addition into the binder phase of WC-Ni improves the corrosion resistance, they also reported that chromium carbide can refine the WC grains. While Kosters, et al., (2005) and Roa, et al., (2020) reported that chromium in the binder of WC-Co increases corrosion resistance by stabilizing the cobalt-based passive oxide layer but also produces a refinement of the WC (Kosters, et al, 2005) & (Roa, et al., 2020).

It has recently been reported that the addition of ruthenium (Ru) in the WC-Co can stabilize the crystal structure of the cobalt binder and improve the corrosion resistance of the

hardmetal while a small addition of vanadium carbide (VC) reduced it (Potgieter, et al., 2011). While Guo, et al., (2020) studied the role of Y_2O_3, Cu, Mo and Mo_2C additives on optimizing the corrosion resistance of WC-6wt%Co in acidic (HCl) and alkaline (NaOH) solutions. It was found that Y_2O_3, Mo and Mo_2C can decrease the grain size and improve the hardness of the cemented tungsten carbide, however, Cu behaves differently. Furthermore, Y_2O_3, Mo and Mo_2C have been reported to improve corrosion resistance in both acidic and alkaline solutions. In comparison, Mo additive was found to be the most effective in improving corrosion resistance cemented tungsten carbide in both solutions whereas Cu only improves corrosion resistance when the hardmetal is exposed to the alkaline solution (Guo, et al., 2020).

2.4.4. The Influence of Various Parameters on Corrosion

Studies have shown that the corrosive environment is one of the last factors that influence the corrosion behaviour of cemented carbides (Bricín, et al, 2019). Temperature and pH can have influence on the corrosion of WC-Co. Bricín, et al., (2019) have found that the use of cobalt binder for woodworking where the pH of wood moves from a value of 3 to that of 8 is detrimental to the cutting tool life. Additionally, they found that the fine-grained WC-Co straight carbide structure degraded when it was exposed to sulphuric acid environment, a loss of hardness was observed (Bricín, et al., 2019).

Sheikh-Ahmad & Bailey (1999) conducted an investigation on the machining of fibreboard and particleboard. They found that the tool material is exposed to reactive gases and vapors produced from thermal decomposition of wood fibers and other board additives at high temperatures. Furthermore, the presence of these reactive agents may be disadvantageous to tool wear (Sheikh-Ahmad & Bailey, 1999).

2.4.5. Effect of organic acid on WC-Co

Cemented tungsten carbide can be used as a cutting tool that can be used to cut a wide variety range of materials including metal, plastic, fibreboard and wood. It is therefore exposed to a variety of environments that may contain highly aggressive compounds. In woodcutting, organic acids such as tannic, acetic acid and others are found in wood and they tend to be highly corrosive, thus, they reduce the tool life. Additionally, studies have shown that the performance of a cutting tool is not determined by its mechanical properties but its dependant on the nature of the environment in which it is being exposed to (Sockel & Pugsley, 2004).

Studies have been conducted on the corrosion of WC-Co in different woodcutting environments. Pugsley, et al., (2001) studied the influence of a corrosive wood-cutting environment on the mechanical properties of hardmetal tools. The materials that were used to investigate this effect were the straight carbide phase (WC-Co) with 10wt%Co and a mixed carbide phase (WC-Co + (WC/TiC/Ta(Nb)C) with 6wt%Co and they were exposed to tannic acid under static load conditions. The formation of defects at the surface of the hardmetals was observed and defects are known that they act as stress raisers that could lead to the reduction in strength of the material. It was reported that the mixed carbide phase hardmetal exhibited a further decrease in strength during the static load conditions. The strength of the straight carbide hardmetal remained unaffected during the static load (Pugsley, et al., 2001).

Gauvent, et al., (2006) studied the corrosion of materials used as cutting tools of wood where carbon steels and tungsten carbide-based alloys were compared to each other exposed to the juice of oak. It was observed that the mechanical resistance of these two cutting tools decreased drastically when the corrosive agents of wood dissolved the metallic matrix. It was proposed that the corrosion behaviour of WC alloys is determined by the composition and the amount of a binder while the corrosion behaviour of carbon steels was determined by nickel and chromium contents in the alloy (Gauvent, et al., 2006). However, studies have not focused yet on the corrosion of WC-Co when it is exposed to an organic acid salt solution.

2.5. Wear

Wear is defined as material removal or surface damage on the one or two surfaces while rolling, sliding or impact motion relative to one another (Jeyaprakash & Yang, 2020). It is part of a wider field called tribology which involves wear, friction, and lubrication (Sacks, 2002) & (Jeyaprakash & Yang, 2020).

Wear processes are usually illustrated in terms of a tribosystem in figure 2.3. The tribosystem often consist of a solid body, a counter body, an interfacial element, and the environment (Sacks, 2002). In addition, the interaction between parameters involved in the tribosystem leads to different types of wear which include rolling, sliding and impact wear (Sacks, 2002).

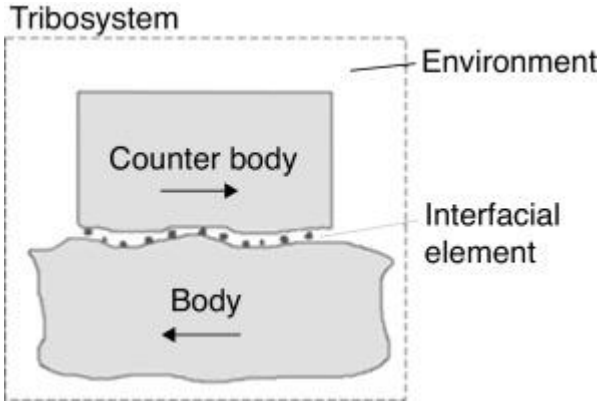


Figure 2.3: Tribosystem (Massola, et al., 2016).

2.5.1. Wear mechanism of WC-Co

Tool wear is a very important aspect for the wood industry because it reflects the tool performance during the cutting of composite materials (Cristovao, 2013) & (Guo, et al., 2014). It was suggested that wear can be divided into two groups depending on the wear mechanisms involved. The first group involves mechanical wear which comes from the mechanical interaction only between counter-faces. The second group involves the chemical interaction such as oxidation or tribo-chemical reaction between counter-faces, as an active wear component (Krakhmalev, et al., 2007). It has been found that the tool geometry, workpiece and cutting parameters influence the wear mechanism greatly. The performance of the cutting tool differs as it is used; the difference in performance can be monitored by observing the change in the edge geometry of the cutting tool and different forces acting on the tool during cutting (Cristovao, 2013) & (Guo, et al., 2014). In addition, the wood moisture which is regarded as the corrosive media plays an important role in the degradation of the cutting tool (Pugsley, et al., 2001) & (Engqvist, et al., 2000).

2.5.1.1. Abrasion Wear

Abrasive wear happens while asperities of a rough and hard particles slide on a softer surface and removes the softer material, and it damages the surface through fracture or plastic deformation (Jeyaprakash & Yang, 2020) & (Affatato & Brando, 2013). This type of wear is often classified according to the type of contact and the contact environment, the type of contact regulates the modes of abrasive wear. There are two modes of abrasive wear which include two-body and three-body abrasive wear (Affatato & Brando, 2013).

The two-body abrasive wear occurs when one surface (often the one with the higher hardness than the other) cuts the material away from the other surface. Furthermore, this mechanism changes to three-body abrasion as the wear debris acts as an abrasive between the two surfaces. The three-body abrasive wear occurs when particles are not restricted but are free to roll and slide down a surface. Therefore, they lead to fissuring, scratching and microcutting of their surface layers, the particles randomly get trapped into one of the layers leading to wear by microcutting (Affatato & Brando, 2013) & (Siczek, 2016). The aforementioned modes of wear experiences the three types of material stresses which include gouging, high and low stress abrasion wear. Gouging happens when the coarse particles impact and cut into the material displacing fairly large material fragments (Sacks, 2002). The high stress abrasion wear occurs when the crushing strength of the abrasive particles is overreached, and they are fragmented during the wear process. In the low stress abrasion wear the particles remain the same (Hutching & Shipway, 2017).

The abrasion resistance of WC-Co is dependent on the material's ability to withstand penetration by abrasive particles and the degree of difficulty in removal of material by fracture or plastic flow (Sacks, 2002). Studies have shown that the abrasive wear mechanism depends on the properties of both the abrasive particles and the hardmetal. The correlative wear ranking of WC-Co has been found to be dependent on the tribosystem and is influenced by factors such as the size and hardness of the abrasive particle used, applied load and to the large on the varying material properties (Pirso, et al., 2009) & (Sacks, 2002).

It has been found that the abrasive wear resistance of the WC-Co increases with increasing carbide content which also cause a gain in the hardness of the hardmetal. Furthermore, the effect of carbide grain size on the wear rate of WC-Co can be different. For example, one of the researchers observed that the coarse grain hardmetals showed a lower abrasive wear rate that the fine-grained ones (Pirso, et al., 2009). Another researcher observed that the fine grain hardmetals are favourable to prevent wear by the large abrasive particles but if the abrasive particles are subjected to intensive fracturing these fine-grained hardmetals lose their advantages and experience high wear rates (Antonov, et al., 2015).

It has been found that WC-Co experiences the following modes of material removal: plastic grooving, binder phase extrusion and removal, fracture of WC grains, Palmqvist crack and subsequent spalling (Pirso, et al., 2009).

2.5.1.2. Corrosive wear

Corrosive/chemical wear happens while sliding takes place in a chemical atmosphere. Chemical wear can arise due to the electrochemical or chemical interaction of the surfaces with the atmosphere. This type of wear occurs in extremely high corrosive atmosphere, high humidity, and temperature atmosphere (Jeyaprakash & Yang, 2020).

A number of studies have been conducted on the wear mechanisms of WC-Co cutting tool under different cutting conditions. Bailey et al., (1983) studied the wear of WC-Co tools in machining oak. The materials that were used for this study were the WC-Co inserts and tannic acid. It was observed that wear occurred through a process of a continuous tool nose rounding when cutting wood with high moisture, this was found when the tool cutting edge was observed through the Scanning Electron Microscope (SEM). It was proposed that the dominant mechanism of wear involves the preferential removal of the binder through chemical reaction with extractives present in the oak. This is followed by the mechanical loss of tungsten carbide grains when the strength of the remaining bond between them and the binder is insufficient to resist the shear forces generated by the motion of the chip. Additionally, it was proposed that adhesive and abrasive processes did not contribute significantly to the tool degradation, though there is some evidence that wear occurred through tool edge chipping (Bailey, et al., 1983).

2.5.2. Effect of the Lubricant

Lubricants are used to reduce friction and wear of two materials rubbing against one another. However, they tend to drive up the wear processes (Sacks, 2002). Studies have shown that the liquid has influence on the wear system and it acts as a leaching reagent. It was observed that the cobalt binder might be selectively leached in certain lubricants and the leaching rate increases as the oxygen concentration decreases in lubricants (Sacks, 2002) & (Lu, et al., 2008). The atmospheric composition can result to the formation of oxides on the metal surfaces, which, however, have low shear strength decreases the contact between abrasive particle and metal (Sacks, 2002).

Friction is defined as the resistance to motion of one moving object relative to one another. It has been shown to be dependent on the normal force and coefficient of the friction. Furthermore, it is independent of the contact area and the sliding velocity (Sacks, 2002). The friction and lubrication are influenced by the surface finish, temperature, sliding velocity,

contact pressure and lubricant characteristics. Therefore, good understanding of the parameters that affect friction is essential for the selection of lubricants. In addition, there are four different types of lubrication which include (1) dry condition, (2) boundary lubrication, (3) mixed-film lubrication and (4) hydrodynamic lubrication. Hence, the Stribeck curve in figure 2.4 is used to show schematically the onset of various types of lubrication mechanisms as a function of lubricant viscosity, sliding velocity and normal pressure (Altan & Tekkaya, 2012) & (Sacks, 2002).

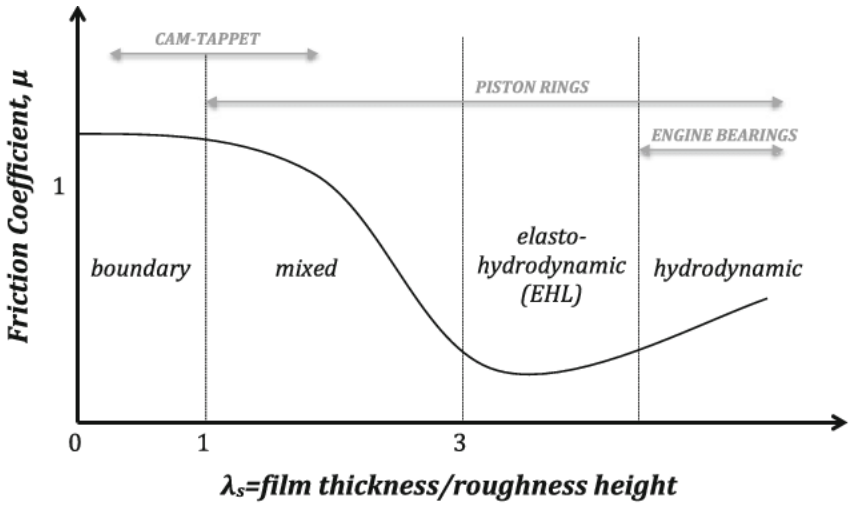


Figure 2.4: The Stribeck curve (Chong & Cruz, 2014)

2.6. Tribocorrosion of WC-Co

The study of tribocorrosion began in the late 1980's where it included the interaction of corrosion and abrasion, erosion, adhesion, fretting and fatigue. WC-Co is a frequent choice for wear parts in the field that demands resistance to abrasion and/or erosion. It has been observed that in cases where abrasion and/or erosion occur with corrosive media, the material loss is mostly found to be greater than would be expected as a result of the corrosive nature of the carrier medium (Wood et al., 2017) & (Gant, et al., 2004).

Wood et al., (2017) studied the implications of tribocorrosion and how it affects the degradation mechanisms of WC-Co. It has been observed that a metal binder that is optimum in one degradation process is not optimum when both corrosion and wear are in place. For example, nickel performs best for corrosion alone but performs poorly in tribocorrosion, this is assumed to be caused by the passive layer which is takes time to form and is mechanically weak which makes it to be susceptible to the removal due to the applied load or its intrinsic material properties are inferior (Wood, et al.,2017). Furthermore, Gant, et al., (2004) studied

the tribocorrosion synergy for WC-Co hardmetals in low stress abrasion by varying the pH values from very acidic to basic conditions in the presence of an abrasive media. It was observed that under acidic conditions (pH 1.1) the WC grains by binder dissolution appeared to be the rate-governing step in determining volume loss, under mild acidic conditions (pH 2.6 and 6.3) there was more evidence of WC grain fracture and correspondingly less of binder dissolution. Under basic conditions (pH 13) caused the least wear (Gant, et al., 2004). However, the mechanism of tribocorrosion for tungsten carbide materials is not fully understood.

2.7. Effect of WC grain size on corrosion

Studies have been conducted on the effect of grain size on the corrosion behaviours in other material system; however, there is limited information on the effect of WC grain size on the corrosion behaviours of WC-Co system when exposed to organic acid environments (Zhang, et al., 2016). Some researchers reported there was no significant influence of the grain size on the corrosion behaviour in acidic environments (Human & Exner, 1997) & (Zheng, et al., 2019). Some found that an increase in grain size increased the passive current density of straight WC-Co alloys in acidic solutions (Tomlinson & Linzell, 1988).

3. Experimental Methods

This chapter focus on the methods used to investigate wear corrosion and tribocorrosion behaviour of WC-Co when it is exposed to organic acid environment. Different experimental techniques were used to assess the microstructural properties that influence the corrosion and tribocorrosion behaviour.

3.1. Materials

3.1.1. Sample characterization

The materials that were being investigated were obtained from the WC cutting blades with different binder contents. They were procured from Brelko Conveyor Products (Pty) Ltd. The chemical composition of the samples is shown in table 3.1. The EDS analysis peaks for the chemical compositions in the table are found in the appendix.

Table 3.1: Compositions for all samples from the EDS analysis

	Composition (wt%)					
Sample	W	Co	Ni	Cr	V	Cu
1 = COR	91.9	0.08	8.0	0	0	0
2 = M	90.9	6.5	1.8	0	0	0.8
3 = UM	83.7	6.4	3.2	1.9	4.8	0
4 = TC	84.2	10.1	4.59	0.65	0	0.41
5 = T3	82.5	11.1	4.64	1.54	0.22	0

3.1.2. Sample Preparation

Samples were prepared for metallography studies such as scanning electronic microscope analysis, hardness testing and grain size test. The sample preparation involved cutting, mounting, grinding, polishing and etching. Four cemented tungsten carbide (blades) samples with different binder compositions and contents were cut into small pieces with a 0.24 cm^2 surface area using a diamond-cutter wheel. The pieces were mounted using Bakelite. Since cemented tungsten carbide is a very hard material it was grounded using three blades and two consumables. Grinding was not done manually but a machine was used for accuracy. The force applied during grinding was 30 kgf. The samples were polished, and they were etched using the Murakami reagent which consists of a mixture of 10 g of potassium ferrocyanide

($K_3Fe(CN)_6$), 10g of potassium hydroxide (KOH) and 100ml of distilled water (Polini, et al., 2006) before using the SEM. Table 3.2 illustrate the material used to prepare the four samples:

Table 3.2: Activities to prepare the samples for material characterization (Elssner, et al., 1999)

Step	Activity	Consumables
Step 1	Mounting	Bakelite
Step 2	Grinding	Diamond disc 600grit, Water
Step 3	Roughing	Diamond disc 220grit, Water
Step 4	Polishing first lap	Woven cloth and 9micron diamond paste
Step 5	Polishing second lap	Woven cloth and 3micron diamond paste
Step 6	Polishing final lap	Woven cloth and 1micron aluminium silicon

3.1.3. Material Characterization

This section will be focusing on the study of the microstructure of a material to understand the properties and engineering characteristics. The as-received samples were characterized for elemental compositions and microstructures using the Carl Zeiss Sigma scanning electronic microscopy (SEM) combined with the energy dispersive X-ray spectroscopy (EDX) to work out the elements present in the samples.

3.2. Methods

3.2.1. Density Measurement

The density of the samples was measured using the density laboratory balance scale. The density scale was set to measure the density of the sample in air as well as water and as a result the scale generates the final density. Table 3.3 shows the density of the samples.

Table 3.3: The density results of the WC-Co samples.

	0.1%Co-8.0%Ni	6.5%Co-1.8%Ni-0.8%Cr	10.1%Co-4.6%Ni-0.7%Cr-0.4%Cu	11.1%Co-4.6%Ni-1.5%Cr-0.2%V	6.4%Co-3.2%Ni-2.0%Cr-4.8%V
Density (g/cm^3)	14.45	13.93	14.45	14.00	14.04

3.2.2. Microhardness Test

The Vickers microhardness test was performed on the samples using the Vickers microhardness machine. The machine consists of a pyramid diamond indenter that is used to make an impression on the surface of the sample. The diamond indenter has a square base with opposite sides joining at the apex at an angle of 136° (Whitefield, 2017). A load of 300 gf (0.3 kgf) was released and was applied for 15 seconds and two diagonals of the indentation were observed. The Vickers microhardness machine calculated the average of these two diagonals and the hardness value ($HV_{0.3}$) was generated. A diamond shape indenter was indented on the surface of a material five times in a straight line. The HV values that were computed by the Vickers microhardness machine followed this equation 1 with P as an applied load and L being the shape of the indenter:

$$HV_{0.3} = \frac{2\,P \sin\frac{136^\circ}{2}}{L^2} \qquad \textbf{Equation 1}$$

Table 3.4 shows the microhardness of the samples.

Table 3.4: The microhardness results of the WC-Co samples.

	0.1%Co-8.0%Ni	6.5%Co-1.8%Ni-0.8%Cr	10.1%Co-4.6%Ni-0.7%Cr-0.4%Cu	11.1%Co-4.6%Ni-1.5%Cr-0.2%V	6.4%Co-3.2%Ni-2.0%Cr-4.8%V
Hardness (HV)	1413	1582	1428	1699	1730

3.2.3. Grain size Measurement

The grain size measurements were taken using the SEM micrographs. ImageJ 2009 software was used to analyse the WC grains. Table 3.5 illustrates the grain size results.

Table 3.5: Grain size results of the WC-Co samples.

	0.1%Co-8.0%Ni	6.5%Co-1.8%Ni-0.8%Cr	10.1%Co-4.6%Ni-0.7%Cr-0.4%Cu	11.1%Co-4.6%Ni-1.5%Cr-0.2%V	6.4%Co-3.2%Ni-2.0%Cr-4.8%V
Mean WC grain size (μm)	0.33	0.54	0.49	0.51	0.17

3.2.4. Wear Test

A CSM Tribometer ball-on-disc PAAR instrument was used to perform friction and sliding wear tests on all five samples under dry conditions. A 6 mm alumina ball was used as recommended by the ASTM G99-05. The initial load applied was 10 N, however it was too heavy hence the machine stopped, and the load was reduced to 5 N. The CSM Tribometer instrument was set to automatically stop scanning at sliding distance of 450 m. The sliding speed was set to 0.1 m/s. The ball and the sample wear taken for SEM/EDS for surface analysis. The volume loss of the sample was determined using equation 2:

$$\text{Volume loss } (mm^3) = \frac{\pi(\boldsymbol{wear\ track\ radius} * \boldsymbol{track\ width^3})}{\boldsymbol{6}(\boldsymbol{sphere\ radius})} \qquad \textbf{Equation 2}$$

The wear rates were obtained by using the equation 3 below:

$$\text{Wear rate } (mm^3/Nm) = \frac{\boldsymbol{disk\ volume\ loss}}{\boldsymbol{sliding\ distance} \times \boldsymbol{load\ applied}} \qquad \textbf{Equation 3}$$

The contact pressure of the ball against the surface of a hardmetal was also computed which is the ratio between the load applied to the contact area. Equation 4:

$$\text{Contact pressure } (N/mm^2) = \frac{\boldsymbol{load\ applied}}{\boldsymbol{contact\ area}} \qquad \textbf{Equation 4}$$

3.3. Corrosion Tests

A Flat Corrosion Cell was used with a graphite rod as the counter electrode (anode). The electro-chemical potential was determined using a silver/silver chloride reference electrode. The working electrode (cathode) was mounted with on the side of the cell with an exposed

surface area of 0.283 cm^2 to the solution. The compositions of the working electrodes are found in section 3.1.1 table 3.1. The electrolyte samples that were used during the corrosion tests of tungsten carbide materials were collected for an AAS analysis and the results are found in table 4.5. Six 3.5% NaCl solutions were prepared to simulate a corrosive environment in which a tool will generally be used. One was mixed with acetic acid and the other with sulphuric acid with varying pH levels (see table 3.6). The acetic acid was used because it is an organic acids found in wood while most literature explores the effect of tannic acid this study will focus on the effects of the question. Sulphuric acid as a strong acid was used to compare the effect each acid has on the hardmetal. The tests were carried out at room temperature (25°C).

3.3.1. Open Circuit Potential (OCP) and Cyclic Potentiodynamic Polarization Measurements

An open circuit potential (OCP) was measured for 1 hour after the sample was exposed to the acid-salt solution before a potential scan was performed. The polarization scan was started from a potential scan of -100 mV to 100 mV. An electrochemical polarisation was done at a scan rate of 0.17 V/s based on ASTM G5. In this study a cyclic potentiodynamic polarization scan which is similar to a potentiodynamic scan was conducted in which the voltage is swept across a range but reversed back to the starting potential. This scan enables the sensitivity of metallic materials to pitting corrosion when exposed to certain media. The Nova Software was used to determine the current density (i_{corr}) and corrosion potential (E_{corr}) from the polarization curve.

3.3.2. Determining the Corrosion Rate

After the potentiodynamic polarization measurement is complete, a reverse polarization scan is generated which consists of the potential versus the log current density shown in figure 3.1. The current density is obtained by extrapolating the linear sections of the cathodic and anodic parts of the forward polarization scan. The current density is one of the requirements used to find the corrosion rate in µm/yr units. Equation 3 is used to calculate the corrosion rate of a metal:

$$CR = \frac{K_2.a.i_{corr}}{n.D} \qquad \textbf{Equation 5}$$

Where: K_2 is the constant $3.272 \times 10^6 \, {}^{\mu m}/_{yr}$

a is the atomic mass (g/mol)

n is the number of electrons

D is density of a metal

i_{corr} is the current density (µm/cm^2)

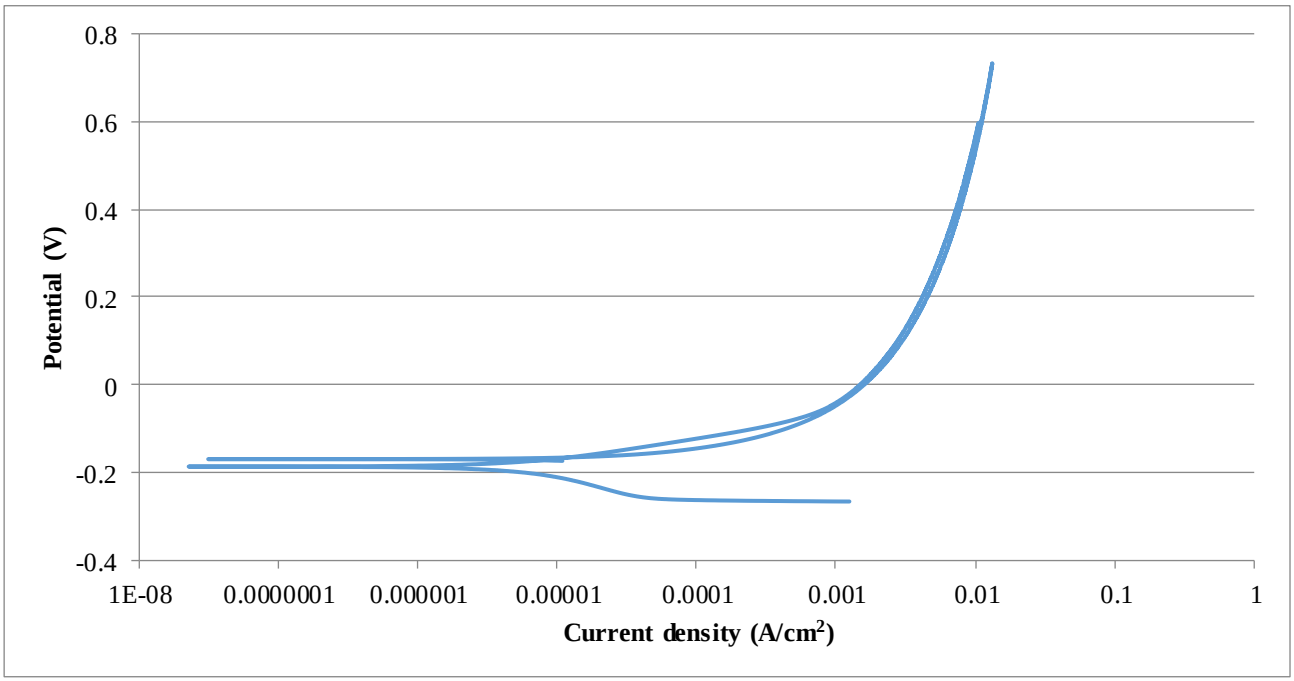


Figure 3.1: Polarisation curve of sample 6.5%Co-1.8%Ni-0.8%Cr exposed to 3.5%NaCl acetic acid solution at pH 2.

The table below shows the different pH levels that were used in this study. These values were selected because they range around the pH levels that are found in wood.

Table 3.6: These are different electrolytes that were used for corrosion tests at room temperature.

Acetic acid	Sulphuric acid
3.5% NaCl	
pH	pH
2	2
3.5	3.5
5	5

After each corrosion test, the solutions were collected and taken for the AAS analysis to identify the elements that are present in the solution.

3.4. Tribocorrosion Tests

Tribocorrosion test was performed using the same equipment and solution as that of the electrochemical test except that there was a ball-on-disc with a 6 mm alumina ball used and a load of 5 N was applied. The OCP scan ran for 2400 seconds (40 minutes) where there was scratching of the surface of the sample and with no scratching at different time intervals. The sample was not scratched for the first ten minutes while the potential applied was measured simultaneously. The following ten minutes was when the sample was scratched as the potential was being measured, the following ten minutes was when the running motor was turned off while the potential was measured. In the last ten minutes, the motor was turned on where the sample was scratched, and the electrochemical scan took place simultaneously. The electrochemical polarisation was scanned at a scan rate of 0.4 mV/s. Figure 3.2 illustrates a schematic diagram that shows the principles of tribocorrosion.

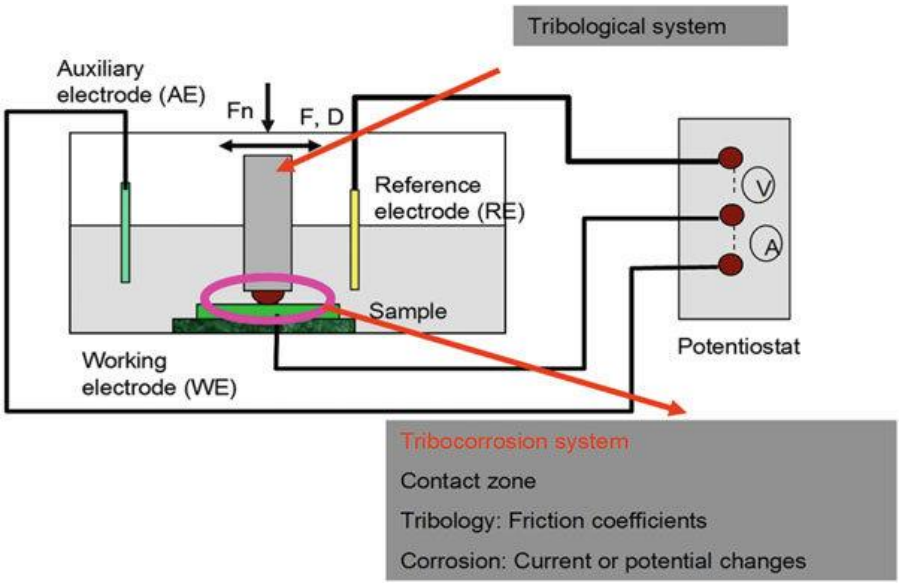


Figure 3.2: Tribocorrosion schematic diagram (Barao, et al., 2013).

4. Results

This chapter consists of the results of the experimental work conducted to assess the corrosion of tungsten carbide when it is exposed to organic acid environments. Some of the relationships are outlined in a graphical form and microstructural pictures are shown.

4.1. Material Characterisation

This section illustrates and describes the results of the properties of both the material and mechanical properties that will be required to gain an understanding of wear, corrosion and tribocorrosion in this study.

4.1.1. Optical Microscopy

The microstructures of the cemented tungsten carbide hardmetal are illustrated in figure 4.1. The lighter and darker phases can be observed of which they correspond to tungsten carbide and cobalt, respectively. A very fine microstructure was observed at a magnification of x50.

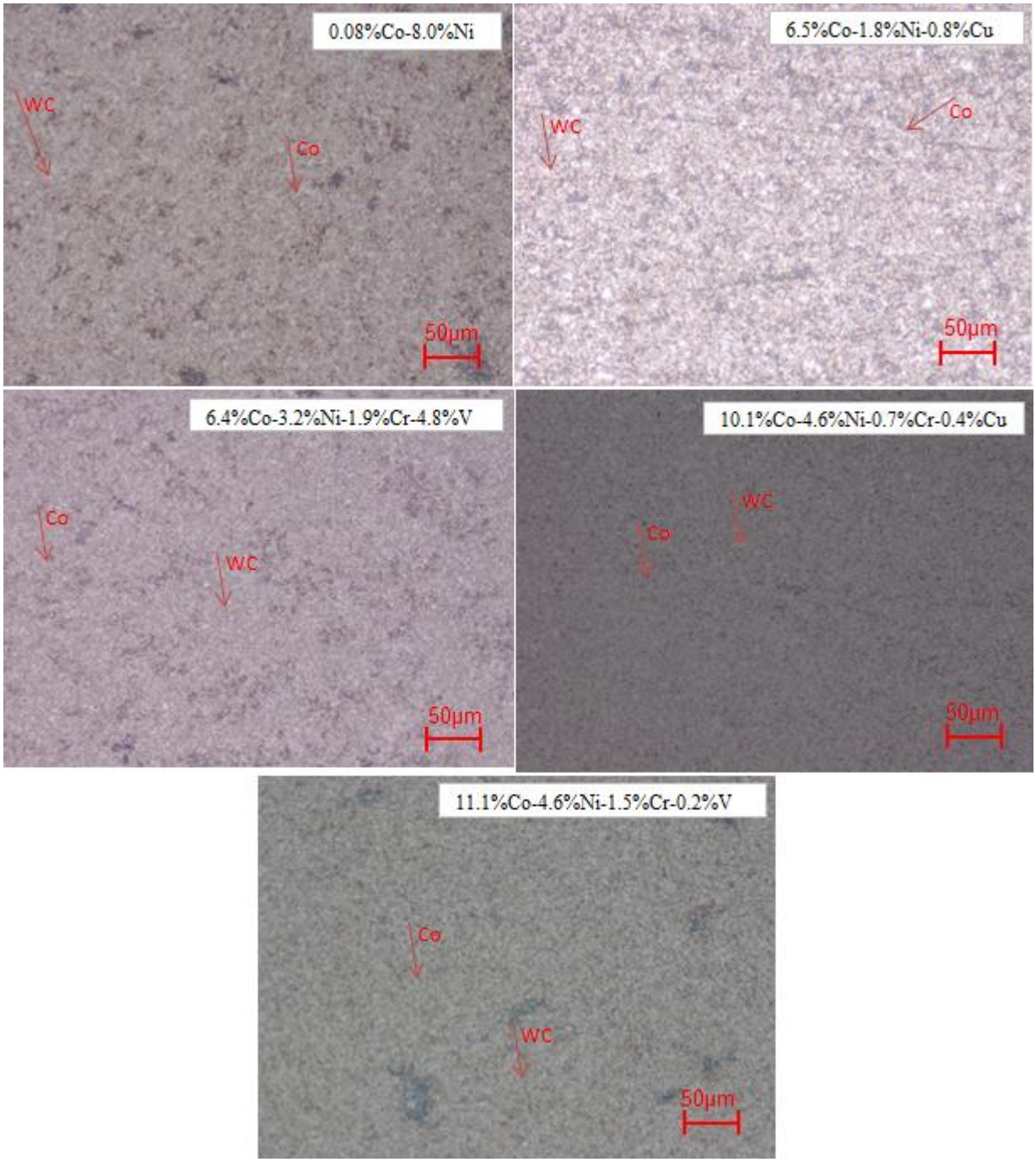


Figure 4.1: Optical micrographs of the WC alloys: a) 0.08%Co-8.0%Ni, b) 6.5%Co-1.8%Ni-0.8%Cu, c) 6.4%Co-3.2%Ni-1.9%Cr-4.8%V, d) 10.1%Co-4.6%Ni-0.7%Cr-0.4%Cu and e) 11.1%Co-4.6%Ni-1.5%Cr-0.2%V.

4.1.2. Scanning Electron Microscope (SEM)

The surfaces of the five samples were characterized before corrosion to obtain the micrographs and the elemental compositions using the SEM/EDS, the micrographs are given in figure 4.2.

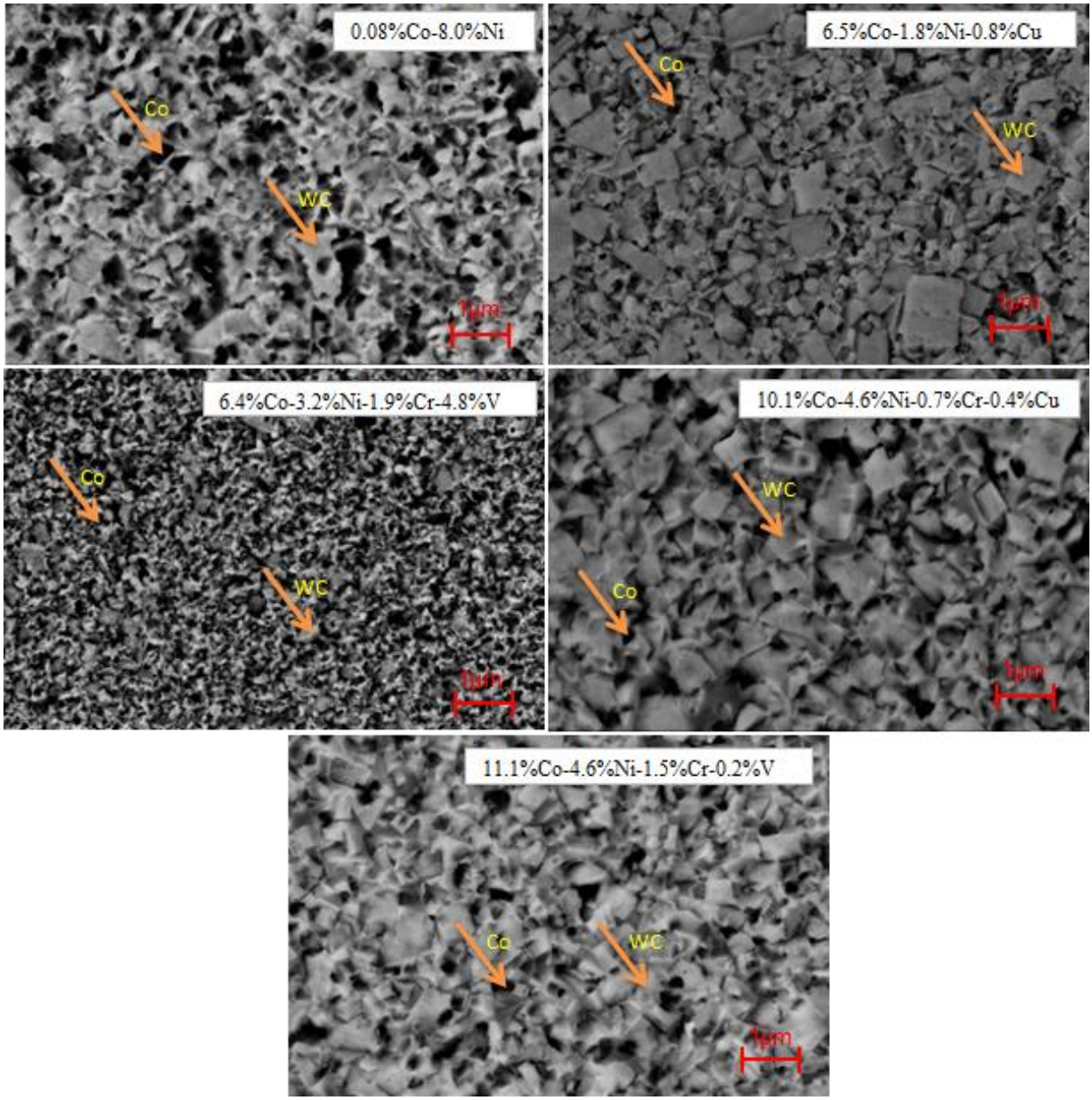


Figure 4.2: SEM micrographs of the WC alloys: a) 0.08%Co-8.0%Ni, b) 6.5%Co-1.8%Ni-0.8%Cu, c) 6.4%Co-3.2%Ni-1.9%Cr-4.8%V, d) 10.1%Co-4.6%Ni-0.7%Cr-0.4%Cu and e) 11.1%Co-4.6%Ni-1.5%Cr-0.2%V.

The figure above illustrates the microstructures of the polished surfaces of the WC alloy before corrosion. There are two phases that can be observed in the micrographs which include the lighter and darker phase. The lighter phase corresponds to tungsten carbide grains and the darker phase corresponds to cobalt binder. It can be observed that 6.4%Co-3.2%Ni-1.9%Cr-4.8%V had shown a very fine-grained microstructure compared to the other alloys and it had a very high hardness value. A coarse-grained microstructure was observed in carbides 10.1%Co-4.6%Ni-0.7%Cr-0.4%Cu and 0.08%Co-8.0%Ni they also have similar

hardness values. The EDX analysis is found in the appendix, in which the W peaks were observed to be the highest for each hardmetal.

4.2. Wear tests

This section describes the results of the five alloys in which they were subjected to sliding wear in rotary motion under dry conditions. The wear responses of the hardmetals are described with respect to the contact pressure, sliding speed and the distance. The wear damages are described using the wear track that was observed as a result of this wear procedure which was then used to determine the wear rates of the hardmetals. The alumina balls used for each alloy did not show any sign of wear scars.

4.2.1. Wear rates under dry conditions

Table 4.1 shows the data obtained for the wear tests conducted under dry conditions for WC-Co alloys after sliding wear in rotary motion at a sliding speed of 0.1 m/s and distance of 450 m. The radius of the wear track was found to be almost same for all the hardmetals. Equation 2, 3 and 4 was used to obtain the disk volume loss, wear rate, and contact pressure, respectively.

Table 4.1: Raw wear rate data

Sample	0.08%Co-8.0%Ni	6.5%Co-1.8%Ni-0.8%Cu	6.4%Co-3.2%Ni-1.9%Cr-4.8%V	10.1%Co-4.6%Ni-0.7%Cr-0.4%Cu	11.1%Co-4.6%Ni-1.5%Cr-0.2%V
Ball radius (mm)	6	6	6	6	6
Wear track radius (mm)	3.57	3.58	3.50	3.55	3.60
Wear track width (mm)	0.202	0.212	0.110	0.209	0.245
Disk volume loss (mm)	0.092	0.107	0.015	0.101	0.165
Sliding distance (m)	450	450	450	450	450
Load (N)	5	5	5	5	5
Wear rate (mm^3/Nm)	0.00102	0.00119	0.000162	0.00112	0.00183
Contact Pressure (N/mm^2)	4.531	4.773	2.419	4.654	5.532

Figure 4.3. illustrates the wear rates of the hardmetals. It can be observed that the alloy containing 6.4%Co-3.2%Ni-1.9%Cr-4.8%V had a lower wear rate compared to the other hardmetals. The alloy containing 11.1%Co-4.6%Ni-1.5%Cr-0.2%V had shown a higher wear rate. The wear rate between 0.08%Co-8.0%Ni and 10.1%Co-4.6%Ni-0.7%Cr-0.4%Cu seem to be similar to one another. The wear rate has been observed to increase with an increasing cobalt content.

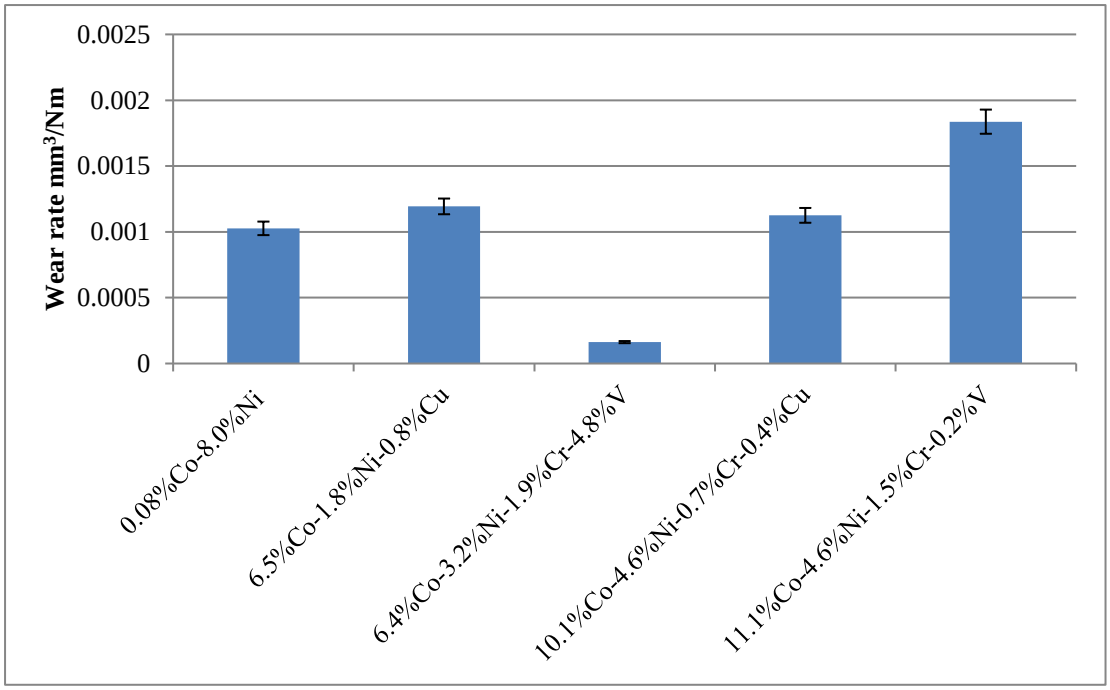


Figure 4.3: Wear rates of the WC-Co alloys under dry conditions

When two surfaces, the ball and the hardmetal come into contact stresses are involved as a result of normal and tangential forces that arise from sliding wear. The heat is generated at the sliding-contact is due to friction. The stress and heat generated from friction lead to wear at sliding-contact interface. Therefore, the wear rates and wear mechanisms are determined from these instances. Figure 4.5 presents a relationship between the coefficient of friction (CoF) and distance. It can be observed that the CoF increased as the distance was increasing. The alloy containing 6.4%Co-3.2%Ni-1.9%Cr-4.8%V had shown a lower CoF values with increasing distance as compared to the other alloys while it had shown a lower wear rate. The alloy containing 0.08%Co-8.0%Ni had shown a higher CoF values as compared to the others. Therefore, CoF and wear rate increases with increasing sliding distance. The presence of the wear debris at the surface of the hardmetal can cause the CoF to increase. It can have a positive or negative influence on the CoF and it can act as a "lubricant" at the interface.

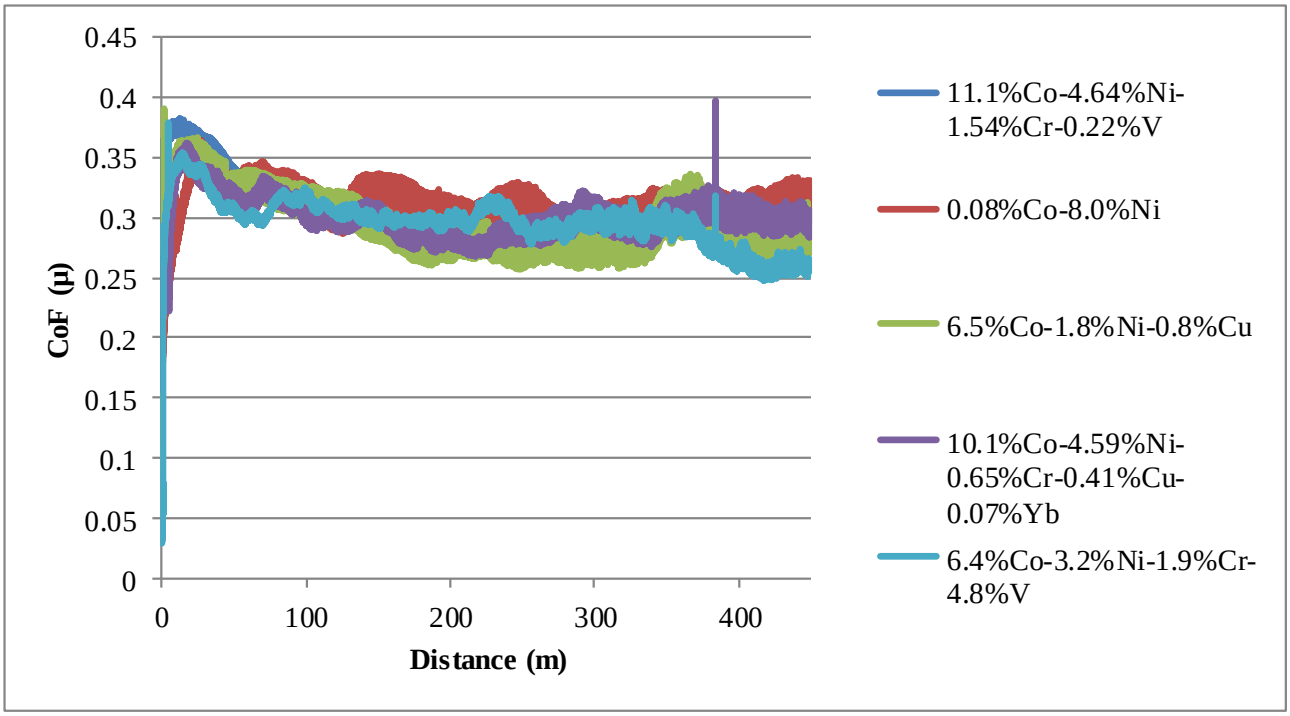


Figure 4.4: Relationship between the coefficient of friction and sliding distance.

The contact pressure was calculated, illustrated in figure 4.5. A correlation can be observed between the wear rate and the contact pressure. The contact pressure increased with increasing wear rate.

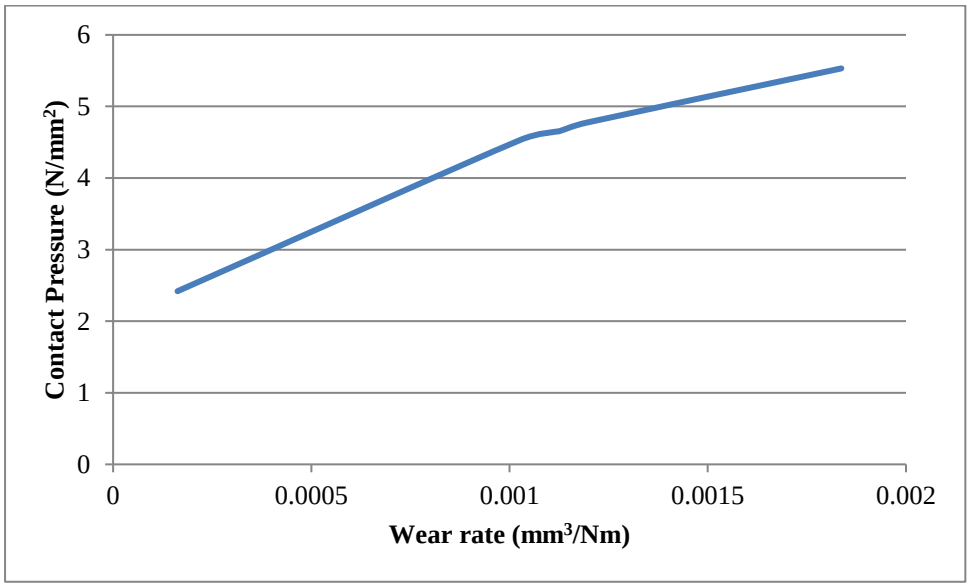


Figure 4.5: Contact pressure vs wear

4.2.2. Microstructural analysis

The worn out hardmetal surfaces were examined using the SEM in order to obtain microstructural information. It is possible from the micrographs to gain an impression of the effect the alumina ball had on different hardmetals. From this study, pits are observed at the surface of the hardmetals which can be due to the wear processes.

The wear profiles of the hardmetals are illustrated in figure 4.6. The micrographs show that sliding was the main wear process that the hardmetals were subjected to since the surfaces were damaged. The damage involved a progressive loss of material due to the sliding-contact between surfaces. It can be observed that 0.08%Co-8.0%Ni had shown transgranular cracks and pits which also shown the signs of plastic deformation. The hardmetal containing 6.5%Co-1.8%Ni-0.8%Cu had shown abrasive scratches and pits. The abrasive scratches indicate the chip flow at the surface that became hard due to oxidation.

Wear debris was observed in the micrograph containing 11.1%Co-4.6%Ni-1.5%Cr-0.2%V which consists of the fragments of the material. Pits were observed at the surface of the same hardmetal, it can be noted that this hardmetal had the highest wear rate compared to other hardmetals. The hardmetal containing 10.1%Co-4.59%Ni-0.65%Cr-0.41%Cu had shown the sliding direction of the alumina ball and pits.

The hardmetal containing 6.4%Co-3.2%Ni-1.9%Cr-4.8%V had shown pits. Features marked A illustrates fatigue cracks which is indicative of the maximum shear stresses of the samples are at the surface during the sliding conditions and cracks propagates along the interface.

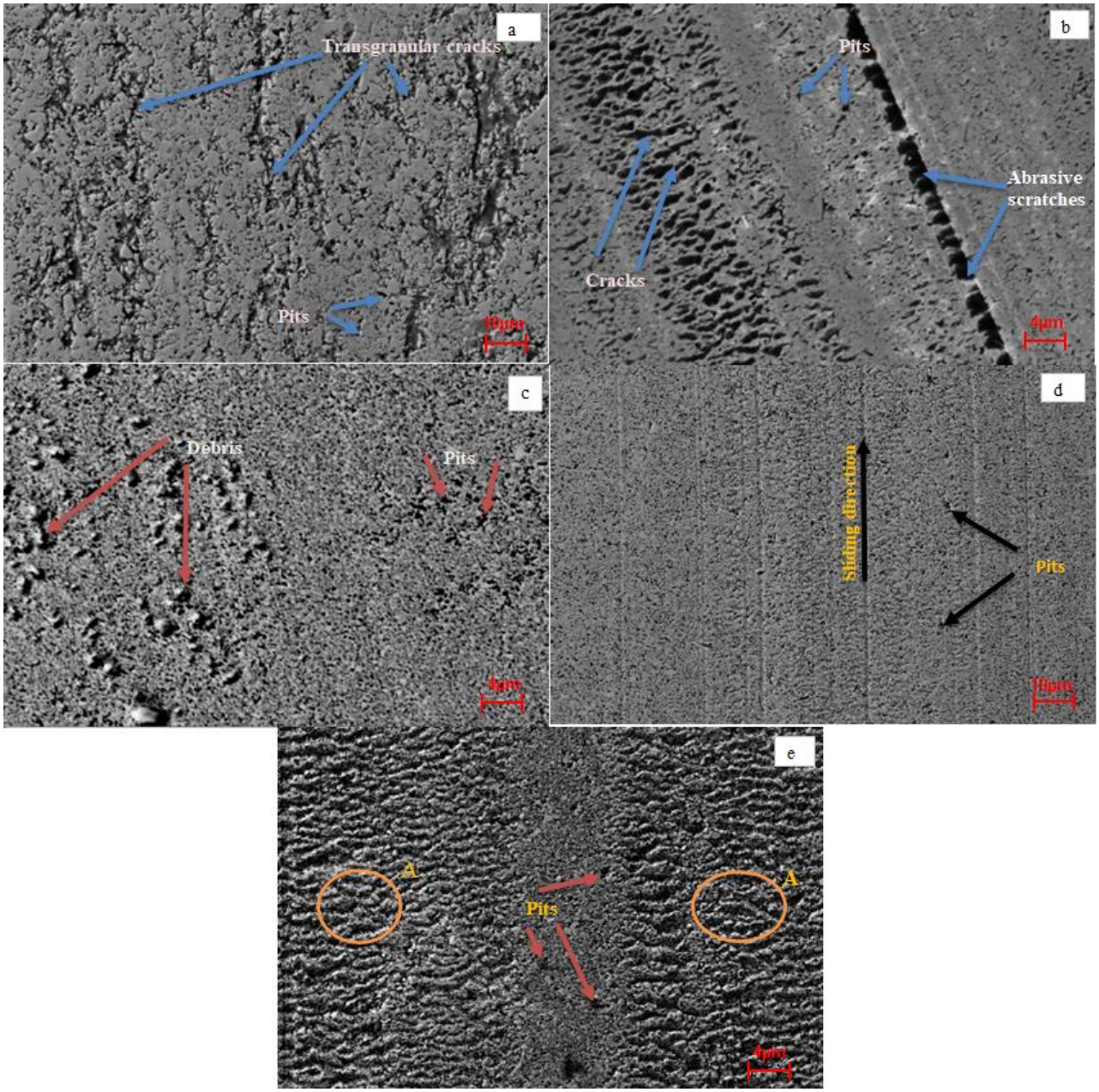


Figure 4.6: Wear micrographs: a) 0.08%Co-8.0%Ni, b) 6.5%Co-1.8%Ni-0.8%Cu, c) 11.1%Co-4.6%Ni-1.5%Cr-0.2%V, d) 10.1%Co-4.6%Ni-0.7%Cr-0.4%Cu and e) 6.4%Co-3.2%Ni-1.9%Cr-4.8%V.

4.3. Corrosion tests

This section describes the results of the electrochemical behaviour of the hardmetals in which the grades 0.08%Co-8.0%Ni; 6.5%Co-1.8%Ni-0.8%Cu; 11.1%Co-4.6%Ni-1.5%Cr-0.2%V; 10.1%Co-4.6%Ni-0.7%Cr-0.4%Cu and 6.4%Co-3.2%Ni-1.9%Cr-4.8%V were subjected to corrosion tests under various conditions. The corrosion response of the hardmetals are described with respect to the variation of acetic and sulphuric acid pH conditions and the influence of 3.5% NaCl solution addition to the electrolyte. The 3.5% NaCl solution was used because it simulates the corrosive environment, and it is the driving force for corrosion. The

cyclic potentiodynamic results are illustrated with potential plotted along the y-axis and the current density along the x-axis. In tables 4.3, 4.4 and 4.5; important corrosion parameters are listed for testing conducted in acetic and sulphuric acid electrolytes. The current densities found in this testing were low. Table 4.6 illustrates the electrolyte analysis from the AAS to identify the amounts of elements present in each solution after the corrosion tests.

4.3.1. Open Circuit Potential Values

4.3.1.1. Acetic and Sulphuric Acid pH 2

The differences in the OCP values of the WC alloys measured for one hour in acetic and sulphuric acid electrolytes are shown in figure 4.8. It can be observed that the hardmetals behaved differently when they were exposed to acetic and sulphuric acid electrolytes. For the hardmetal containing 0.08%Co-8.0%Ni in the acetic acid electrolyte, had shown a positive OCP value and is most noble at 0.242V. This could be that there was pseudopassivity formed at the surface of the hardmetal. From literature it is caused by the WC-Co alloy with high W content which decreases the dissolution rate by reducing further the dissolution of the binder in acidic environments (Sutthiruangwong & Mori, 2003) & (Kosters, et al, 2005). When the aforementioned hardmetal was exposed to sulphuric acid electrolyte, the behaviour was similar to that of the hardmetal 11.1%Co-4.6%Ni-1.5%Cr-0.2%V. It can be noted that the OCP values increased with increasing nickel content for two hardmetals in question.

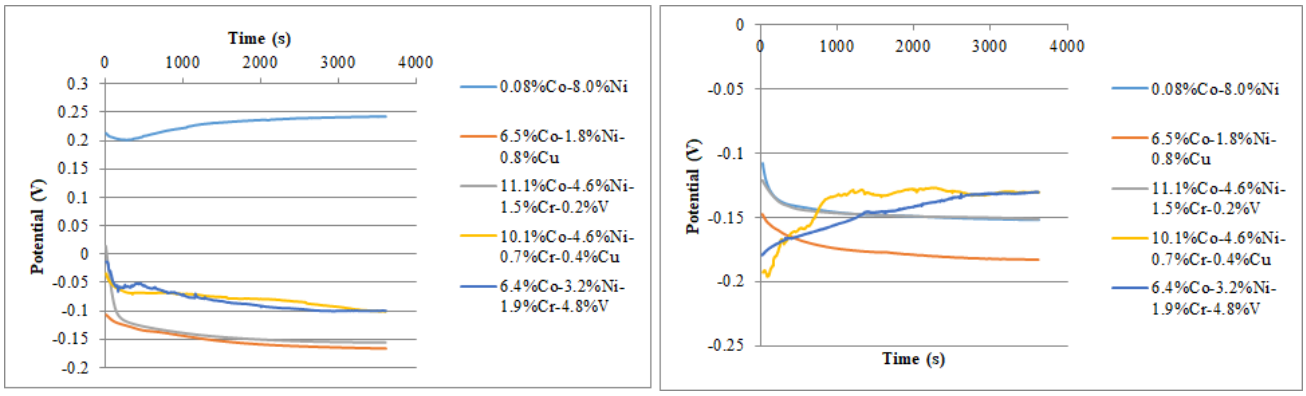


Figure 4.7: OCP of acetic and sulphuric acid electrolytes at pH 2.

The hardmetal containing 10.1%Co-4.6%Ni-0.7%Cr-0.2%V had shown signs of instability. It had shown more fluctuations in the OCP values when exposed to sulphuric acid electrolyte as compared to when it was exposed to acetic acid electrolyte. The hardmetals 6.5%Co-1.8%Ni-

0.8%Cu and 11.1%Co-4.6%Ni-1.5%Cr-0.2%V behaved in a similar way when exposed to acetic acid electrolyte.

4.3.1.2. Acetic and Sulphuric Acid pH 3

Variations in the OCP values of the hardmetals measured for one hour in acetic and sulphuric acid electrolytes are shown in figure 4.9. It can be observed that the hardmetal containing 6.5%Co-1.8%Ni-0.8%Cu had shown unstable OCP values in both acetic and sulphuric acid electrolytes. Initially, the values increased with time and suddenly the hardmetal reduced to more negative potentials. The hardmetal containing 0.08%Co-8.0%Ni had shown an increase to more positive OCP values when it was it exposed to acetic acid electrolyte, however, as the time progresses there was a slight drop in potential. When the hardmetal was exposed to sulphuric acid electrolyte, it was observed that it had shown an increase in potential with time by stabilizing with a negative potential. It can be observed that a hardmetal containing 10.1%Co-4.6%Ni-0.7%Cr-0.4%Cu had shown a decrease in potential with increasing time when it was exposed to acetic acid electrolyte. The potential had a slight increase which was followed by a decrease and as the time progresses it stabilized at high potential values. When it was exposed to sulphuric acid electrolyte, a decrease in potential was observed; however, an increase in potential values as time progresses was observed and the hardmetal started stabilizing at a constant OCP value of -0.1V.

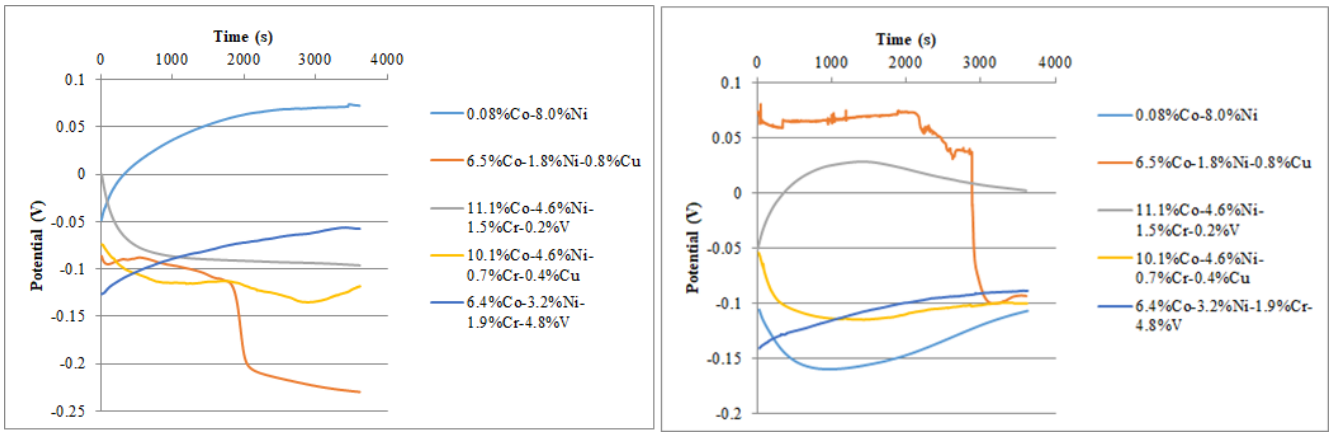


Figure 4.8: OCP of acetic and sulphuric acid electrolytes at pH 3.

4.3.1.3. Acetic and Sulphuric Acid pH 5

Variations in the OCP values of the hardmetals measured for one hour in acetic and sulphuric acid electrolytes are shown in figure 4.10. It can be observed that the hardmetal containing 11.1%Co-4.6%Ni-1.5%Cr-0.2%V had shown a similar behaviour in OCP values when

exposed to both acetic and sulphuric acid electrolytes. The OCP values decreased as time progresses. The same behaviour was observed in a hardmetal containing 6.4%Co-3.2%Ni-1.9%Cr-4.8%V it started with a decrease in the OCP values and as the time progresses it had shown an increase in the OCP values. The other hardmetals had also shown a similar behaviour when exposed to acid electrolytes except for 0.08%Co-8.0%Ni. This hardmetal had shown an increase in the OCP values with time to more noble values when exposed to acetic acid electrolyte, however, the behaviour was different in sulphuric acid electrolyte as the OCP values started by decreasing and as the time progresses an increase was observed where it stabilized at -0.1V. The hardmetals containing 6.5%Co-1.8%Cr-0.8%Cu and 10.1%Co-4.6%Ni-0.7%Cr-0.4%Cu had shown unstable potentials with random flactuations, however, they became stable as the time progressed.

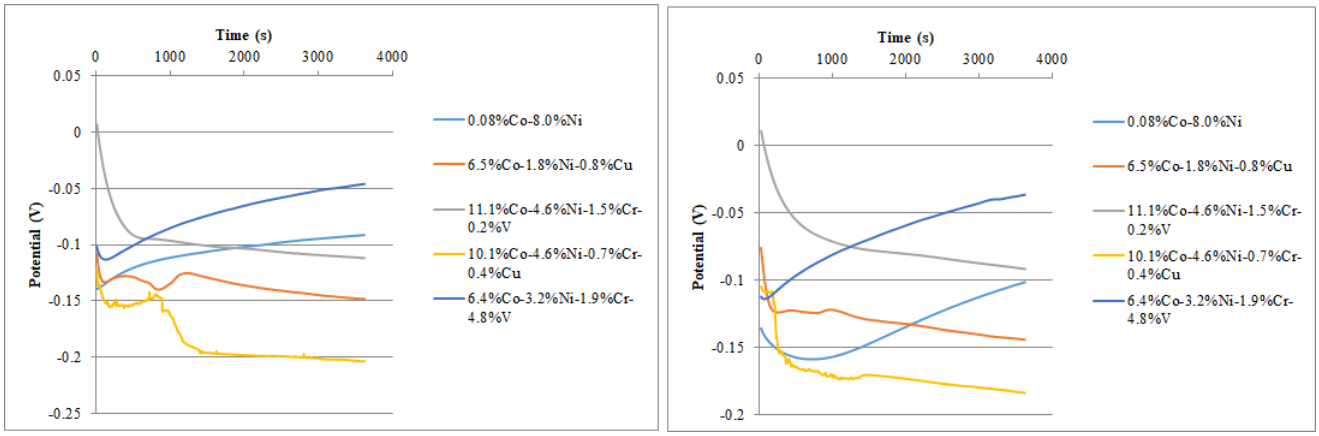


Figure 4.9: OCP of acetic and sulphuric acid electrolytes at pH 5.

4.3.2. Cyclic Polarization Curve

This section presents all the cyclic polarization curves of the five hardmetals exposed to acetic and sulphuric acid electrolytes. The cyclic potentiodyamic polarization test mainly evaluates the material susceptibility to localized corrosion such as pitting and crevice corrosion (Esmailzadeha, et al., 2018). The cyclic polarization curves have the quantities which provide information on pit formation which include the hysteresis and repassivation potential. The hysteresis consists of negative and positive loops. The negative hysteresis loop forms when the current density of the reverse scan is less than that of the forward scan (Tait, 2018). The positive hysteresis loop forms when the current density of the reverse scan is greater than that of the forward scan. These loops determine whether they will be a formation of pits and whether or not the surface of the hardmetal will repassivate to prevent the

formation of pits. Repassivation help by replacing the aggressive ions in the pit with passive layer at more negative potentials.

4.3.2.1. Acetic and Sulphuric Acid pH 2

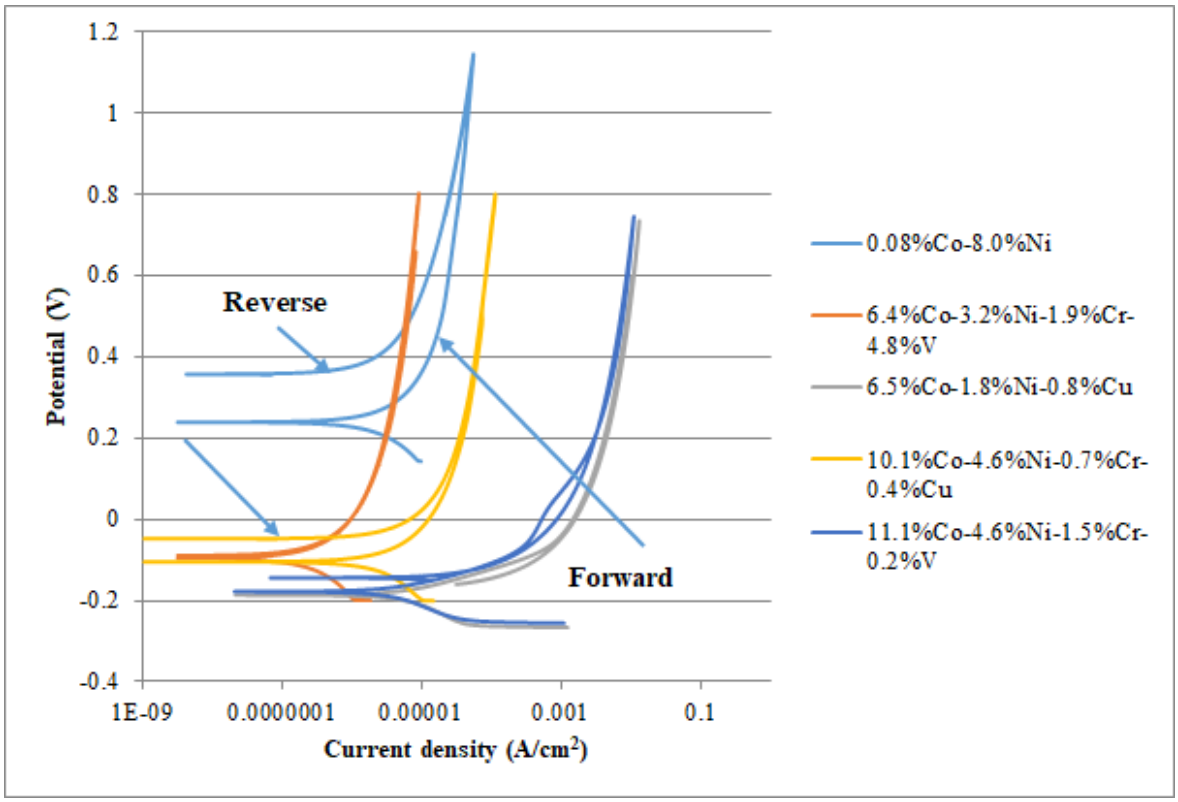


Figure 4.10: Cyclic polarization curve of acetic acid electrolyte at pH 2.

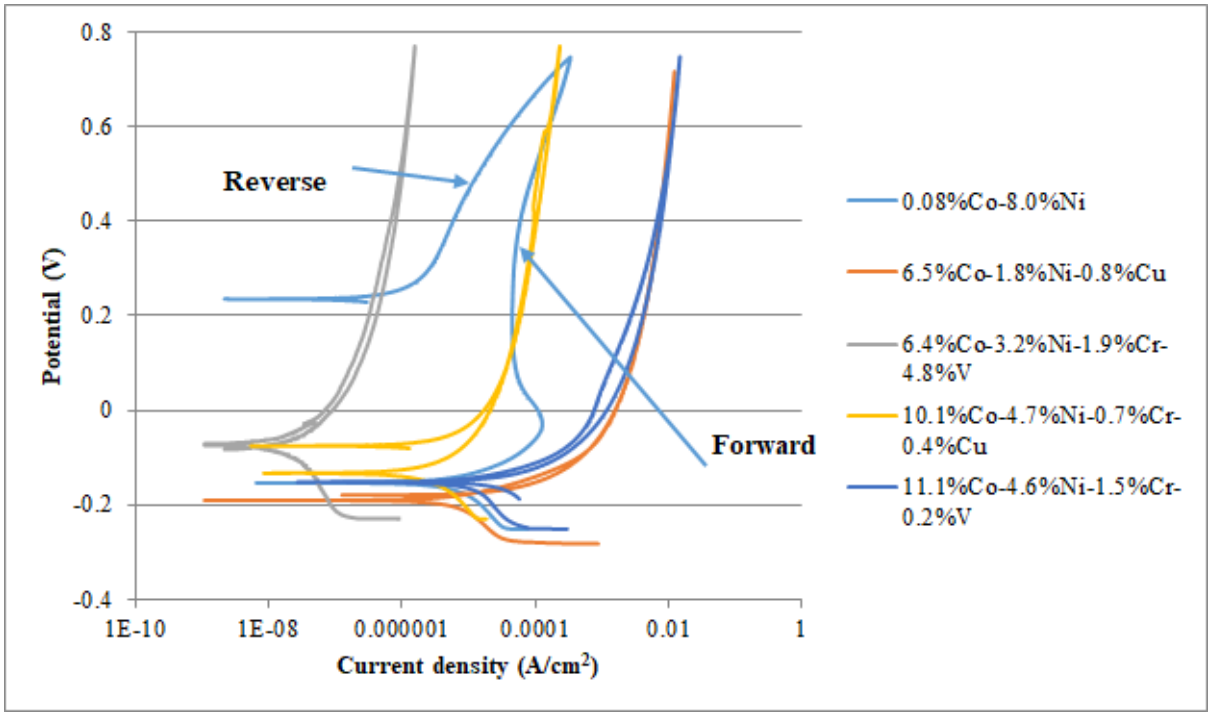


Figure 4.11: Polarization curve of sulphuric acid electrolyte at pH 2.

Figure 4.11 and 4.12 shows the cyclic polarization curves at pH 2 with a forward and reverse potential scan. This reverse potential scan provides information about the pitting corrosion. It can be observed in Figure 4.12 that the hardmetal containing 0.08%Co-8.0%Ni had formed a weak passive region and it also shows a large and negative hysteresis loop. The negative hysteresis is said to occur when the current density of the reverse scan is less than that of the forward scan (Tait, 2018). The hardmetal had shown signs of repassivation during the reverse scan and the pit formation was less likely to occur. In figure 4.11, it did not show any formation of pit corrosion, however, it had high potential values as compared to the others. Some hardmetals did not show any passive region or any formation of pitting corrosion on both acid electrolytes. The hardmetal containing 6.4%Co-3.2%Ni-1.9%Cr-4.8%V had a low current density on both acid electrolytes. In figure 4.11 it had shown that it had experienced general corrosion as the forward scan coincides with the reverse scan.

The polarization characteristics of all the hardmetal grades in all electrolytes are not similar. It can be observed in figure 4.11 that the hardmetals containing 6.5%Co-1.8%Ni-0.8%Cu and 11.1%Co-4.6%Ni-1.5%Cr-0.2%V had similar cathodic and anodic slopes, however, the latter had a slightly higher reverse potential (E_{rev}) of 0.75V. In figure 4.12, 11.1%Co-4.6%Ni-1.5%Cr-0.2%V had a similar cathodic slope as that of the 0.08%Co-8.0%Ni, however, the

anodic slope of 11.1%Co-4.6%Ni-1.5%Cr-0.2%V is similar to that of 6.5%Co-1.8%Ni-0.8%Cu with an E_{rev} of 0.76V which is higher than that of the latter.

The corrosion rates are shown in figure 4.13 for five hardmetals exposed to acetic and sulphuric acid electrolytes at pH 2. Table 4.3 shows the raw data of acetic and sulphuric acid electrolytes corrosion rates. The corrosion rates for both acetic and sulphuric acid electrolytes did not follow any trend in terms of an increase in binder or grain size. It can be observed that the current densities kept on increasing as the environment became more aggressive. This could be due to the presence of Cl^-. The alloy containing 6.4%Co-3.2%Ni-1.9%Cr-4.8%V had a low corrosion rate on both acid electrolytes as compared to the other hardmetals. This could be due to the presence of chromium and nickel contents in the binder or it could be the low grain size.

Table 4.2: Raw data for acetic and sulphuric acid at pH 2

Acetic Acid			
Sample	i_{corr} (A/cm^2) $\times 10^{-6}$	E_{corr} (V)	Corrosion rate (µm/yr)
COR	1.5	0.23	4.69
M	5.0	-0.191	16.1
T3	3.9	-0.185	11.25
TC	1.1	-0.12	3.15
UM	0.07	-0.1	0.20
Sulphuric Acid			
COR	7.5	-0.175	23.5
M	3.1	-0.191	9.96
T3	7.9	-0.162	22.8
TC	1.8	-0.135	5.15
UM	0.014	-0.081	0.04

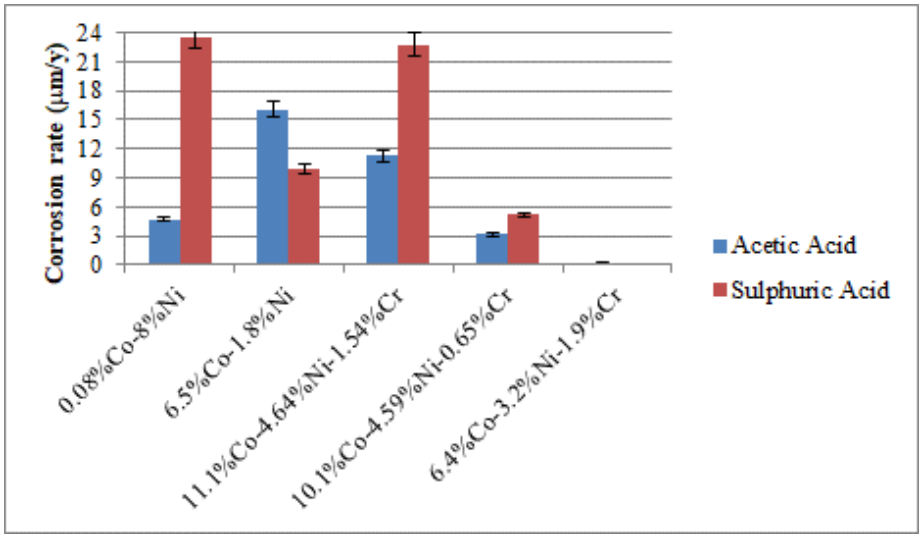


Figure 4.12: Corrosion rates against cobalt content at pH 2.

4.3.2.2. Acetic and Sulphuric Acid pH 3

The hardmetal containing 11.1%Co-4.6%Ni-1.5%Cr-0.2%V had shown a decrease in potential values until it stabilized at -0.09V when it was exposed to acetic acid electrolyte. When it was exposed to sulphuric acid electrolyte, the potential values increased with time to more positive potential values. The hardmetal had shown a positive hysterical loop The hardmetal containing 6.4%Co-3.2%Ni-1.9%Cr-4.8%V had shown an increase in potential with time when it was exposed to both acetic and sulphuric acid electrolytes, however, a

slight decrease in potential values was observed in acetic acid electrolytes. The behaviour of the hardmetals at pH 2 is different from that of pH 3.

Figure 4.14 presents the polarization curves for the WC-Co hardmetal in acetic acid electrolyte at pH 3. A shift in corrosion potential values towards more noble values with increasing nickel and chromium into the binder was observed in the hardmetals. The hardmetal containing 0.08%Co-8.0%Ni had shown a more positive corrosion potential value as compared to the other WC-Co hardmetals. It had also shown a low current density of $0.5\times 10^{-6}\,{}^{A}/_{cm^2}$. The hardmetal containing 6.4%Co-3.2%Ni-1.9%Cr-4.8%V had shown an increasing anodic slope that increased with potential and current density, it can be observed that there was a slight decrease in the current density which indicated a pseudopassive current. However, as the potential increases the anodic slope increases with increasing current density. It can be observed that all the curves did not show any signs of repassivation during the reverse scan. The hardmetals containing 10.1%Co-4.6%Ni-0.7%Cr-0.4%Cu had shown unstable potential values in the reverse scan, the values were fluctuating with decreasing potential and current density values.

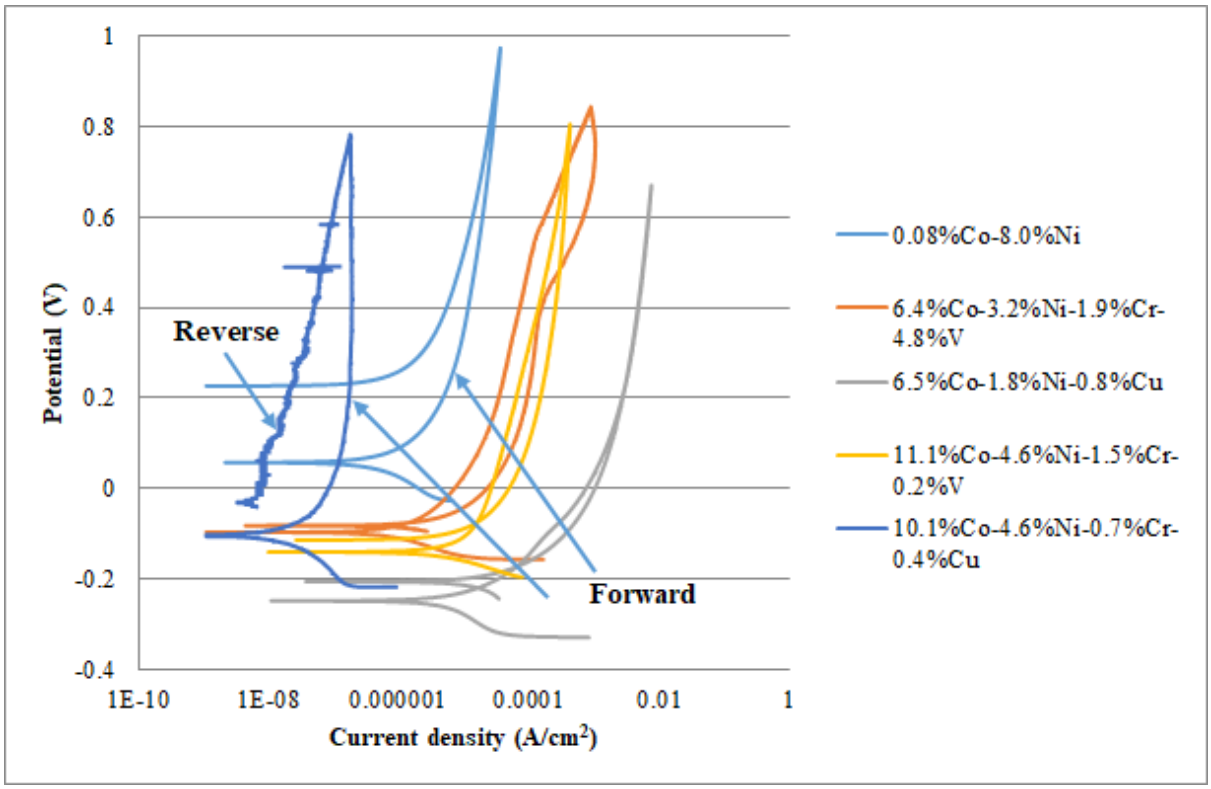


Figure 4.13: Polarization curves of the Acetic acid at pH 3.

Figure 4.15 presents the polarization curves for the WC-Co alloy in sulphuric acid electrolyte at pH 3. It can be observed that the hardmetals had shown a similar behaviour except for 11.1%Co-4.6%Ni-1.5%Cr-0.2%V that had shown to have a more noble corrosion potential as compared to the others. This behaviour can be observed as the pH values start to increase. The hardmetals had shown a decrease in current densities as the chromium content into the binder decreases. The anodic slopes had shown an increase with increasing potential and current density. It can be observed that the hardmetal containing 0.08%Co-8.0%Ni had shown an increase in current density as the potential increases, however, the anodic slope had shown a steep increase with decreasing current density. At 0.44V, an increase in current density was observed. The hardmetals containing 6.4%Co-3.2%Ni-1.9%Cr-4.8%V had shown a sharp increase anodic slope with increasing current density and potential. The reverse scan of this hardmetal had shown signs of repassivation as the scan decreased with decreasing current density and potential. Increasing current density was observed as the potential values continue to decrease. The hardmetal containing 10.1%Co-4.6%Ni-0.7%Cr-0.4%Cu had shown an increase in the current density which was followed by a constant anodic slope with a decrease in current density.

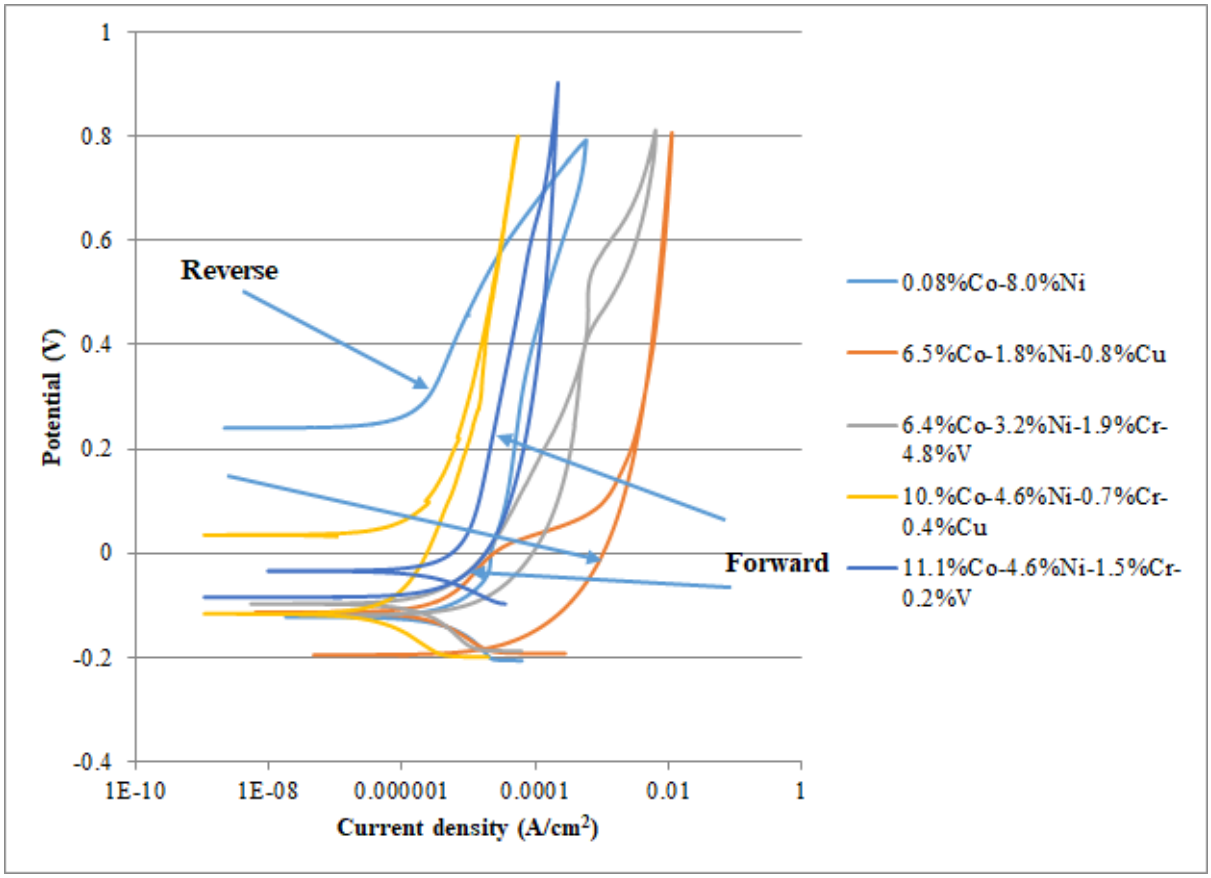


Figure 4.14: Polarization curves of Sulphuric acid at pH 3.

Figure 4.16 presents the corrosion rates of acetic and sulphuric acid electrolyte that were extracted from the Table 4.4. It can be observed that the alloy containing 10.1%Co-4.6%Ni-0.7%Cr-0.4%Cu had a low corrosion rate on both acetic and sulphuric acid electrolyte as compared to the other hardmetals. An increase in corrosion rates did not follow a particular trend in this case. It can be observed that 10.1%Co-4.6%Ni-0.7%Cr-0.4%Cu and 0.08%Co-8.0%Ni had low corrosion rates with a high grain size when exposed to acetic acid salt solution.

Table 4.3: Raw data of acetic and sulphuric acid corrosion rates at pH 3

Acetic Acid			
Sample	i_{corr} (A/cm^2) $\times 10^{-6}$	E_{corr} (V)	Corrosion rate (µm/yr)
COR	0.5	0.05	1.56
M	8.8	-0.28	28.3
T3	4.8	-0.13	13.9
TC	0.019	-0.1	0.05
UM	0.8	-0.093	2.30
Sulphuric Acid			
COR	3.2	-0.132	10.0
M	2.2	-0.121	7.07
T3	1.85	-0.04	5.34
TC	0.175	-0.117	0.5
UM	1.6	-0.118	4.60

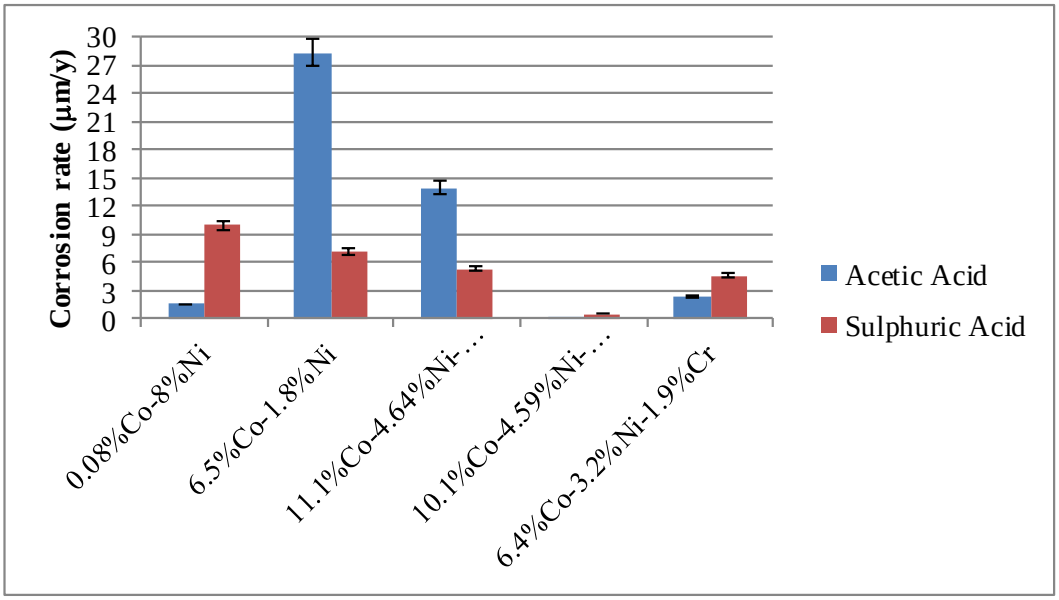


Figure 4.15: Corrosion rates of acetic and sulphuric acid at pH 3.

4.3.2.3. Acetic and Sulphuric Acid pH 5

The polarization curves of the WC-Co hardmetals in acetic acid electrolyte are presented in Figure 4.17. It can be observed that the potential values were increasing with increasing chromium. The hardmetal containing 6.4%Co-3.2%Ni-1.9%Cr-4.8%V had shown a low current density as compared to the other alloys. A trend was observed in the current density with had shown an increase with increasing cobalt and nickel. The hardmetals containing 0.08%Co-8.0%Ni and 6.4%Co-3.2%Ni-1.9%Cr-4.8%V had shown a similar increase in the

anodic slope with increasing current density and potential values, however, the current density of the latter continued to increase with increasing potential.

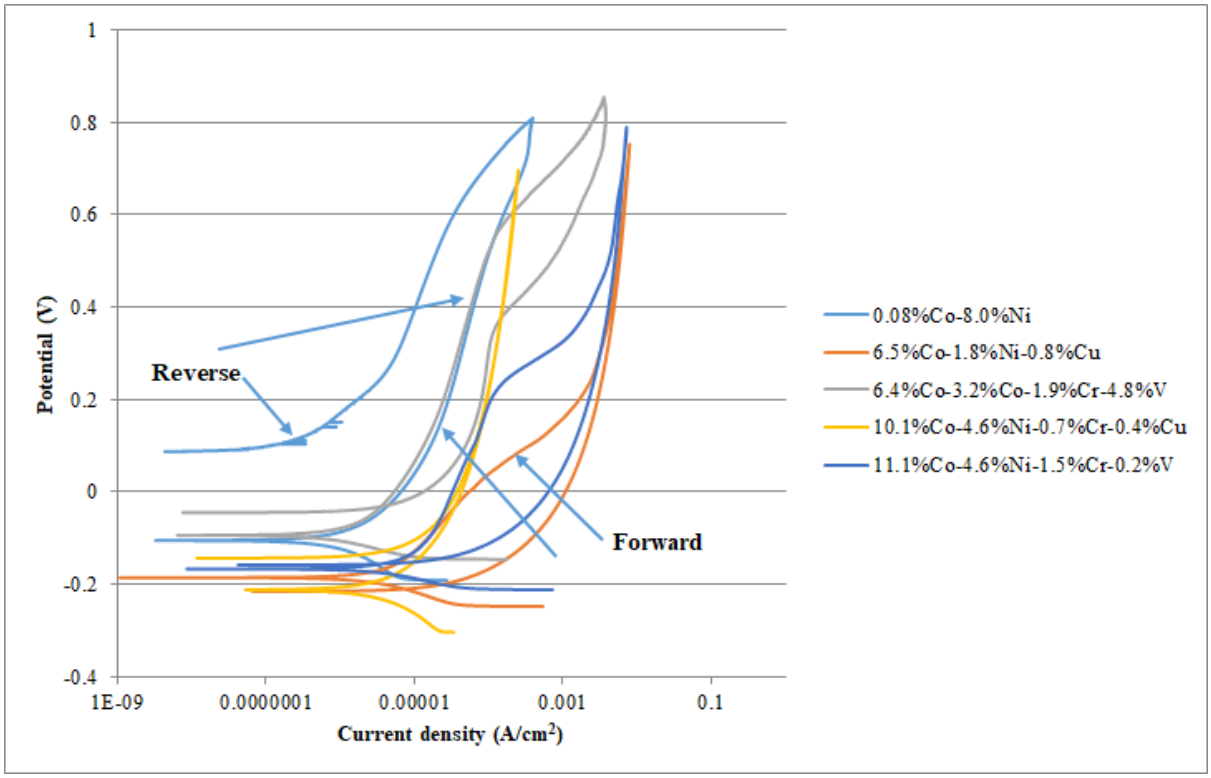


Figure 4.16: Polarization curves of Acetic acid at pH 5.

The polarization curves of WC-Co hardmetals in sulphuric acid salt solution were presented in Figure 4.18. It can be observed that the hardmetals had a similar behaviour which was the same as the hardmetals exposed to acetic acid eletrolyte. However, the current density increased with increasing cobalt and a decrease in chromium.

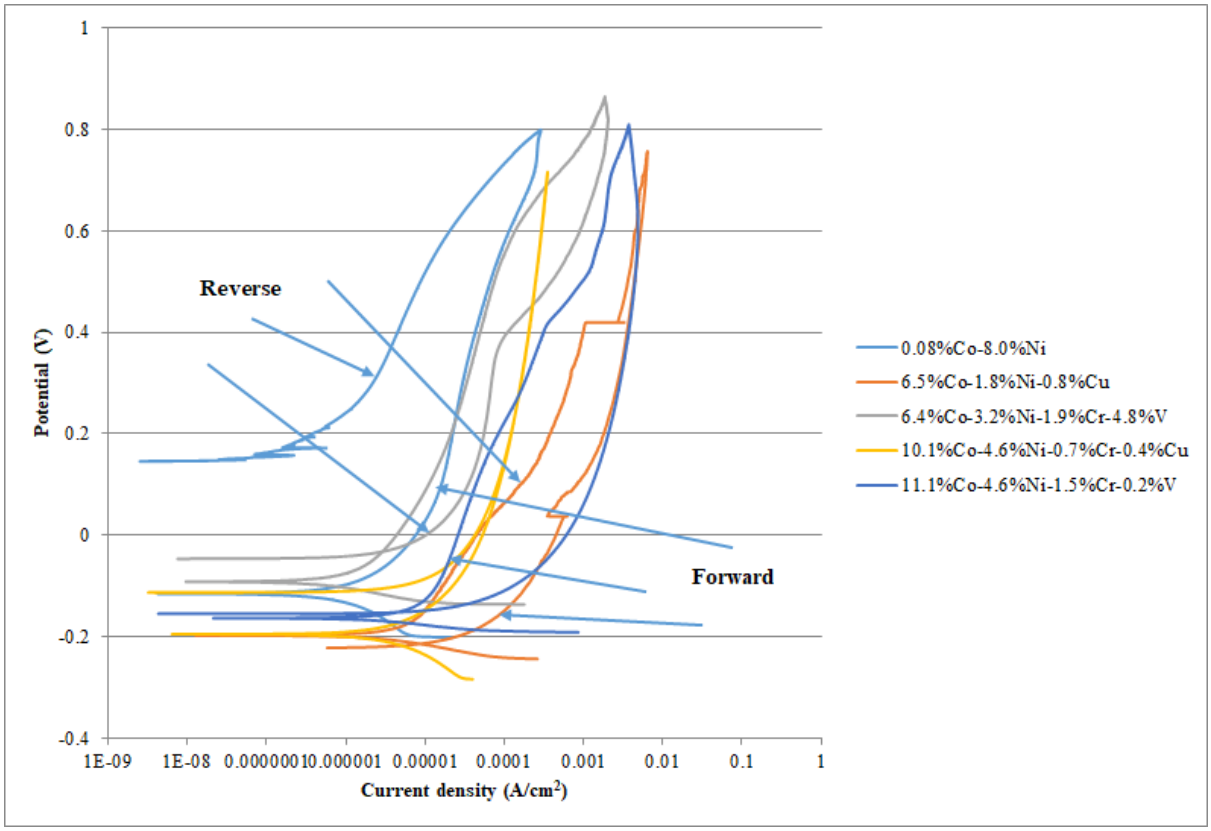


Figure 4.17: Polarization curves of Sulphuric acid at pH 5.

Figure 4.19 presents the corrosion rates of acetic and sulphuric acid at pH 5. Table 4.5 shows the raw data of acetic and sulphuric acid corrosion rates. It can be observed that 6.4%Co-3.2%Ni-1.9%Cr-4.8%V had the same corrosion rate in both acetic and sulphuric acid. It had a low corrosion rate when it was exposed to acetic acid salt solution followed by 0.08%Co-8.0%Ni. All the corrosion rates on both corrosion solutions increased with increasing cobalt and nickel. A solution analysis was conducted and the hardmetal containing 10.1%Co-4.6%Ni-0.7%Cr-0.4%Cu did show any primary binder concentration in the solution when it was exposed to acetic acid salt solution. The hardmetal containing 6.4%Co-3.2%Ni-1.9%Cr-4.8%V had large amounts of cobalt concentration in the acetic acid corrosion solution.

Table 4.4: Raw data for acetic and sulphuric acid at pH 5

Acetic Acid			
Sample	i_{corr} (A/cm^2) $\times 10^{-6}$	E_{corr} (V)	Corrosion rate (μm/yr)
COR	0.82	-0.11	2.56
M	3.0	-0.192	9.64
T3	3.3	-0.17	9.52
TC	1.8	-0.22	5.15
UM	0.69	-0.1	1.98
Sulphuric Acid			
COR	0.5	-0.119	1.56
M	3.3	-0.205	10.6
T3	3.0	-0.12	8.66
TC	2.1	-0.201	6.01
UM	0.69	-0.09	1.98

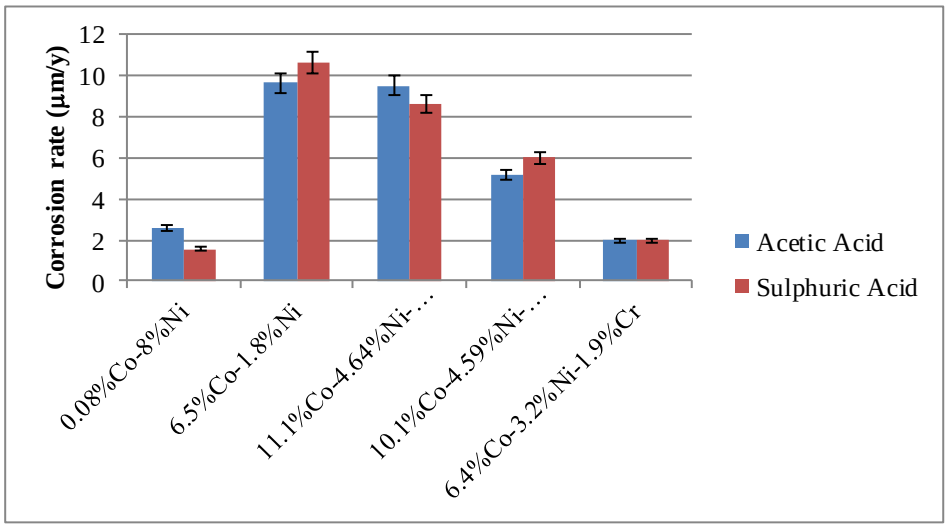


Figure 4.18: Corrosion rates of acetic and sulphuric acid at pH 5.

A solution analysis was conducted using the AAS to determine the concentrations of elements passed into the solution during corrosion at pH 2 in Table 11. The primary binder content, Co, was present in high concentrations into acetic and sulphuric acid salt solution. However, small amounts of Ni were detected in the acetic acid salt solution and there was an increase in the Ni concentration as the conditions became aggressive in the presence of sulphuric acid salt solution.

A solution analysis was conducted to identify the concentration of the elements present in the corrosion solution at pH 3, the concentrations are found in Table 4.6. It can be observed that the primary binder was not dictated in the acetic acid corrosion solution of the hardmetal 10.1%Co-4.6%Ni-0.7%Cr-0.4%Cu, however, it was dictated in the sulphuric acid corrosion solution in high concentrations. It had shown small amounts of nickel concentrations in both acetic and sulphuric acid corrosion while chromium had shown higher concentrations in both corrosion solutions. This could mean that the presence of nickel into the binder had lowered the corrosion rate.

Table 4.5: AAS analysis for corrosion tests solutions.

Acetic Acid			
pH 2			
Sample	Cr (mg/l)	Ni(mg/l)	Co(mg/l)
COR	2.540	0.647	3.394
M	4.862	0.865	4.403
UM	1.235	0.591	2.719
T3	2.731	0.588	4.021
TC	1.409	0.585	3.064
pH 3			
COR	0.176	0.266	0.908
M	0.226	0.233	0.534
UM	0.390	0.175	0.147
T3	0.038	0.225	1.070
TC	1.037	0.087	-0.041
pH 5			
COR	0.131	0.299	1.109
M	0.108	0.286	0.618
UM	0.223	0.284	1.209
T3	0.042	0.228	0.978
TC	0.791	0.102	-0.073
Sulphuric Acid			
pH 2			
COR	1.575	0.629	3.301
M	5.531	0.958	2.855
UM	1.432	0.594	3.721
T3	4.005	0.701	5.008
TC	1.678	0.604	3.843
pH 3			
COR	0.028	0.210	0.881
M	0.290	0.199	0.277
UM	0.031	0.267	1.081
T3	2.264	1.048	4.515
TC	1.068	0.175	2.233
pH 5			
COR	0.202	0.257	0.715
M	0.109	0.293	1.193
UM	0.056	0.226	0.846
T3	0.141	0.260	0.906
TC	0.630	0.163	0.078

4.4. Tribocorrosion tests

This section describes the results of the tribo-electrochemical behaviour of the hardmetals in which the grades 0.08%Co-8.0%Ni; 6.5%Co-1.8%Ni-0.8%Cu; 11.1%Co-4.6%Ni-1.5%Cr-

0.2%V; 10.1%Co-4.6%Ni-0.7%Cr-0.4%Cu and 6.4%Co-3.2%Ni-1.9%Cr-4.8%V were subjected to tribocorrosion tests under various conditions. The tribocorrosion response of the hardmetals is described with respect to the variation of acetic and sulphuric acid pH conditions and the influence of 3.5% NaCl solution addition to the electrolyte. The potentiodynamic results are illustrated with potential plotted along the y-axis and the current density along the x-axis. In tables 4.7, 4.8 and 4.9; important corrosion parameters are listed for testing conducted in acetic and sulphuric acid electrolytes. The current densities found in this testing were low compared to those found in corrosion testing. Table 4.10 illustrates the electrolyte analysis from the AAS to identify the amounts of elements present in each solution after the corrosion tests. Table 4.11 illustrates the comparison of dry wear rates with the tribocorrosion wear rates.

4.4.1. Open Circuit Circuit

4.4.1.1. Acetic and Sulphuric Acid at pH 2

The variations in the OCP values of the WC-Co alloys for a period of 40 minutes after exposure to acetic acid electrolyte are presented in Figure 4.20. The first part of the scan took place in the first ten minutes without scratching the surface of the hardmetals. It can be observed that the OCP values decreased as time progresses, however, 6.4%Co-3.2%Ni-1.9%Cr-4.8%V had shown an increase in the OCP values which was followed by a slight decrease. In the next ten 10 minutes, the motor was switched on and there scratching of the surface. It can be observed that all hardmetals had shown a sharp increase in the OCP values. The hardmetal containing 6.4%Co-3.2%Ni-1.9%Cr-4.8%V had shown unstable OCP values and random fluctuations as the OCP values were decreasing. The other hardmetals had shown a slight increase in OCP values and a decrease as time progresses. In the next ten minutes, the motor was switched off and there was no scratching of the surface. It can be observed that the potential values were decreasing. In the last ten minutes, the motor was switched on and there was scratching of the surface. It can be observed that the alloys had shown an increase in the potential values and they started to stabilize except for 11.1%Co-4.6%Ni-1.5%Cr-0.2%V. It had shown unstable potential values before stabilizing at -0.135V. It can be noted that the scratching of the surface raised the potential values.

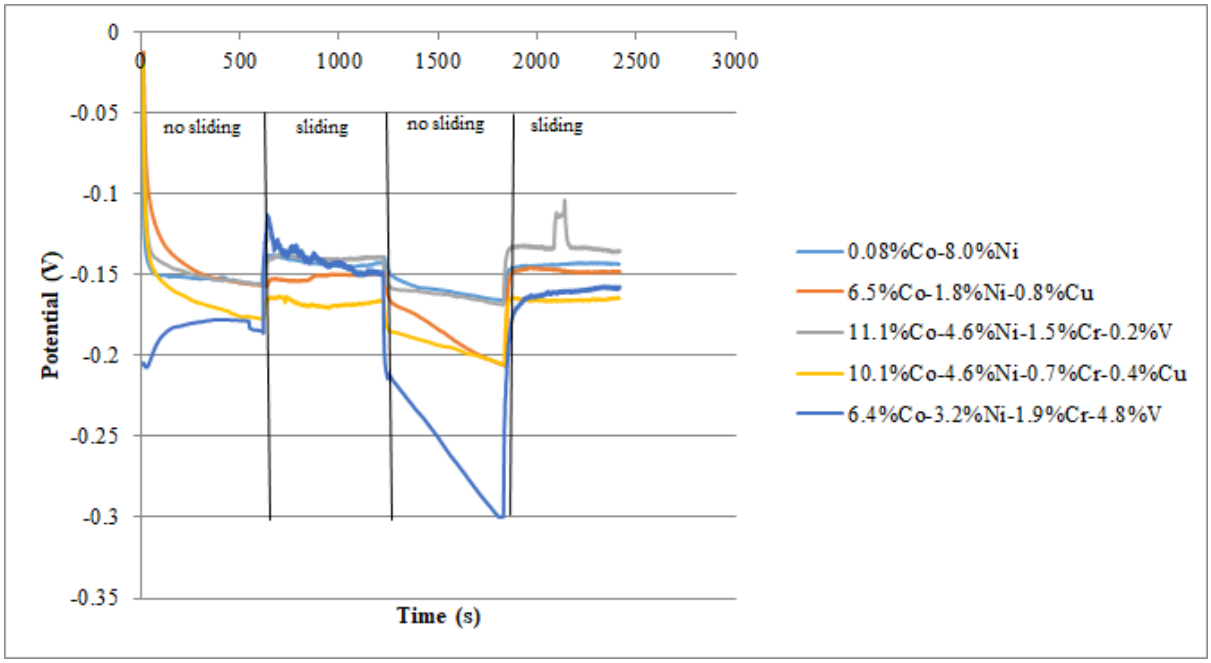


Figure 4.19: OCP scans of the WC-Co alloys in acetic acid electrolyte at pH 2.

Figure 4.21 presents the OCP scans of the WC-Co hardemetals in sulphuric acid electrolyte. It can be noted that in the first ten minutes of no scratching of the surface, the hardemetals had shown a decrease in the potential values. The hardemetal containing 11.1%Co-4.6%Ni-1.5%Cr-0.2%V had shown to be unstable and had fluctuating potential values. In the next ten minutes the motor was switched on, the alloys had shown an increase in the potential values which was followed by a decrease. The hardemetal containing 6.4%Co-3.2%Ni-1.9%Cr-4.8%V had shown unstable potential values. In the next ten minutes with no surface scratching, a decrease in the potential was observed and 6.4%Co-3.2%Ni-1.9%Cr-4.8%V and 10.1%Co-4.6%Ni-0.7%Cr-0.4%Cu were stable at potential values of -0.435 and -0.44V, respectively. In the last ten minutes the motor was on, an increase of the potential values was observed. It can be noted that the hardemetal with less nickel was the most noble as compared to the others.

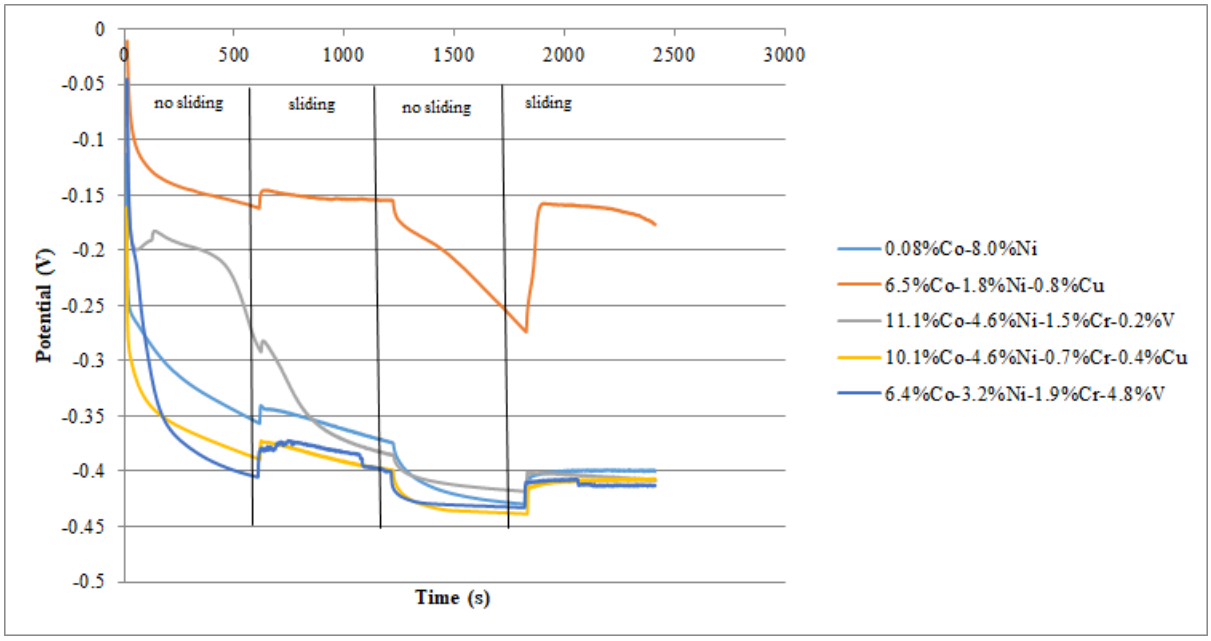


Figure 4.20: OCP scans of WC-Co alloys in sulphuric acid electrolyte at pH 2.

4.4.1.2. Acetic and Sulphuric Acid at pH 3

The variations in the OCP values of the WC-Co hardemetals for a period of 40 minutes after exposure to acetic acid electrolyte are presented in Figure 4.22. In the first ten minutes with no surface scratching, the hardemetal containing 10.1%Co-4.6%Ni-0.7%Cr-0.4%Cu and 6.4%Co-3.2%Ni-1.9%Cr-4.8%V had an increase in the potential to more positive values which was followed by a decrease. In the next ten minutes with the motor switched on, the hardemetals had shown an increase in potential values which was followed by a decrease where the hardemetals were unstable as they were showing fluctuating OCP values. In the next ten minutes of no scratching, the alloys had shown an increase in the potential which was then reduced as time progresses and they were unstable with fluctuating potential values. The last ten minutes had shown an increase of potential values and the alloys were stabilizing. The hardemetal containing 11.1%Co-4.6%Ni-1.5%Cr-0.2%V continued to show unstable potential values. It can be observed that hardemetals with increasing amounts of chromium are nobler than those without chromium.

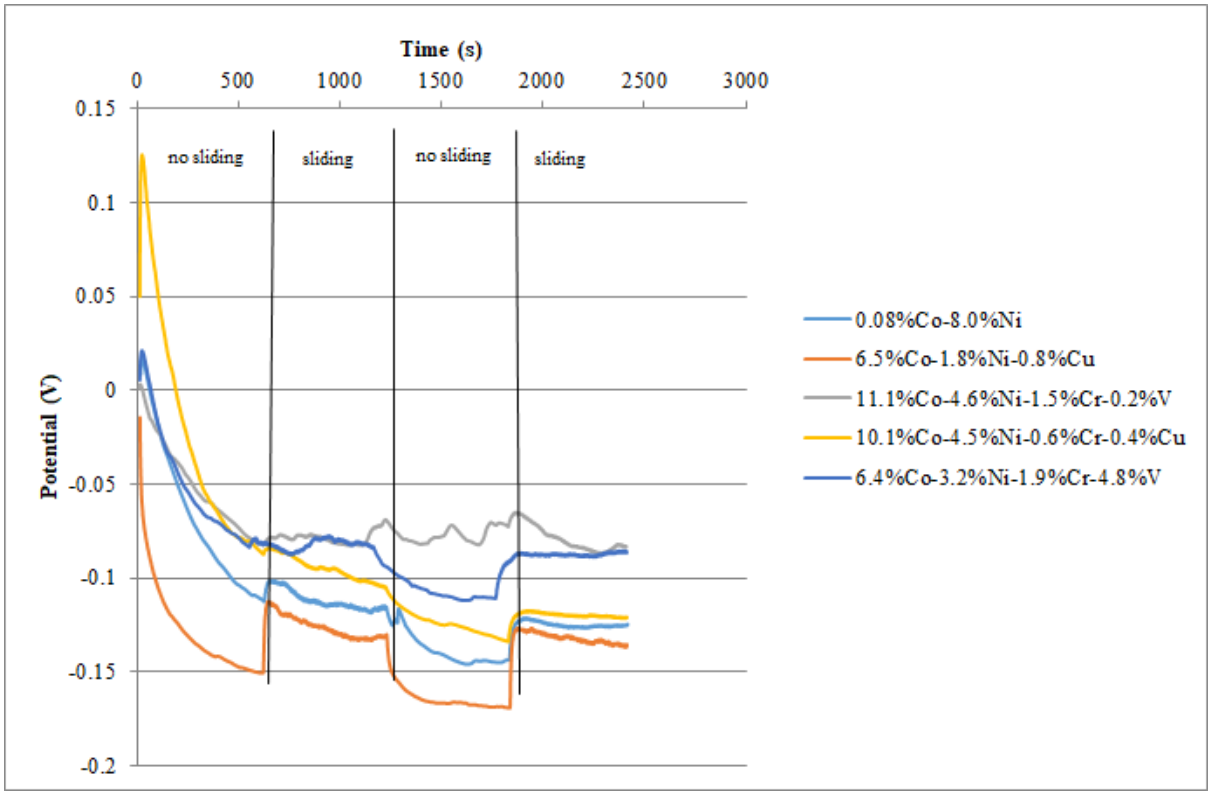


Figure 4.21: OCP scans of WC-Co alloys in acetic acid electrolytes at pH 3.

Figure 4.23 illustrates the OCP scans of the WC-Co hardemetals in sulphuric acid. It can be noted that in the first ten minutes all hardemetals had shown decreasing potential values. In the next ten minutes the potential values increased which was followed by a fluctuating potential. The OCP values at 2400s show that the hardemetals with increasing cobalt are nobler than the one with lower cobalt and high nickel content.

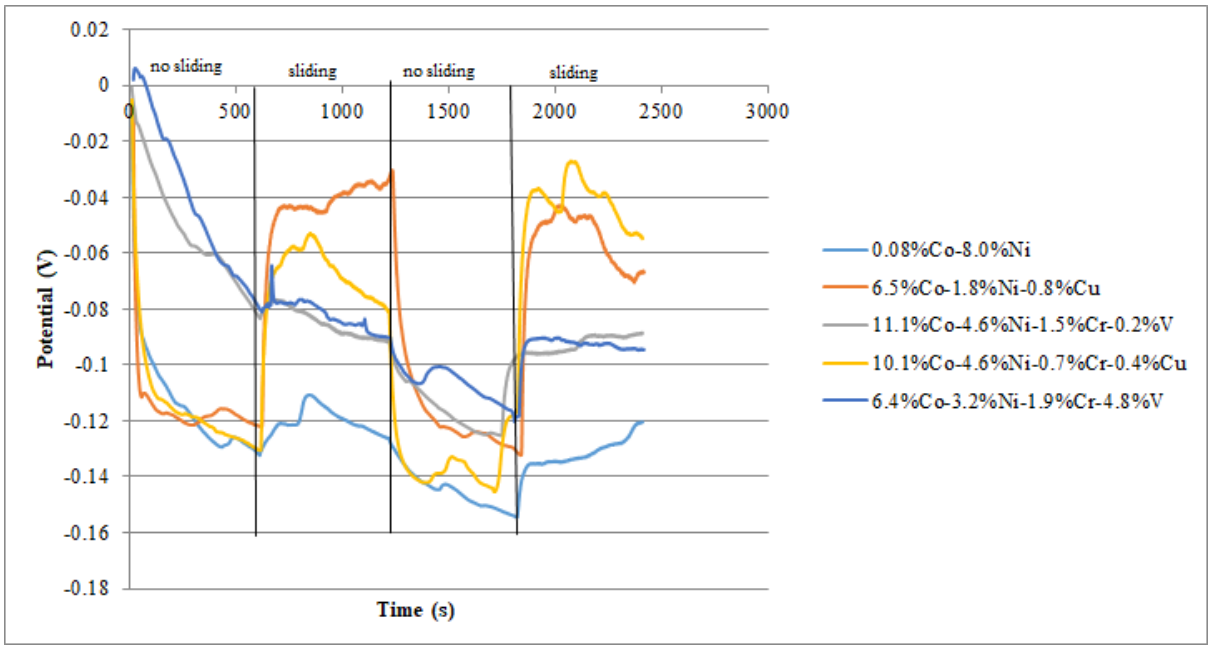


Figure 4.22: OCP scans of the WC-Co alloys in sulphuric acid electrolytes at pH 3.

4.4.1.3. Acetic and Sulphuric acid pH 5

The variations of the OCP values of the WC-Co hardemetals for a period of 40 minutes after exposure to acetic acid salt solution are presented in Figure 4.24. In the first ten minutes, 6.5%Co-1.8%Ni-0.8%Cu had shown an increase of potential values which was followed by an decrease. The hardemetals containing 6.4%Co-3.2%Ni-1.9%Cr-4.8%V and 0.08%Co-8.0%Ni had shown decreasing potential values which was followed by an increase as time progresses. In the next ten minutes 6.5%Co-1.8%Ni-0.8%Cu continued to show decreasing potential value which were unstable. The hardemetals containing 0.08%Co-8.0%Ni and 6.4%Co-3.2%Ni-1.9%Cr-4.8%V had shown a decreasing potential values, however, as time progresses the latter had shown increasing OCP values to more noble values as compared to the other hardemetals. In the next ten minutes, the hardemetals had shown decreasing OCP values. The last ten minutes had shown increasing potential values, however, the values were fluctuating. It can be observed that the hardemetals with the presence of vanadium had nobler values as compared the other hardemetals without vanadium.

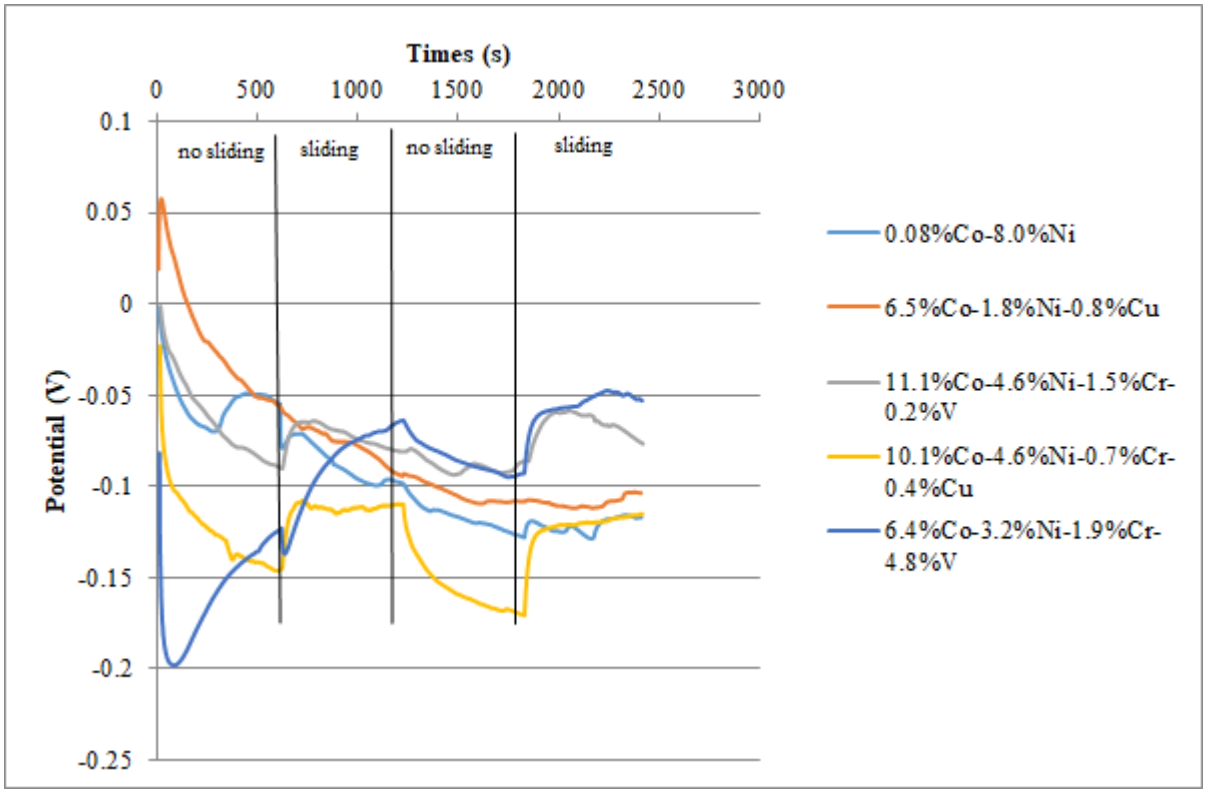


Figure 4.23: OCP scan of WC-Co alloys in acetic acid at pH 5.

Figure 4.25 illustrates the OCP values of the WC-Co hardemetals for a period of 40 minutes after exposure to sulphuric acid salt solution. In the first ten minutes, the hardemetals had shown decreasing potential values. In the next ten minutes, the hardemetal containing 6.4%Co-3.2%Ni-1.9%Cr-4.8%V had shown unstable potential values. In the last ten minutes, the same hardemetal had continued to show unstable potential values. It can be noted that the OCP values at 2400s with decreasing vanadium and chromium had increasing improved potential values.

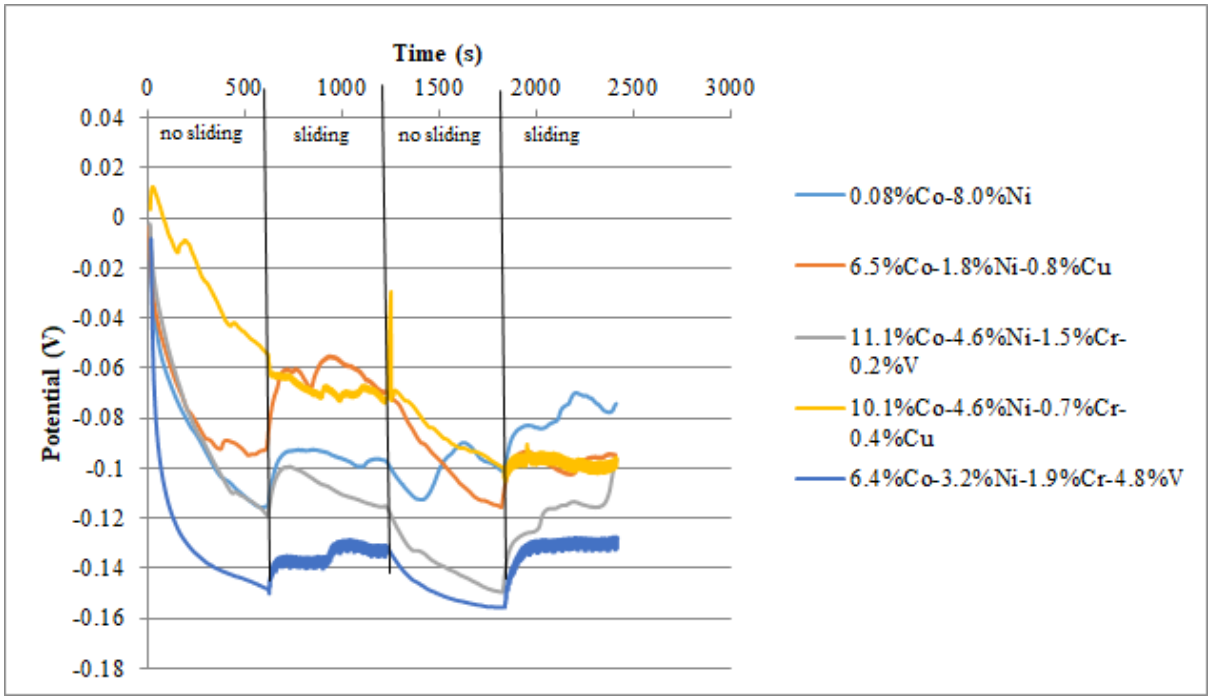


Figure 4.24: OCP scans of the WC-Co alloys in sulphuric acid electrolyte at pH 5.

4.4.2. Polarization Curves

4.4.2.1. Acetic and Sulphuric Acid at pH 2

The polarization curves of the WC-Co hardemetals in acetic acid electrolytes are illustrated in figure 4.26. It can be observed that the hardemetals did not show a similar behaviour. However, it can be noted the hardemetals with increasing amounts of cobalt had the noblest values as compared to the other hardemetals. The current densities decreased with decreasing cobalt.

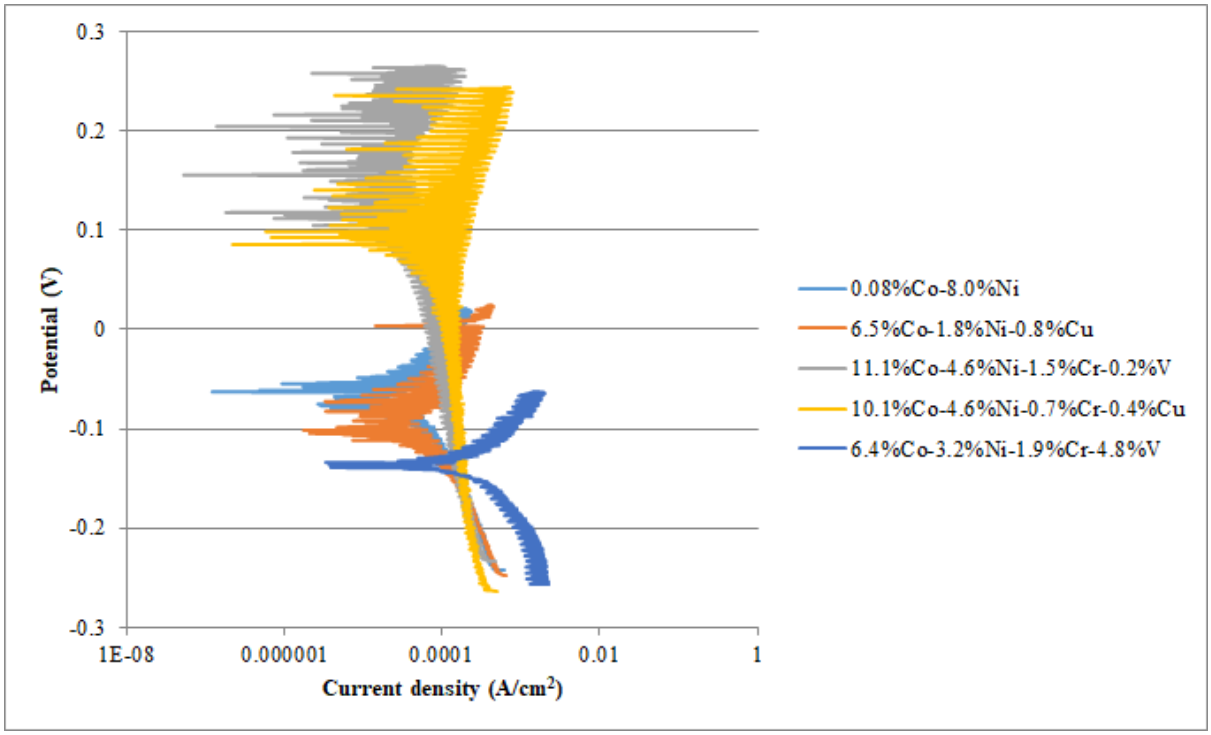


Figure 4.25: Polarization curves of WC-Co alloys in acetic acid electrolyte at pH 2.

Figure 4.27 illustrates the tribocorrosion rates of the WC-Co hardemetals in acetic and sulphuric acid electrolytes which are taken from Table 4.7. It can be observed that for acetic acid electrolyte, the rates increased with decreasing grain size. The tribocorrosion rates of the hardemetals in sulphuric acid electrolyte had shown higher rates as compared to the acetic acid electrolyte rates. These rates are so much higher when compared to the corrosion rates of both acid electrolytes at pH 2.

Table 4.6: Raw data for acetic and sulphuric acid at pH 2

Acetic Acid			
Sample	i_{corr} (A) $\times 10^{-6}$	E_{corr} (V)	Corrosion rate (µm/yr)
COR	29.0	-0.069	90.7
M	39.0	-0.095	125.3
T3	40.0	0.175	115.5
TC	150.0	0.069	429.2
UM	178.0	-0.135	511.3
Sulphuric Acid			
COR	189.0	0.84	590.9
M	75.0	0.97	241.0
T3	150.0	-0.045	433.1
TC	250.0	0.05	715.4
UM	73.0	0.097	209.7

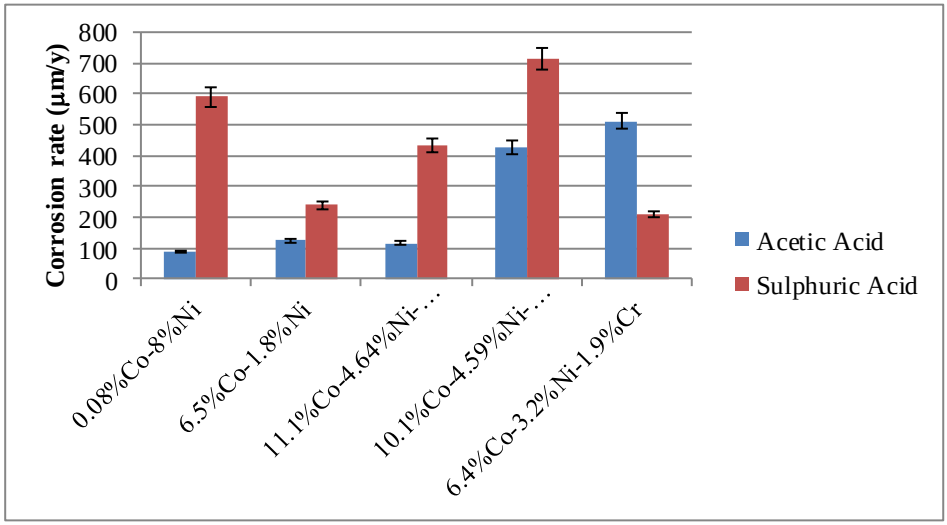


Figure 4.26: Tribocorrosion rates of the hardmetals in acetic and sulphuric acid at pH 2.

4.4.2.2. Acetic and Sulphuric Acid at pH 3

The polarization curves of the WC-Co hardemetals in sulphuric acid electrolyte are presented in Figure 4.28. It can be observed that the corrosion potential values increased and the current density decreased with increasing cobalt.

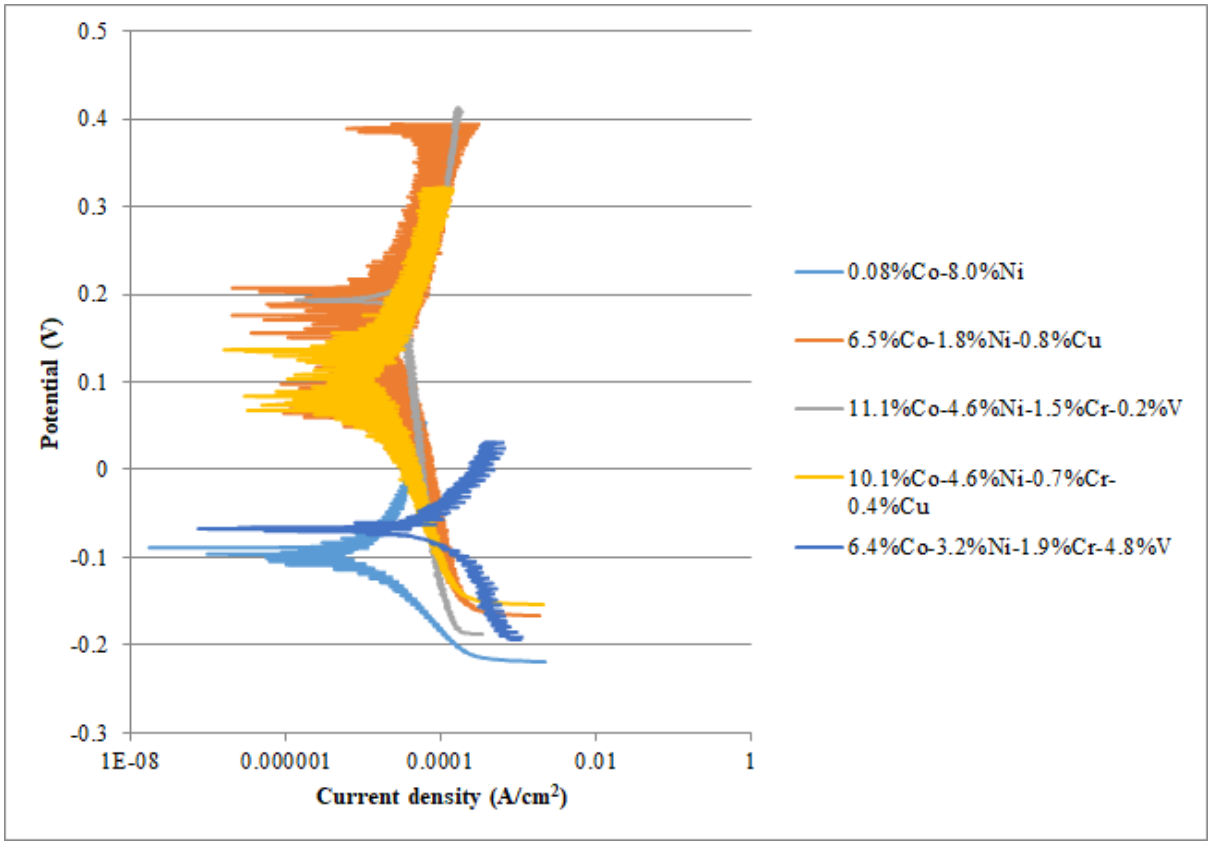


Figure 4.27: Polarization curves for WC-Co in sulphuric acid electrolytes at pH 3.

Figure 4.29 illustrates the tribocorrosion rates of the hardmetals in acetic and sulphuric acid electrolytes which were extracted from Table 4.8. The acetic acid electrolyte had shown higher tribocorrosion rates as compared to that those of sulphuric acid electrolyte. It can be observed that the rates for the sulphuric acid electrolyte increased with increasing cobalt content.

Table 4.7: Raw data for acetic and sulphuric acid at pH 3

Acetic Acid			
Sample	i_{corr} (A) $\times 10^{-6}$	E_{corr} (V)	Corrosion rate (µm/yr)
COR	39.0	0.01	121.9
M	28.0	0.03	90.0
T3	24.0	0.112	69.3
TC	40.0	0.119	114.5
UM	50.0	0.094	143.6
Sulphuric Acid			
COR	7.1	-0.111	22.2
M	32.2	0.137	103.5
T3	35.2	0.201	101.6
TC	18.0	0.1	51.5
UM	6.9	-0.065	19.8

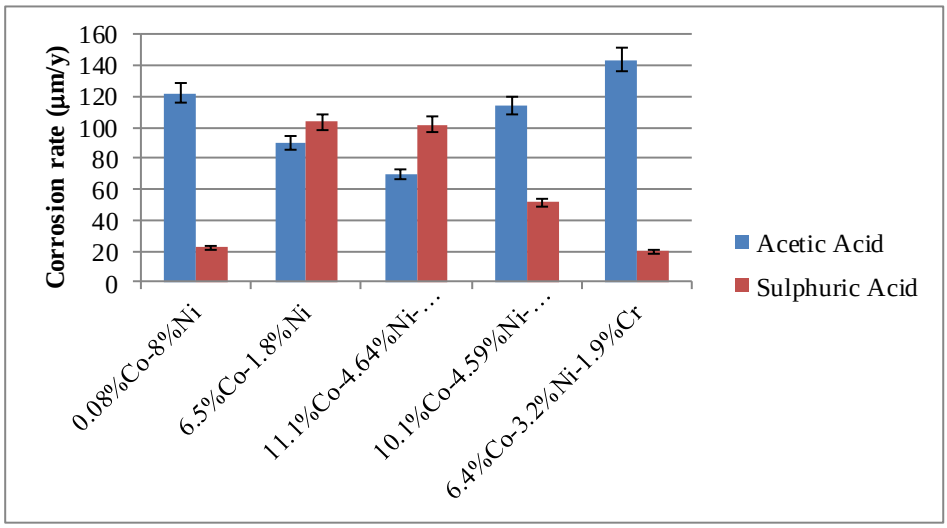


Figure 4.28: Tribocorrosion rates of hardmetals in acetic and sulphuric acid at pH 3.

4.4.2.3. Acetic and Sulphuric acid pH 5

The polarization curves of WC-Co hardemetals in acetic acid electrolyte are illustrated in Figure 4.30. It can be observed that the current density decreased with increasing vanadium and chromium. The hardemetals containing 6.4%Co-3.2%Ni-1.9%Cr-4.8%V and 11.1%Co-4.6%Ni-1.5%Cr-0.2%V had shown a similar behaviour as it can be noted that the latter is behind the 6.4%Co-3.2%Ni-1.9%Cr-4.8%V alloy.

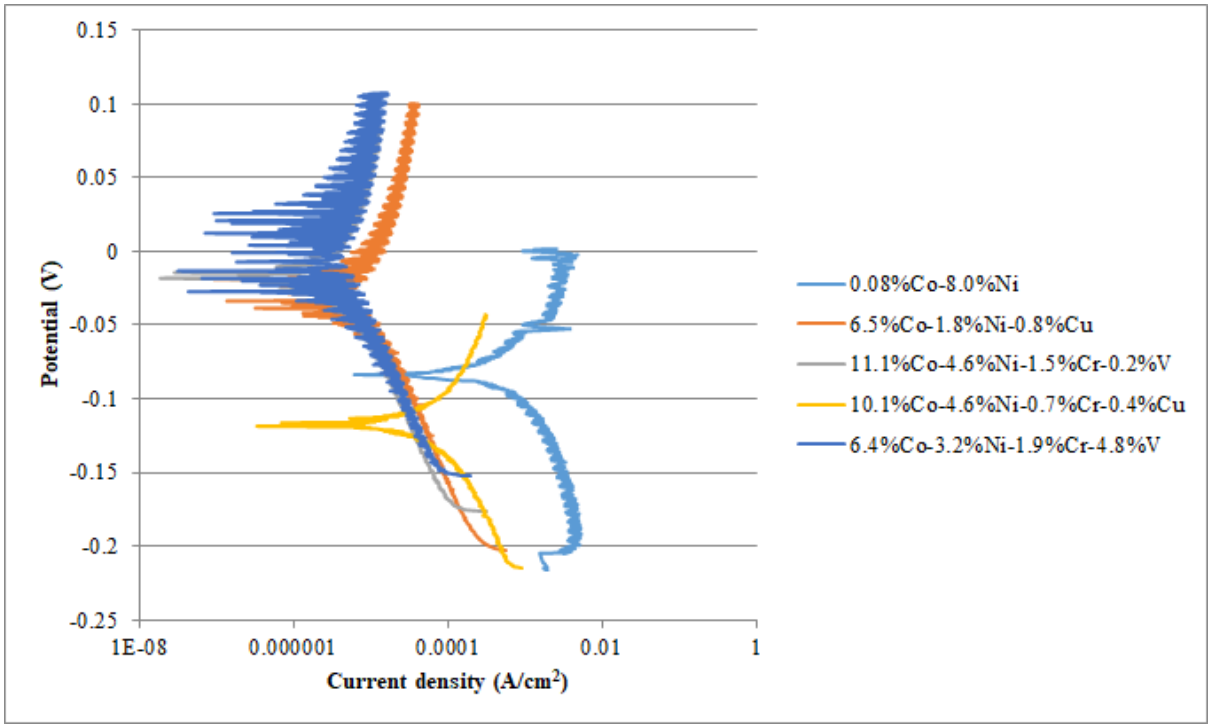


Figure 4.29: Polarization curves of the WC-Co alloys in acetic acid electrolyte at pH 5.

Figure 4.31 illustrates the tribocorrosion rates of the WC-Co hardemetals after exposure to acetic and sulphuric acid electrolyte and they extracted from Table 4.9. It can be observed that the hardemetal containing 0.08%Co-8.0%Ni had shown a very high tribocorrosion rate when exposed to acetic acid electrolyte as compared to the other hardemetals. However, when it was exposed to sulphuric acid it had shown a low tribocorrosion rate as compared to the other hardemetals with a low cobalt content. The hardemetals with lower tribocorrosion rates had high cobalt content with >6%Co when exposed to acetic acid electrolyte. The tribocorrosion rates increased with increasing chromium content when exposed to sulphuric acid electrolyte.

Table 4.8: Raw data for acetic and sulphuric acid at pH 5

Acetic Acid			
Sample	i_{corr} (A) $\times 10^{-6}$	E_{corr} (V)	Corrosion rate (µm/yr)
COR	300.0	-0.075	937.9
M	6.0	-0.031	19.3
T3	1.3	-0.02	3.8
TC	19.9	-0.115	56.9
UM	4.5	-0.005	12.9
Sulphuric Acid			
COR	2.0	-0.025	6.3
M	6.1	-0.0285	19.6
T3	2.5	-0.029	7.2
TC	24.4	-0.0595	69.8
UM	21.0	-0.122	60.3

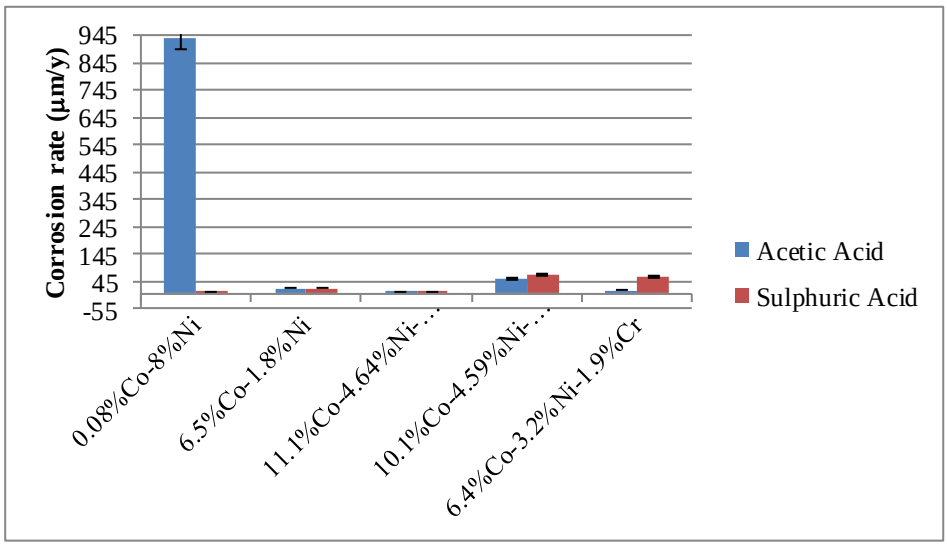


Figure 4.30: Tribocorrosion rates of hardmetals in acetic and sulphuric acid at pH 5.

A solution analysis was conducted using the AAS to determine the concentrations of elements passed into the solution during corrosion at pH 2 in Table 4.10. The primary binder content, Co, was not found into acetic and sulphuric acid salt solution. However, a significant amount of Ni was detected in the sulphuric acid salt solution for sample M as the environment became aggressive for the alloy.

A solution analysis was conducted to identify the concentration of the elements present in the corrosion solution at pH 3, the concentrations are found in Table 4.10. It can be observed that not much of the cobalt was detected in both acidic salt solutions. This could mean that the

presence of cobalt into the binder had lowered the corrosion rate. Small amounts of nickel concentrations were dictated in both acetic and sulphuric acid corrosion while chromium had shown higher concentrations in both corrosion solutions. A solution analysis for pH 5 was conducted as well and little to no cobalt was detected in both acidic salt solutions. However, in sulphuric acid salt solution sample T3 had shown a higher concentration of cobalt detection. Nickel was also detected in small amounts and high concentrations of chromium were observed as.

Table 4.9: AAS analysis for tribocorrosion tests solutions

Acetic Acid			
pH 2			
Sample	Cr (mg/l)	Ni(mg/l)	Co(mg/l)
COR	2.882	0.238	-1.285
M	3.670	0.522	-1.596
UM	2.558	0.517	-0.107
T3	0.528	0.521	1.647
TC	1.719	0.355	0.200
pH 3			
COR	2.038	1.847	1.439
M	2.802	1.591	1.861
UM	1.801	0.035	-2.455
T3	0.326	0.259	0.783
TC	5.359	3.170	-0.886
pH 5			
COR	2.520	0.194	-1.391
M	3.389	0.047	-2.803
UM	2.184	0.190	-1.726
T3	0.577	0.227	-0.121
TC	2.330	1.410	0.167
Sulphuric Acid			
pH 2			
COR	2.390	0.0866	-1.921
M	9.529	3.621	1.355
UM	2.923	0.702	-1.550
T3	0.402	0.259	1.390
TC	1.146	0.859	-0.391
pH 3			
COR	1.947	0.890	-2.016
M	2.335	0.873	0.749
UM	2.460	0.575	-0.895
T3	1.067	0.722	0.785
TC	3.715	1.634	0.452
pH 5			
COR	1.881	0.178	-1.193
M	2.539	0.123	-1.620
UM	2.363	0.065	-1.421
T3	0.602	1.025	2.195
TC	2.450	1.365	-0.566

4.4.3. Comparison of the wear rates under varied pH conditions

The wear rates of the hardmetals under dry, acetic and sulphuric acid conditions are listed in table 4.11. Testing was done on all the hardmetals; however, a few number of hardmetals did not show any wear track even after the second run at different pH conditions. This could mean that no wear took place. The corrosive wear rates were compared to that of dry wear rates. It can be observed that wear rates obtained under wet conditions were mostly higher than those obtained in dry conditions. Normally, the "lubricant" is known to decrease wear rates as it removes the wear debris that acts as the abrasive particles and possibly add to the wear process. In this case, the presence of an aggressive Cl^- and the corrosive influence from the acids could have could have led to such wear rates.

From the table it can be observed that 6.5%Co-1.8%Ni-0.8%Cu is common in all the pH conditions in both acid electrolytes. It can be noted that at pH 2 of both acid electrolytes it had shown a very high wear rate when compared to the dry conditions. This could be that the acid was very aggressive especially the weak acid. The hardmetal containing 6.4%Co-3.2%Ni-1.9%Cr-4.8%V had shown a very high wear rate at pH 3 in sulphuric acid electrolyte. A hardmetal containing 0.08%Co-8.0%Ni had shown a very high wear rate at pH 2 in sulphuric acid electrolyte when compared to dry conditions.

Table 4.10: Corrosive and dry wear rates information for the WC-Co alloys

Dry wear	
Sample	Wear rate (10^{-4} mm^3/Nm)
COR	10.3
M	11.9
T3	18.4
TC	11.3
UM	1.63
Acetic Acid	
pH 2	
M	6500
UM	37.5
pH 3	
COR	18.2
M	40.8
TC	18.0
pH 5	
M	5.48
T3	2.79
TC	11.7
UM	22.4
Sulphuric Acid	
pH 2	
COR	3.79
M	13.7
pH 3	
COR	25.5
M	11.9
UM	163.5
pH 5	
COR	99.7
M	4.87
T3	83.1
TC	1.82
UM	0.314

The wear rates of the hardmetals are illustrated graphically in figure 4.32 under dry conditions and for when they are exposed to acetic and sulphuric acid electrolytes at pH 5. The hardmetals containing 0.08%Co-8.0%Ni and 11.1%Co-4.6%Ni-1.5%Cr-0.2%V had shown a very high wear rate in sulphuric acid compared to when it is under dry conditions.

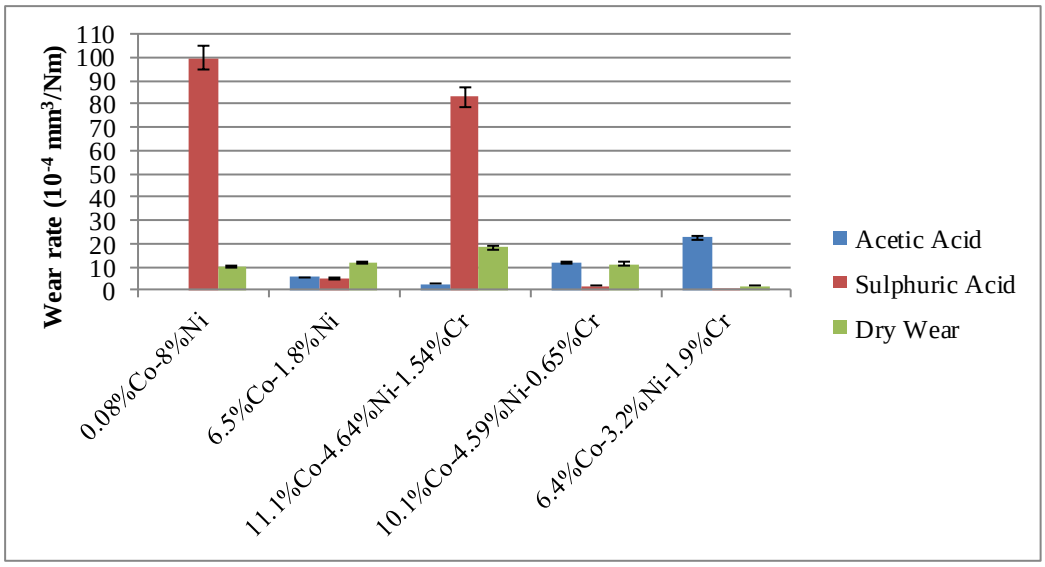


Figure 4.31: Comparisons of the WC-Co hardmetals wear rates under dry and pH 5 conditions.

4.4.4. Microstructural Analysis

The microstructural examinations of the worn hardmetals were done to help determine the wear mechanisms that took place. The comparisons between the corrosive wear under varied pH conditions were made in addition to the comparison between the hardmetal grades. The microstructures from varying pH conditions are similar but the severity of the damage is different.

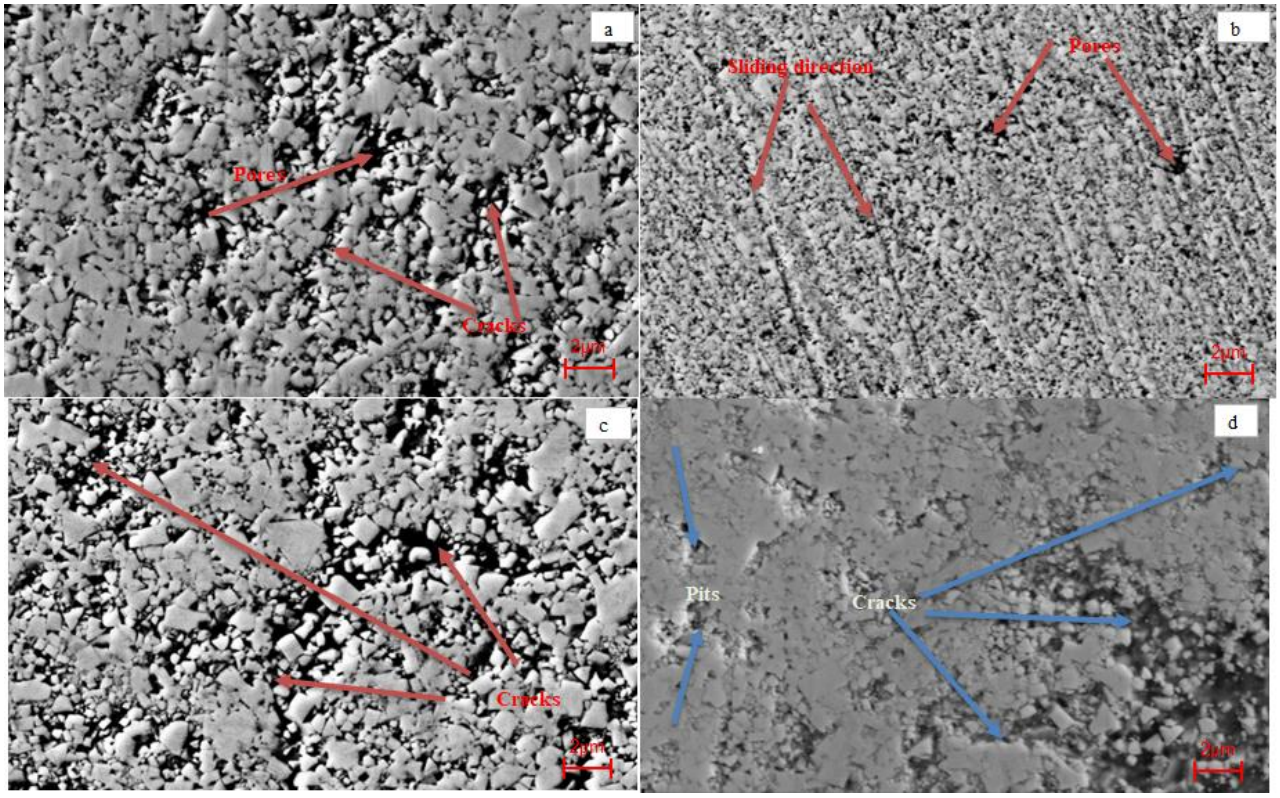


Figure 4.32: Worn surfaces at pH 2. (i) when exposed to acetic acid: a) 6.5%Co-1.8%Ni-0.8%Cu and b) 6.4%Co-3.2%Ni-1.9%Cr-4.8%V and (ii) when exposed to sulphuric acid: c) 0.08%Co-8.0%Ni and d) 6.5%Co-1.8%Ni-0.8%Cu.

It can be observed in Figure 4.33 that the hardmetals containing 6.5%Co-1.8%Ni-0.8%Cu in (a) and 0.08%Co-8.0%Ni in (c) had a similar microstructure. They both illustrated fragmented grains and pits. This could be the result of the aggressive conditions that the hardmetals were subjected to. The hardmetal containing 6.4%Co-3.2%Ni-1.9%Cr-4.8%V had shown a sliding direction, the microstructure is similar to that found in Figure 4.6. The hardmetal in (d) had shown cracks and pits formed at the surface of the of the material. These micrographs are showing transgranular cracks as all hardmetals show fragmented grains. It can be observed that the transgranular cracks primarily attributed to the formation of pits that propagated along the grains. It could also mean that cobalt was preferentially removed because of acid influence.

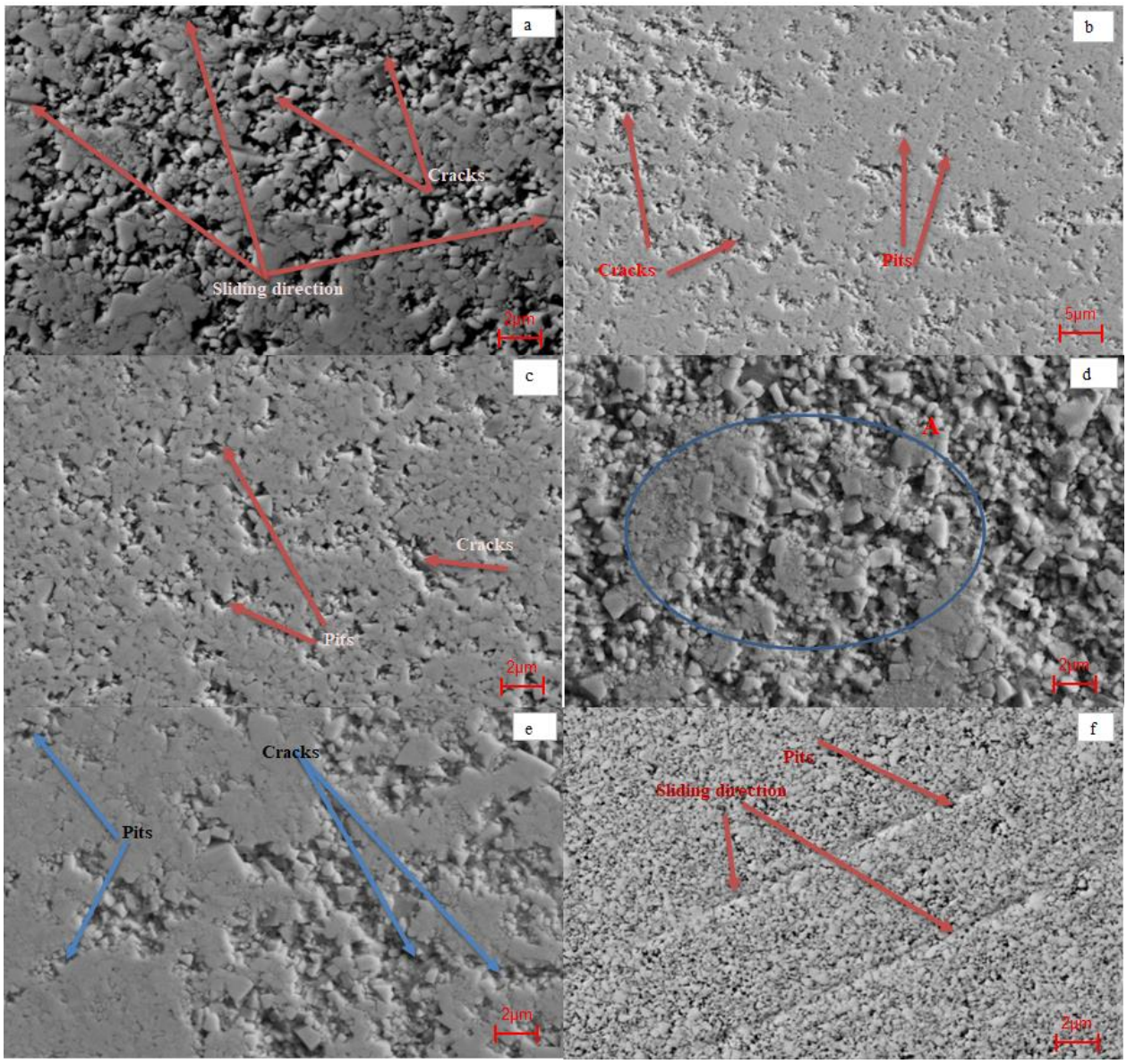


Figure 4.33: Worn surfaces at pH 3 when exposed to acetic acid: a) 0.08%Co-8.0%Ni, (b) 6.5%Co-1.8%Ni-0.8%Cu and (c) 10.1%Co-4.6%Ni-0.7%Cr-0.4%Cu and when exposed to sulphuric acid: d) 0.08%Co-8.0%Ni, e) 6.5%Co-1.8%Ni-0.8%Cu and f) 6.4%Co-3.2%Ni-1.9%Cr-4.8%V

It can be observed in figure 4.34 that the hardmetal containing 0.08%Co-8.0%Ni in (a) shown a fragmented grains and sliding distance of the alumina ball. It was also observed in (d) that the grains were severely damaged. This could be due to the aggressive environment. Most of the microstructures illustrates fragmented cracks and pits at the surface of the hardmetals. The hardmetal containing 6.4%Co-3.2%Ni-1.9%Cr-4.8%V did not show much damage except the sliding direction of the ball and small holes which are not that visible.

In figure 4.35 (a) the wear direction and pits of this hardmetal can be observed. The hardmetals containing 6.5%Co-1.8%Ni-0.8%Cu had shown more cracks and pits compared to figure 4.34 (b) and (e), grain pull out can be observed. The hardmetal containing

10.1%Co-4.6%Ni-0.7%Cr-0.4%Cu (d) had shown similar features as of the one in figure 4.6, sliding direction.

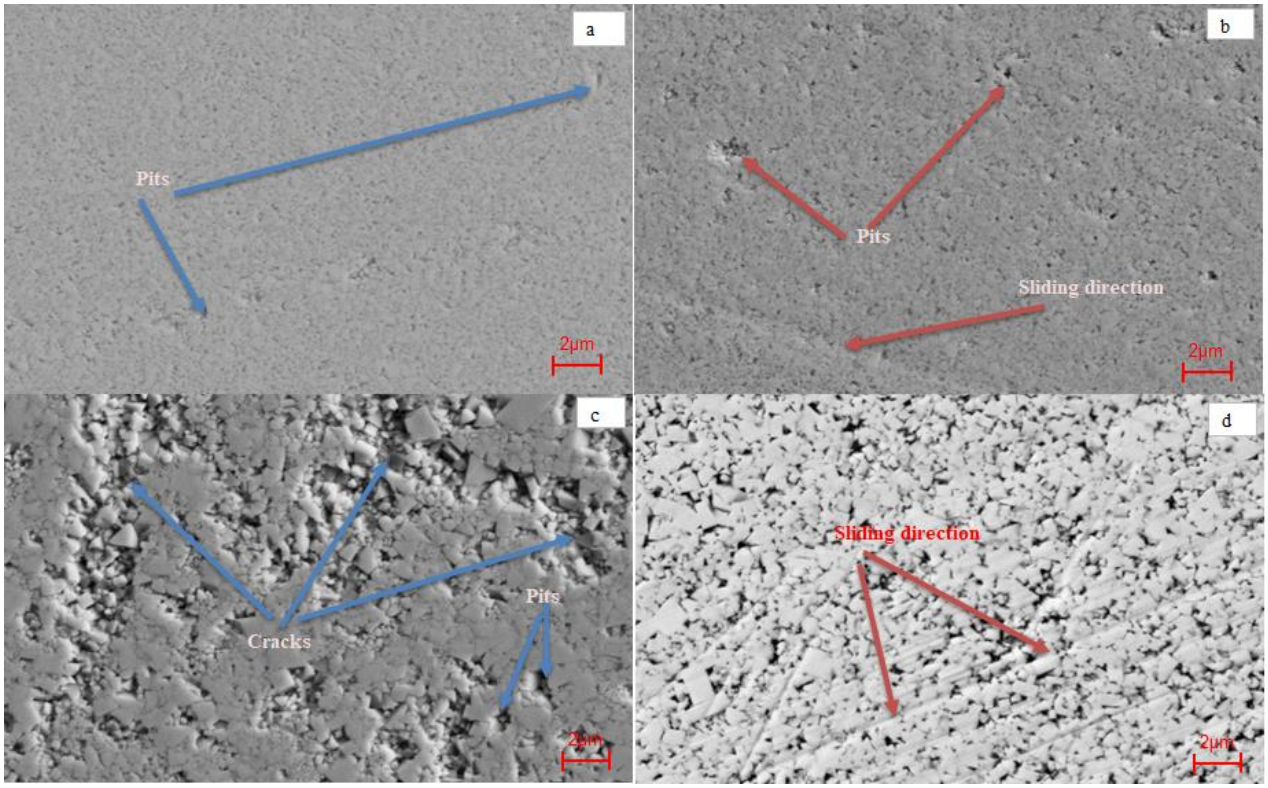


Figure 4.34: Worn surfaces Acetic acid pH 5: a) 11.1%Co-4.6%Ni-1.5%Cr-0.2%V, b) 6.4%Co-3.2%Ni-1.9%Cr-4.8%V, c) 6.5%Co-1.8%Ni-0.8%Cu and d) 10.1%Co-4.6%Ni-0.7%Cr-0.4%Cu.

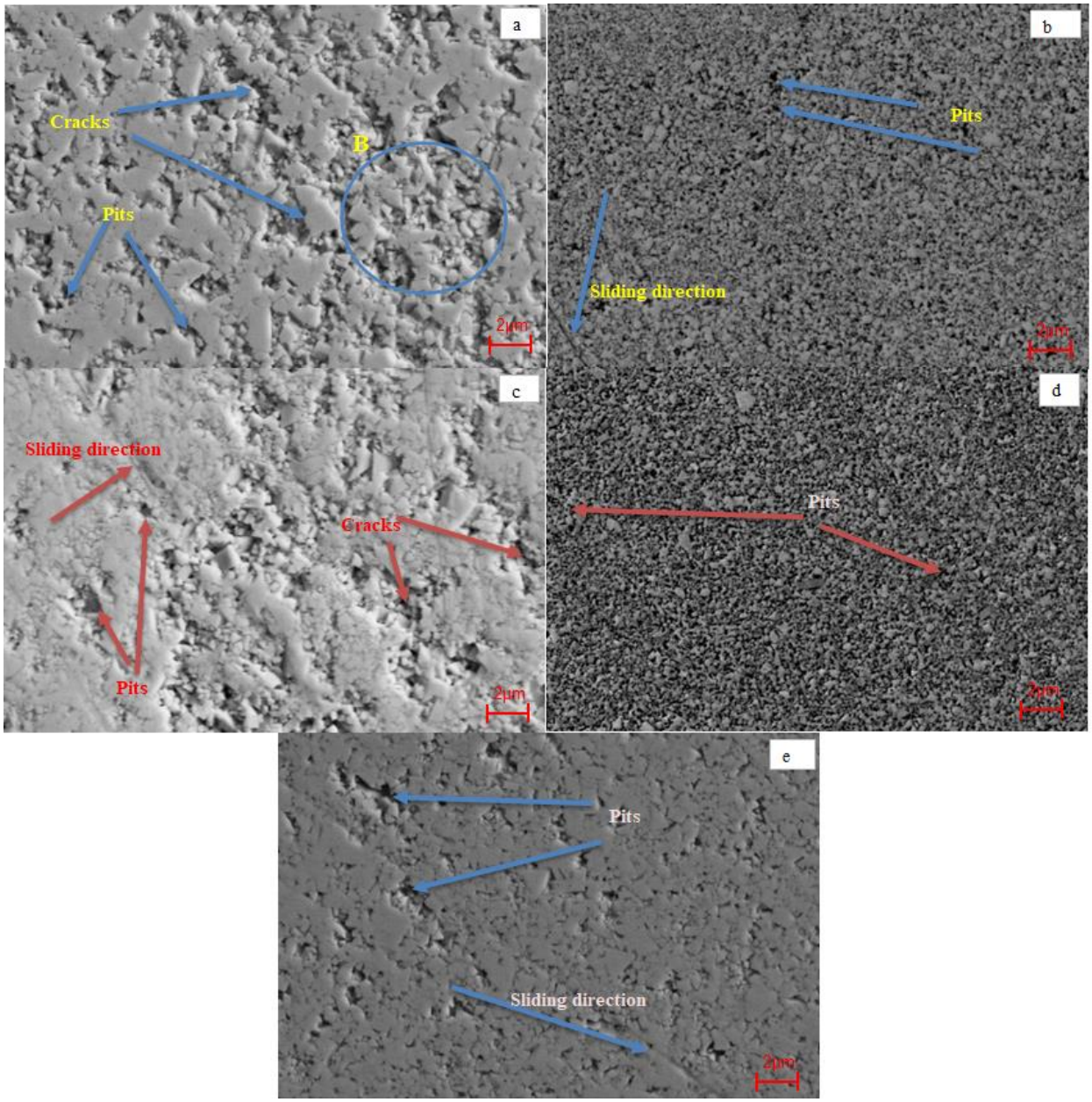


Figure 4.35: Worn surfaces in Sulphuric acid pH 5: a) 0.08%Co-8.0%Ni, b) 6.4%Co-3.2%Ni-1.9%Cr-4.8%V, c) 10.1%Co-4.6%Ni-0.7%Cr-0.4%Cu, d) 11.1%Co-4.6%Ni-1.5%Cr-0.2%V and e) 6.5%Co-1.8%Ni-0.8%Cu.

In figure 4.36, it was observed that the 0.08%Co-8.0%Ni in (a) had shown fractured grains marked B and localized pits. The hardmetal containing 10.1%Co-4.6%Ni-0.7%Cr-0.4%Cu in (c) had shown cracks, sliding direction and pits. The alloys containing 6.5%Co-1.8%Ni-0.8%Cu and 6.4%Co-3.2%Ni-1.9%Cr-4.8%V in (e) and (b) had shown pits and grinding lines. The hardmetal containing 11.1%Co-4.6%Ni-1.5%Cr-0.2%V in (d) had shown small pits, it shows similar features as that found in figure 4.6 except the wear debris.

5. Discussion

In this chapter the corrosion, wear and tribocorrosion response of the WC-Co alloys are discussed. The influence of the testing procedures used and environment is evaluated. The corrosion response of hardmetals is evaluated under different condtions which was followed by their wear response when they were subjected to a ball-on-disc in a rotary motion wear.

5.1. Corrosion response of the WC-Co hardmetals

The corrosion response of the hardmetal can be explained in contrast with the galvanic couple. The cobalt assumes an anodic role when exposed to corrosive environments and would want to provide cathodic protection to the tungsten carbide. The tungsten carbide has a more noble position than cobalt in the electrochemical series. In chapter 4.3, some polarization curves illustrated the formation of pits which indicated that the cobalt binder was preferentially removed from the hardmetal matrix during corrosion. It could be possible that the weak acid and strong acid in different conditions had initiated the galvanic effect in the corrosion environment.

Corrosion rates are influenced by the cathode and anode in a typical electrochemical reaction. The rates are controlled by the amount of cobalt binder phase and the properties. Studies had shown that corrosion rates are accelerated by higher cobalt binder contents (Sacks, 2002); (Human & Exner, 1996). In this investigation the observations were different; the corrosion behaviour of the alloys did not follow the aforementioned trend. It was observed that the corrosion response of the WC-Co alloys was different in all the investigated solutions under varied pH conditions. Figure 5.1 illustrates that the corrosion rates decreased with increasing pH values. For the weak acid, it could mean that the oxygen reduction has taken place at a greater degree than the hydrogen evolution (Sacks, 2002). It can be noted from the graph that acetic acid had lower corrosion rates compared to sulphuric acid at pH 3. Ige, et al., 2017 had studied the cause of high corrosion rates in the presence of sulphuric acid. It was found that the high corrosion rates are ascribed to the significant galvanic coupling effect arising from large potential differences between cobalt and WC (Ige, et al., 2017).

The results revealed that the hardmetal with 10.1%Co-4.6%Ni-0.7%Cr-0.4%Cu had shown better corrosion rate on both acids at pH 3. The alloy containing 6.4%Co-3.2%Ni-1.9%Cr-4.8%V had a better corrosion rate on both acids at pH 2 and 5. This could be the presence of chromium and vanadium into the binder as they are present in high amounts they produced an

improve corrosion resistance. These observations are in agreement with the study (Wood, et al, 2017) conducted. In this study the corrosive media dictated the binder composition. The study proved that the corrosive media is the one that can dictate the exact binder composition (Gant, et al, 2004). The influence of the grain size was observed when the alloys were exposed to the acetic acid electrolyte at pH 5. The current density increased with increasing grain size. However, (Zhang, et al, 2016) mentioned that there is still limited information on the effect of the grain size on the corrosion behaviour of alloys exposed to organic acid environments. No conclusion can be drawn from this as there still need to be further investigations where a variety of grain size distribution is investigated. The study conducted by (Human & Exner, 1997) & (Zheng, et al, 2019) they did not find any effect of the grain size on the corrosion behaviour of the alloys in acidic environment. This observation is in agreement with the corrosion behaviour observed at pH 5 of sulphuric acid electrolyte.

In the polarization curves two different types of hysteresis loops were observed which include positive and negative. The positive hysteresis loop is defined as the loop that is related to a reduced passivity which is due to the formation of localized corrosion causing the current density to increase in the reverse scan (Esmailzadeha, et al, 2018). The alloys containing 6.5%Co-1.8%Ni-0.8%Cu and 11.1%Co-4.6%Ni-1.5%Cr-0.2%V had shown this particular loop with slow decreasing current density in the reverse scan at pH 3 in sulphuric acid electrolyte. A study that was conducted by Esmailzadeha, et al., 2018, had found that this behaviour would be due to the difficulty in surface repassivation or the pits stopped growing. The presence of the Cl^- ion in the solution could progress the growth of pits and also the presence of the aggressive acid can accelerate that growth. The negative hysteresis loop occurs when the level of surface passivation is greater at more noble potentials; this causes the current density to decrease in the reverse scan to be less than that of the forward scan (Esmailzadeha, et al, 2018). The alloy containing 0.08%Co-8.0%Ni had shown this hysteresis loop at pH 2 in acetic and sulphuric acid.

Pit formation also known as localized corrosion was also from the curves was observed and the process becomes stronger when the solution contains chloride ions. Pits form when the oxide film is chemically damaged and the alloy does not repassivate immediately. The chloride ion is responsible for damaging the passive film for the pits to initiate as the oxides breaks.

It was difficult to detect corrosion products on the surface of the alloys using the EDS analysis which makes it hard to define the reactions that took place between the cobalt and the acetic or sulphuric acid electrolytes. The organic acid and the strong acid have a very complex structure. Since there was air exposure, this could mean that the reduction of oxygen had taken place at a greater degree than hydrogen evolution. It can be observed that the corrosion rates at low pH levels were high; this could mean that the oxide film formed was thin especially in the presence of a strong acid as well as NaCl. It could be possible that a chelation reaction occurred between the organic acid and the cobalt metal. Chelation is the reaction between a metal ion and an organic acid resulting in the formation of a ring structure (Dixon, 2013). The absence of the corrosion products could be the formation of the chelates between the cobalt and organic acid which were soluble.

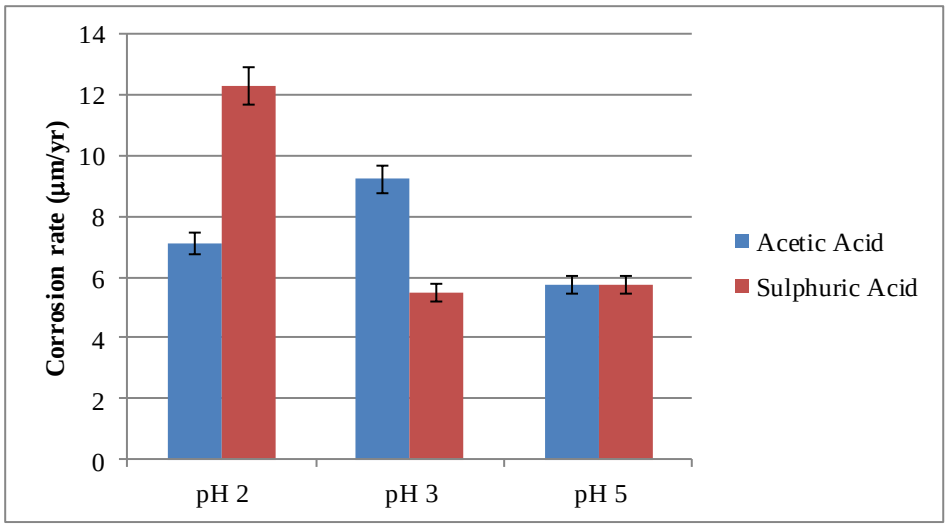


Figure 5.1: Averaged corrosion values under varied pH conditions.

5.2. Wear response of the WC-Co alloys

During the ball-on-disk test the ball is pressed against the surface (disk) of the hardmetal at a 5N load. After the tests, the wear scar on the pin was not visible even after the second run under dry conditions. This could be that the ball had a higher hardness compared to the hardmetals. The WC-Co alloys had shown wear tracks which were examined under the SEM to identify the wear type the alloys showed.

Deformation of a hardmetal can be evaluated by considering the deformation properties of each phase. The WC phase is found to be able to accommodate a considerable amount of plastic deformation without fracture compared to the cobalt phase. This could be due to its

slip system which is able to withstand continuity under extreme deformation (Sacks, 2002). In most hardmetals, the cobalt binder phase is ductile which means it has FCC crystal structure. This feature is favourable in performance perspective, since more ductile and fracture resistant material is achieved with FCC structure than with the HCP structure (Sacks, 2002). This crystal structure can transform to HCP structure when the cobalt phase is plastically deformed. The binder phase is associated with the stacking faults. The stacking faults tend to act as nucleation planes for the HCP lamellae formation as deformation continues the stacking faults increase their thickness and then coalesce to form observable HCP lamellae and this may take place by gliding (Yang, et al., 2014). Crack formation in WC-Co hardmetals is closely related with cobalt phase FCC and HCP transformation. The HCP structure only has one easy slip plane, compatibility becomes difficult as deformation proceeds (Sarin & Johannesson, 1975); (Yang, et al., 2014). Therefore, when certain fraction of the FCC binder phase is transformed to HCP, cracks start to form and the carbide skeleton breaks (Yang, et al., 2014).

The wear rate can be influenced by the grain size and cobalt content. It was found that 6.4%Co-3.2%Ni-1.9%Cr-4.8%V had a better wear rate compared to the other alloys and the original microstructure had shown a very fine-grained microstructure and has a higher hardness. The effects of adding high amounts of vanadium and chromium into the binder were strong. A study has indicated that these elements are regarded as good grain growth inhibitors in the cemented tungsten carbide (Sacks, 2002). This alloy had a high amount of these two elements, which improved wear resistance and hardness. This could be due to the fact that vanadium has a high electron affinity for carbon which promotes the formation of stable carbide whilst chromium is a good grain growth inhibitor. It also had a fine-grained microstructure which can be observed in figure 4.2. However, the alloy containing 11.1%Co-4.64%Ni-1.54%Cr-0.22%V had a higher wear rate compared to the other alloys irrespective of the presence of vanadium and chromium. It was also the second alloy with high hardness. This proves that a material with high hardness does not guarantee high wear resistance. The wear track microstructure of this material had shown that the alloy had wear debris and holes. The alloy containing 0.08%Co-8.0%Ni was the second alloy with low wear rate and it was tough. The wear track microstructure of this alloy had shown plastic deformation. The cracks were observed in this alloy where crack propagation is prevented due to some constrain in plastic flow.

5.3. Tribocorrosion response of the WC-Co alloy

This process consists of wear and corrosion which has a variation of mechanical and chemical mechanisms when integrated they mostly result in a notable increase of material loss. Furthermore, these mechanisms are still not fully understood as they are still debates on which one contributes more to the volume loss when they are both in operation. This study investigated the effect corrosion has on wear, the wear-corrosion combination is controlled by the electrolyte, the alloy used and wear conditions.

It can be observed that the fluids have a very great influence on the wear rates of materials when compared to the dry conditions. This investigation recorded high wear rates in the wet environment compared to the dry environment. The presence of fluids in this case has proven to be very aggressive to the material by accelerating the wear rates. However, the behaviour of the fluids was different at higher pH levels. The wear rates of some alloys were lower compared to the dry environment as the fluids might have acted as lubricants. In some cases, other alloys did not show a wear track which could mean corrosion was the most dominant mechanism.

It can be observed in Figure 5.2 that sulphuric acid had high corrosion rates at pH 2 compared to the other pH levels. This could be the aggressiveness of the environment that drove the corrosion rates up. The increase in corrosion rates can be the resultant of an increase in surface roughness which increases the surface area. However, in Figure 5.3 the material loss was very low compared to the other pH levels. This could mean that the presence of cobalt had improved wear resistance of the materials under these aggressive conditions. Wood et al., 2017 studied the implications of tribocorrosion and how it affects the degradation mechanisms of WC-Co. It has been observed that a metal binder that is optimum in one degradation process is not optimum when both corrosion and wear are in place. For example, nickel performs best for corrosion alone but performs poorly in tribocorrosion, this is assumed to be caused by the passive layer which is takes time to form and is mechanically weak which makes it to be susceptible to the removal due to the applied load or its intrinsic material properties are inferior (Wood, et al.,2017).

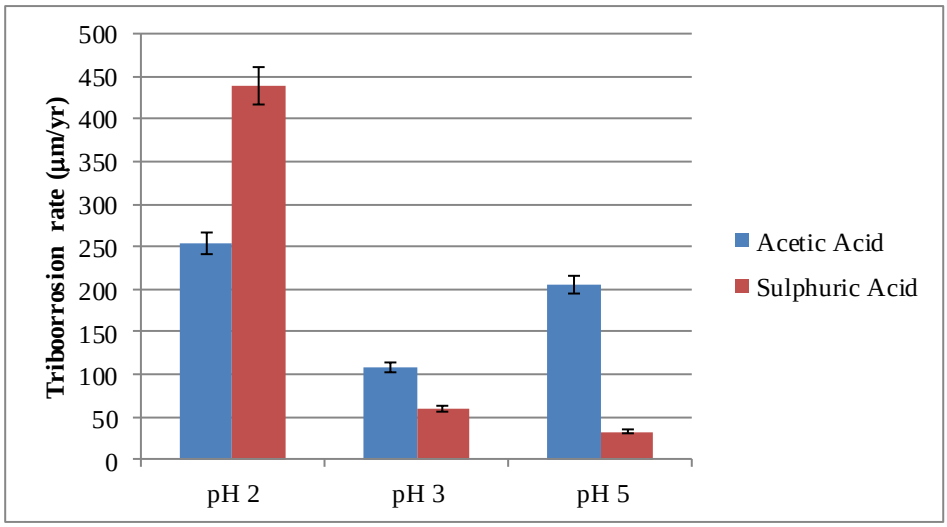


Figure 5.2: Averaged tribocorrosion rates under varied pH conditions.

It can be noted that the material loss increased with decreasing corrosion rates when the alloys were exposed to sulphuric acid. However, the acetic acid had shown the opposite. This could be due to the removal of the oxide film during the mechanical process in the case of sulphuric acid or the formation of oxide surface which caused less mass loss.

The microstructure had shown cracks, pits and grain fracture. It can be concluded that these high corrosion rates are driven by the propagation of cracks. These mentioned features elevate the anodic behaviour of a material, hence, allowing corrosion attack as the ball continues to slide causing more material loss and this in turn decreases the strength of a material. Gant, et al., 2004 studied the tribocorrosion synergy for WC-Co hardmetals in low stress abrasion by varying the pH values from very acidic to basic conditions in the presence of an abrasive media. It was observed that under mild acidic conditions (pH 2.6 and 6.3) there was more evidence of WC grain fracture and correspondingly less of binder dissolution. Grain pull-out was also observed, it could be caused by the corrosive-wear combination which could increase the exposure of the grains to mechanical action. Pereira, et al., 2022, studied that the grain pull-out was caused by the preferential removal of the binder and dissolution of the binder around the carbide grains. The preferential removal of the binder leads to a gap around the carbide grains which increases due to chemical and mechanical action that also results to the formation of pits (Pereira, et al., 2022). Therefore, results to high material removal from the surface, thus, the high measured wear rates.

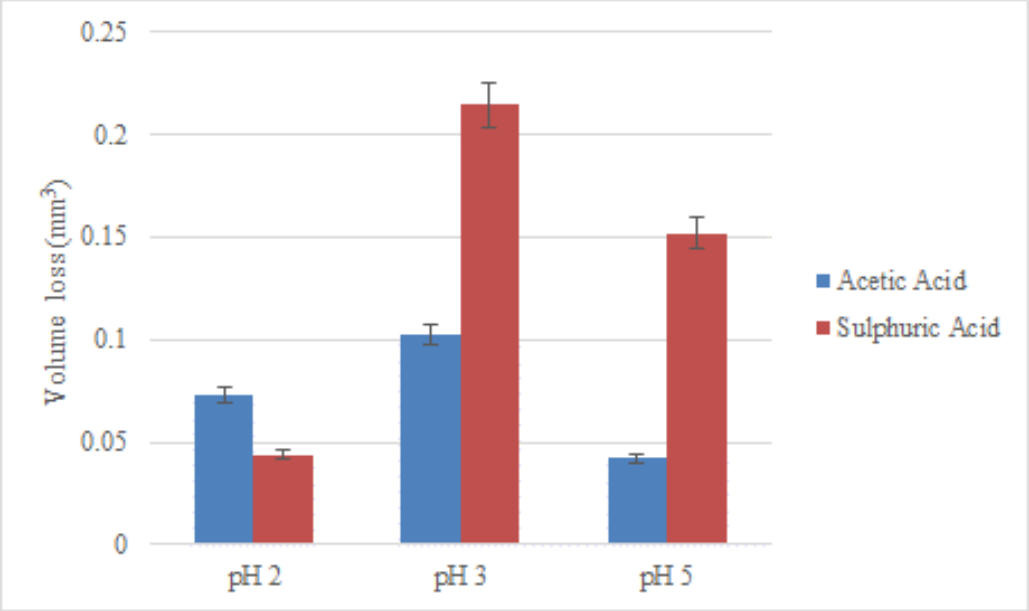


Figure 5.3: Disk volume loss under varied pH condition.

The alloy containing 6.5%Co-1.8%Ni-0.8%Cu had shown high wear rates at the pH range of 2-3 of both the weak and strong acid. Most of the grain fracture and cracks were observed in the microstructure of this alloy, this could mean that they acted as active sites that accelerated the corrosion attacks since it had shown high corrosion rates as well. At high pH levels, the alloy had very low wear rates and it had shown the same corrosion rates when it was exposed to acetic and sulphuric acid. The influence of grain size was observed at pH 3 in sulphuric acid; however, the results remain inconclusive as the study of the influence grain size under varied pH levels needs to be conducted on a much broader level.

6. Conclusions

6.1. The effect of binder compositions in the corrosion behaviour of alloys

- This study proved that the corrosive environment dictates the exact binder composition that will be suitable for that condition.
- The additions of chromium and nickel did have an effect in stabilizing the cobalt binder phase at pH 2 and 5 this can be observed from the alloy 6.4%Co-3.2%Ni-1.9%Cr-4.8%V.
- High amounts of cobalt did not affect the performance of the alloys under varied pH conditions.
- The grain size did not have much influence on the corrosion behaviour of the alloys.

6.2. The corrosion behaviour of the WC-Co alloys under varied pH conditions

- Hysteresis loops were observed from the curves as they determine whether they will be formation of localized corrosion or not.
- Positive hysteresis loop was observed at higher pH levels, where it was found that the presence of Cl- ions and that of acid might accelerate the growth of pits.
- Negative hysteresis loop was observed at lower pH levels for the alloy 0.08%Co-8.0%Ni as the reverse scan had shown decreasing current density.

6.3. The tribocorrosion behaviour of the WC-Co alloys

- It was found that the wear conditions, alloy, and electrolyte they control the wear-corrosion interaction.
- Some alloys had shown the dominant corrosion behaviour as there was no wear took place.
- The presence of fluids in the wear process has an influence on the wear rates.
- The varied pH conditions have great influence on the wear rates of the alloys which in turn accelerate the corrosion attack with increasing acid strength.
- The material removal is presented by the formation of pits, cracks, and fractured grains.
- Under dry conditions, some alloys had shown wear debris and cracks which might have caused material loss.

- Less than 1wt% of cobalt content had shown low corrosion rates at pH 2 in acetic acid and pH 5 sulphuric acid.
- Less vanadium additions had shown improved corrosion rates at pH 3 and 5 of acetic acid. High additions of vanadium had shown improved corrosion rates at pH 2 and 3 of sulphuric acid.

Recommendations

- Studies have proved that high amounts of vanadium have an influence on the corrosion behaviour of the WC-Co alloys. Vanadium additions are made with respect to the varying of pH conditions.
- High amounts of cobalt (>6wt%) had shown that they can improve the corrosion resistance of the alloys under varied pH conditions.

References

1. Affatato, S., & Brando, D. (2013). Introduction to Wear Phenomena of Orthopaedic Implants. *Wear of Orthopaedic Implants and Artificial Joints*, 3-26.

2. Allen, C., & Wentzel, E. (1995). Erosion-Corrosion Resistance of Tungsten Carbide Hard metals with different Binder Compositions. *Wear*, 63-69.

3. Altan, T., & Tekkaya, A. (2012). Chapter 7: Friction and Lubrication. In H. Kim, & N. Kardes, *Sheet Metal Forming - Fundamentals* (pp. 89-98). ASM International .

4. Antonov, M., R.Veinthal, D-L.Yung, D.Katušin, & I.Hussainova. (2015). Mapping of Impact-Abrasive Wear Performance of WC–Co Cemented Carbides. *Wear*, 971-978.

5. AZoM. (2002). Tungsten Carbide - An Overview.

6. Bailey, J. A., Bayoumi, A.-M., & Stewart, J. S. (1983). Wear of some Cemented Tungsten Carbide Tools in Machining Oak. *Wear*, 69-79.

7. Barao, V., Sukotjo, C., & Mathew, M. T. (2013). Fundamentals of Linking Tribology and Corrosion (Tribocorrosion) for Medical Applications: Bio-tribocorrosion.

8. Barcík, Š., Pivolusková, E., Kminiak, R., & Wieloch, G. (2009). The Influence of Cutting Speed and Feed Speed on Surface Quality at Plane Milling of Poplar Wood. *Wood Research*, 109-116.

9. Bendikiene, R., & Keturakis, G. (2017). The Influence of Technical Characteristics of Wood Milling Tools on its Wear Performance. *Journal of Wood Science*, 606-614.

10. Bozzini, B., Gaudenzi, G. P., Fanigliulo, A., & Mele, C. (2004). Electrochemical Oxidation of WC in Acidic Sulphate Solution. *Corrosion Science*, 453-469.

11. Bricín, D., Pomahač, J., & Kříž, A. (2019). Degradation of Sintered Carbides in Different Corrosion Environment.

12. Chiniforush, A., Akbarnezhad, A., Valipour, H., & Malekmohammadi, S. (2019). Moisture and Temperature Induced Swelling/Shrinkage of Softwood and Hardwood Glulam and LVL: An Experimental Study. *Construction and Building Materials*, 70-83.

13. Chong, W. W., & Cruz, M. D. (2014). Elastoplastic Contact of Rough Surfaces: A line Contact Model for Boundary Regime of Lubrication. *Meccanica*, 1177-1191.

14. Cristovao, L. (2013, Doctoral Thesis). Machining Properties of Wood: Tool Wear Cutting Force and Tensioning Blades. Sweden, Skelleftea, Lulea University of Technology.

15. Crosky, A., Allen, B., Hoffman, M., & Munroe, P. (n.d.). *Material Engineering Online Tutorials.* Elsevier.

16. Darmawan, W., Rahayu, I., Nandika, D., & Marchal, R. (2011). Wear Characteristics of Wood Cutting Tools caused by Extractive and Abrasive Materials in some Tropical Woods. *Journal of Tropical Forest Science*, 345-353.

17. Darmawan, W., Rahayu, I., Nandika, D., & Marchal, R. (2012). The Importance of Extractives and Abrasives in Wood Materials on the Wearing of Cutting Tools. *Bioresources*, 1-15.

18. Dixon, J. (2013). Chemica Weathering in Cold Climates. *Earth Systems and Environmental Sciences* , 245-257.

19. Engqvist, H., Beste, U., & Axen, N. (2000). The Influence of pH on Sliding Wear of WC-based Materials. *International Journal of Refractory Metals & Hard Materials*, 103-109.

20. Esmailzadeha, S., Aliofkhazraeia, M., & Sarlakb, H. (2018). Interpretation of Cyclic Potentiodynamic Polarization Test Results for Study of Corrosion Behavior of Metals: A Review. *Protection of Metals and Physical Chemistry of Surfaces*, 976-989.

21. Ettmayer, P. (1989). Hardmetals and Cermets. *Annual Reviews Material Science*, 145-164.

22. Eyma, F., Meausoone, P.-J., & Martin, P. (2004). Strains and Cuting Forces involved in the Solid Wood Rotating Cutting Process. *Journal of Materials Processing Technology*, 220-225.

23. Fang, Z. Z., & Eso, O. O. (2005). Liquid Phase Sintering of Functionally Graded WC–Co Composites. *Scripta Materialia*, 785–791.

24. Fangab, S., & Llanesb, L. (2020). Microstructural Characterization of Cemented Carbides by 3D Volume Reconstruction. *Materials Characterization*.

25. Fazili, A., Derakhshandeh, M. R., Nejadshamsi, S., Nikzad, L., Razavi, M., & Ghasali, E. (2020). Improved Electrochemical and Mechanical Performance of WC-Co Cemented Carbide by Replacing a Part of Co with Al2O3. *Journal of Alloys and Compounds*.

26. Gant, A., Gee, M., & May, A. (2004). The Evaluation of Tribo-corrosion Synergy for WC-Co Hardmetals in Low Stress Abrasion. *Wear*, 500-516.

27. Garcia, E. M., S.Santos, J., Pereira, E. C., & Freitas, M. (2008). Electrodeposition of Cobalt from Spent Li-Ion Battery Cathodes by the Electrochemistry Quartz Crystal Microbalance Technique. *Journal of Power Sources* , 549-553.

28. Garcia, J., & Strelsky, W. (2010). Process Development and Scale up of Cemented Carbide Production . *Scale-up in Metallurgy*, 235-266.

29. García, J., Ciprés, V. C., Blomqvist, A., & Kaplan, B. (2019). Cemented carbide microstructures: a review. *International Journal of Refractory Metals and Hard Materials*, 40-68.

30. Gauvent, M., Rocca, E., Meausoone, P., & Brenot, P. (2006). Corrosion of Materials used as Cutting Tools of Wood. *Wear*, 1051-1055.

31. Gibson, L. T., & Watt, C. M. (2010). Acetic and Formic Acids Emitted from Wood Samples and their Effect on Selected Materials in Museum Environments . *Corrosion Science*, 172-178.

32. Guo, S., Bao, R., Li, S., Ye, Y., Zhu, E., Wan, W., . . . Ye, Y. (2020). The Role of Y2O3, Cu, Mo and Mo2C Additives on Optimizing the Corrosion Resistance of WC-6Co Cemented Carbide in HCl and NaOH Solutions. *Journal of Alloys and Compounds*.

33. Guo, S., Yan, W., Yi, J., Wang, S., Huang, X., Yang, S., . . . Ye, Y. (2020). The Optimization of Mechanical Property and Corrosion Resistance of WC-6Co Cemented Carbide by Mo2C Content. *Ceramics International*.

34. Guo, X., Ekevad, M., Gronlund, A., Marklund, B., & Cao, P. (2014). Tool Wear and Machined Surface Roughness during Wood Flour/Polyethylene Composite Peripheral Upmiling using Cemented Tungsten Carbide Tools. *BioResources.com*, 3779-3791.

35. Human, A. M., & Exner, H. E. (1996). Electrochemical Behaviour of Tungsten-Carbide Hardmetals. *Materials Science and Engineering*, 180-191.

36. Human, A. M., & Exner, H. E. (1997). The Relationship Between Electrochemical Behaviour and In-service Corrosion of WC Based Cemented Carbides. *International Journal of Refractory Metals & Hard Materials*, 65-71.

37. Human, A., Roebuck, B., & Exner, H. (1998). Electrochemical Polarisation and Corrosion Behaviour of Cobalt and Co(W,C) Alloys in 1 N Sulphuric Acid. *Materials Science and Engineering*, 202-210.

38. Hutching, I., & Shipway, P. (2017). Wear by Hard Particles. *Friction and Wear of Engineering Materials* , 165-236.

39. Ige, O., Aribo, S., Obadele, B., Langa, T., Oluwasegun, K., Shongwe, M., & Olubambi, P. (2017). Erosion–corrosion Behaviour of Spark Plasma Sintered WC - 12Co in Aggressive Media. *International Journal of Refractory Metals and Hard Materials*, 36-43.

40. Imasato, S., Tokumoto, K., Kitada, T., & Sakaguchi, S. (1995). Properties of Ultra-Fine Grain Binderless Cemented Carbide 'RCCFN'. *International Journal of Refractory Metals and Hard Materials*, 305-312.

41. Jacobson, F. (2018, October). Wear and Degradation of Co, Fe and Ni-based Cemeted Carbides against Sandstone and Granite. Uppsata, Uppsala Universitet, Sweden.

42. Jeyaprakash, N., & Yang, C. H. (2020). Friction, Lubrication and Wear. *Tribology in Materials and Manufacturing*.

43. Jones, D. A. (1996). *Principles and Prevention of Corrosion* . United States of America : Prentice-Hall.

44. Katiyar, P. K. (2020). A Comprehensive Review on Synergy Effect Between Corrosion and Wear of Cemented Tungsten Carbide Tool Bits: A Mechanistic Approach. *International Journal of Refractory Metals & Hard Materials*, 1-18.

45. Kellner, F., Hildebrand, H., & Virtanen, S. (2009). Effect of WC Grain Size on the Corrosion Behaviour of WC-Co based Hardmetals in Alkaline Solutions. *International Journal of Refractory Metals & Hard Materials*, 806-812.

46. Kim, H., Kim, J., & Kwon, Y. (2005). Mechanical Properties of Binderless Tungsten Carbide by Spark Plasma Sintering. *Novel Materials Processing by Advanced Electromagnetic Energy Sources*, 275-279.

47. Kosaba, T., Muto, I., & Sugawara, Y. (2021). Effect of Anodizing on Galvanic Corrosion Resistance of Al Coupled to Fe or Type 430 Stainless Steel in Diluted Synthetic Seawater. *Corrosion Science*.

48. Kosters, R., Sutthiruangwong, S., & Mori, G. (2005). Passivity and pseudopassivity of cemented carbides. *International Journal of Refractory Metals & Hard Materials*, 129-136.

49. Krakhmalev, P., Sukumaran, J., & Gåård, A. (2007). Effect of Microstructure on Edge Wear Mechanisms in WC–Co. *International Journal of Refractory Metals & Hard Materials*, 171-178.

50. Kříž, A., & Bricín, D. (2017). Properties and Testing of Cemented Carbides. *Powder Metallurgy - Fundamentals and Case Studies*, 273-299.

51. Kruger, J., & Begum, S. (2016). Corrosion of Metals: Overview. *Reference Module in Materials Science and Materials Engineering*.

52. Lassner, E., & Schubert, W.-D. (1999). Tungsten in Hardmetals. In E. Lassner, & W.-D. Schubert, *Tungsten: Properties, Chemistry, Technology of the Element, Alloys and Chemical Compounds* (pp. 321-362). Austria: Kluwer Academics/ Plenum Plushers.

53. Li, G., Peng, Y., Yan, L., Xu, T., Long, J., & Luo, F. (2020). Effects of Cr Concentration on the Microstructure and Properties of WC-Ni Cemented Carbides. *Journal of Materials Research and Technology*, 902-907.

54. Lu, R., Minarro, L., Su, Y.-Y., & Shemenski, R. M. (2008). Failure Mechanism of Cemented Tungsten Carbide Dies in Wet Drawing Process of Steel Cord Filament. *International Journal of Refractory Metals & Hard Materials*, 589-600.

55. Massola, C. P., Chaves, A. P., & Albertin, E. (2016). A Discussion on the Measurement of Grinding Media Wear. *Journal of Materials Research and Technology*.

56. Mohan, G. D., & Klamecki, B. E. (1981). The Susceptibility of Woodcutting Tools to Corrosive Wear. *Wear* , 85-92.

57. Morton, C., Wills, D., & Stjernberg, K. (2005). The Temperature Ranges for Maximum Effectiveness of Grain Growth Inhibitors in WC–Co Alloys. *International Journal of Refractory Metals & Hard Materials*, 287-293.

58. Naylor, A., & Hackney, P. (2013). A Review of Wood Machining Literature with a Special Focus on Sawing. *Bioresources.com*, 3122-3135.

59. Palomar, F., Zambrano, P., Gómez, M. I., Colás, R., & Castillo, A. (2009). Tungsten Carbide and Tantalum Carbide Coatings on Machining Tools. *Ingeniería mecánica, tecnología y desarrollo*.

60. Pereira, P., Vilhena, L., Sacramento, J., Senos, A., Malheiros, L., & Ramalho, A. (2022). Influence of Different Binders and Severe Environmental Conditions on the Tribological and Electrochemical Behaviour of WC-Based Composites. *Lubricants*.

61. Pirso, J., Viljus, M., Juhani, K., & Letunovits, S. (2009). Two-body Dry Abrasive Wear of Cermets. *Wear*, 21-29.

62. Potgieter, J., Thanjekwayo, N., Olubambi, P., Maledi, N., & Potgieter-Vermaak, S. (2011). Influence of Ru Additions on the Corrosion Behaviour of WC–Co Cemented Carbide Alloys in Sulphuric Acid. *International Journal of Refractory Metals and Hard Materials*, 478-487.

63. Pugsley, V., Korn, G., Luyckx, S., Sockel, H., Heinrich, W., Wolf, M., . . . Schulte, R. (2001). The Influence of a Corrosive Wood-cutting Environment on the Mechanical Properties of Hardmetal Tools. *International Journal of Refractory Metals and Hard Materials*, 311-318.

64. Ramage, M. H., Burridge, H., Busse-Wicher, M., Fereday, G., Reynolds, T., Shah, D. U., . . . Scherman, O. (2017). The Wood from the Trees: The Use of Timber in Construction. *Renewable and Sustainable Energy Reviews*, 333-359.

65. Ramasamy, G., & Ratnasingam, J. (2010). A Review of Cemented Tungsten Carbide Tool Wear Durind Wood Cutting Processes. *Journal of Applied Sciences*, 2799-2804.

66. Roa, J., Simison, S., Grasso, J., Arcidiacono, M., Escalada, L., Soldera, F., . . . Sosa, A. (2020). Cyclic Contact Fatigue of Cemented Carbides Under Dry and Wet Conditions: Correlation between Microstructure, Damage and Electrochemical Behavior. *International Journal of Refractory Metals & Hard Metarials*, 1-10.

67. Roulon, Z., Missiaen, J., & Lay, S. (2020). Carbide Grain Growth in Cemented Carbides Sintered with Alternative Binders. *International Journal of Refractory Metals and Hard Materials*.

68. Sacks, N. (2002, December 19). The Wear and Corrosive-Wear Response of Tungsten Carbide-Cobalt Hardmetals Under Woodcutting and Three Body Abrasion Conditions. Erlangen, Thesis, University of Erlangen-Nurnberg.

69. Sandoval, D., Rinaldi, A., Notargiacomo, A., Ther, O., Roa, J., & Llanes, L. (2019). WC-Base Cemented Carbides with Partial and Total Substitution of Co as Binder: Evaluation of Mechanical Response by means of Uniaxial Compression of Micropillars. *International Journal of Refractory Metals and Hard Materials*.

70. Santos, R., Rocha, A. F., Bastos, A., Cardoso, J., Rodrigues, F., Fernandes, C., . . . Malheiros, L. F. (2020). Microstructural Characterization and Corrosion Resistance of WC-Ni-Cr-Mo Composite – The Effect of Mo. *International Journal of Refractory Metals & Hard Materials*, 1-7.

71. Sarin, V., & Johannesson, T. (1975). On the Deformation of WC-Co Cemented Carbides. *Metallurgy Science*, 472-476.

72. Scholl, H., Hofman, B., & Rauscher, A. (1992). Anodic Polarization of Cemented Carbides of the type [(WC,M): M = Fe, Ni or Co] in Sulphuric Acid Solution . *Electrochimica Acta*, 447-452.

73. Sheikh-Ahmad, J. Y., & Bailey, J. A. (1999). High-Temperature Wear of Cemented Tungsten Carbide Tools while Machining Particleboard and Fiberboard. *Journal of Wood Science*, 445-455.

74. Sheikh-Ahmad, J., & Bailey, J. (1999). On The Wear of Cemented Carbide Tools in the Continuous and Interrupted Cutting of Particleboard. (pp. 2-12). Research gate .

75. Sheikh-Ahmad, J., & McKenzie, W. M. (1997). Measurement of Tool Wear and Dulling in the Machining of Particleboard. *Wood Machining an Tooling Research Program* (pp. 1-12). Vancouver: Research Gate.

76. Siczek, K. J. (2016). Valve Train Tribology. *Tribological Processes in the Valve Train System with Lightweight Valves*, 85-180.

77. Sockel, H.-G., & Pugsley, V. (2004). Corrosion Fatigue of Cemented Carbide Cutting Tool Materials. *Materials Science and Engineering: A*, 87-95.

78. Stanciu, V. l., Vitry, V., & Delaunois, F. (2017). Optimization of the Introduction of Grain Growth Inhibitor in Cemented Carbides. *EuroPM 2017* (pp. 1-6). Milano: ResearchGate.

79. Stefaniak, A. B., Day, G. A., Harvey, C. J., Leornard, S. S., Schwegler-Berry, D. E., Chipera, S. J., . . . Chisholm, W. P. (2007). Characteristics of Dusts Encountered during the Production of Cemented Tungsten Carbides. *Industrial Health*, 793-803.

80. Sun, J., Zhao, J., Huang, Z., Yan, K., Shen, X., Xing, J., . . . Li, B. (2020). A Review on Binderless Tungsten Carbide: Development and Application. *Nano-Micro Lett.*, 1-37.

81. Sutthiruangwong, S., & Mori, G. (2003). Corrosion Properties of Co-based Cemented Carbides in Acidic Solutions. *International Journal of Refractory Metals and Hard Materials*, 135-145.

82. Tait, W. S. (2018). Chapter 5 - Electrochemical Corrosion Basics. In W. S. Tait, *Handbook of Environmental Degradation of Materials* (pp. 97-115). Elsevier.

83. Tarragó, J., Fargas, G., Isern, L., Dorvloc, S., Tarres, E., Müller, C., . . . Llanes, L. (2016). Microstructural Influence on Tolerance to Corrosion-Induced Damage. *Materials and Design*, 36-43.

84. Thanjekwayo, N. (2009, June MSc Dissertation). The Influence of Ru Additions on the Corrosion Behaviour of WC-Co Cemented Carbide in Corrosive Media. Johannesburg, Gauteng, University of the Witwatersrand.

85. Tomlinson, W. J., & Linzell, C. R. (1988). Anodic Polarization and Corrosion of Cemented Carbides with Cobalt and Nickel Binders. *Journal Of Material Science*, 914-918.

86. Tracey, V. A. (1992). Nickel in Hardmetals. *Refractory Metals & Hard Materials*, 137-149.

87. Tsuda, K. (2016). History of Development of Cemented Carbides and Cermet. *SEI Technical Review*, 16-20.

88. Upadhyaya, G. S. (1997). *Cemented Tungsten Carbides - Production, Properties and Testing.* Kanpur.

89. Wentzel, E., & Allen, C. (1996). The Erosion-corrosion Resistance of Tungsten-carbide Hard Metals. *International Journal of Refractory Metals & Hard Materials*, 81-87.

90. Whitefield, D. D. (2017). Hardness. Johannesburg, Lecture Slides, University of the Witwatersrand: University of the Witwatersrand.

91. Winandy, J. E., & Rowell, R. M. (1984). Chemistry of Wood Strength. In *Handbook of Wood Chemistry and Wood Composite* (pp. 303-350). Press LLC .

92. Wood, R. J., Herda, S., & Thakare, M. R. (2017). A Critical Review of the Tribocorrosion of Cemented and Thermal Sprayed Tungsten Carbide. *Tribology International*, 491-509.

93. Yang, J., Roa, J., Schwind, M., Oden, M., Johansson-Joesaar, M., & Llanes, L. (2014). Grinding-induced Metallurgical Alterations in the Binder Phase of WC-Co Cemented Carbides.

94. Zhang, L., & Chen, Q. (2017). CALPHAD-Type Modelling of Diffusion Konetics in Multicomponent Alloys. *Handbook of Solid State Diffusion* .

95. Zhang, L., Chen, Y., Wan, Q.-l., Liu, T., Zhu, J.-f., & Tian, W. (2016). Electrochemical Corrosion Behaviors of Straight WC–Co Alloys: Exclusive Variation in Grain Sizes and Aggressive Media. *International Journal of Refractory Metals and Hard Materials*, 70-77.

96. Zhang, X., Zhou, J., Liu, C., Li, K., Shei, W., Lin, Z., & Li, Z. (2019). Effects of Ni Addition on Mechanical Properties and Corrosion Behaviours of Coarse-grained WC-10(Co, Ni) Cemented Carbide. *International Journal of Refractory Metals and Hard Materials*, 123-129.

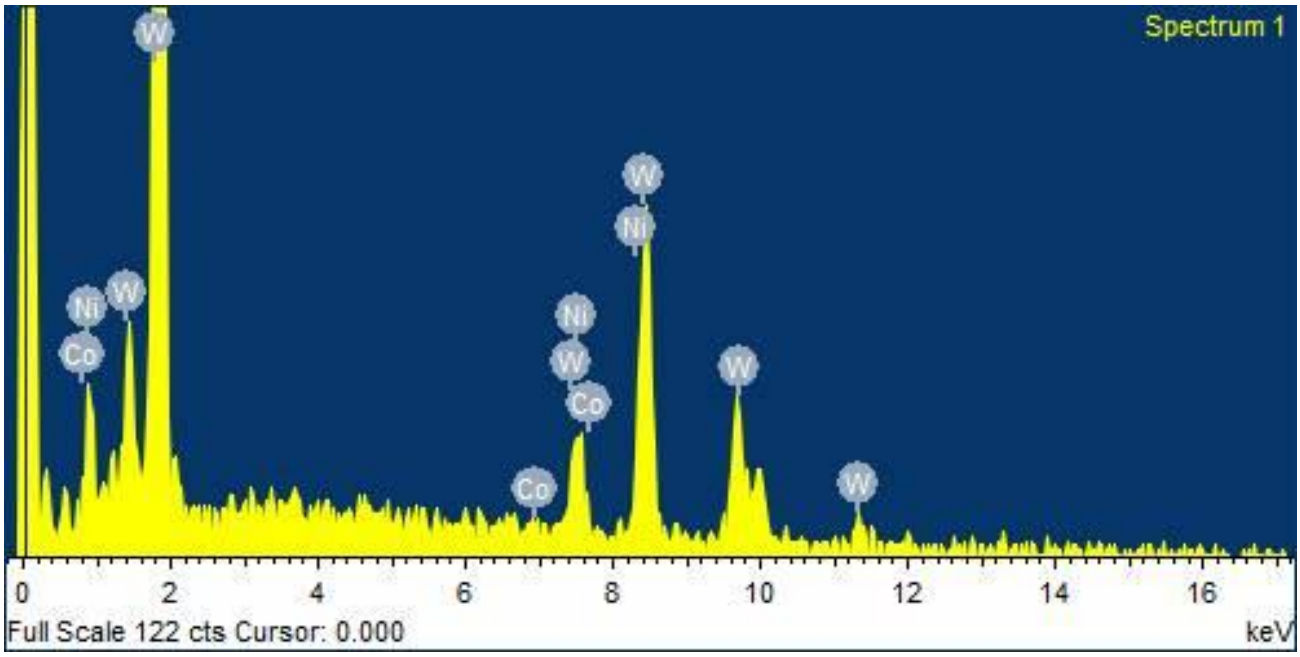
97. Zhao, J., Sun, J., Gong, F., Ni, X., & Li, Z. (2019). Development and Application of WC-Based Alloys Bonded with Alternative Binder Phase. *Critical Reviews in Solid State and Materials Sciences*, 211-238.

98. Zheng, Y., Fargas, G., Armelin, E., Lavigne, O., & Llanes, L. (2019). Corrosion-Induced Damage and Residual Strength of WC-Co,Ni Cemented Carbides: Influence of Microstructure and Corrosion Medium. *Metals*, 1-11.

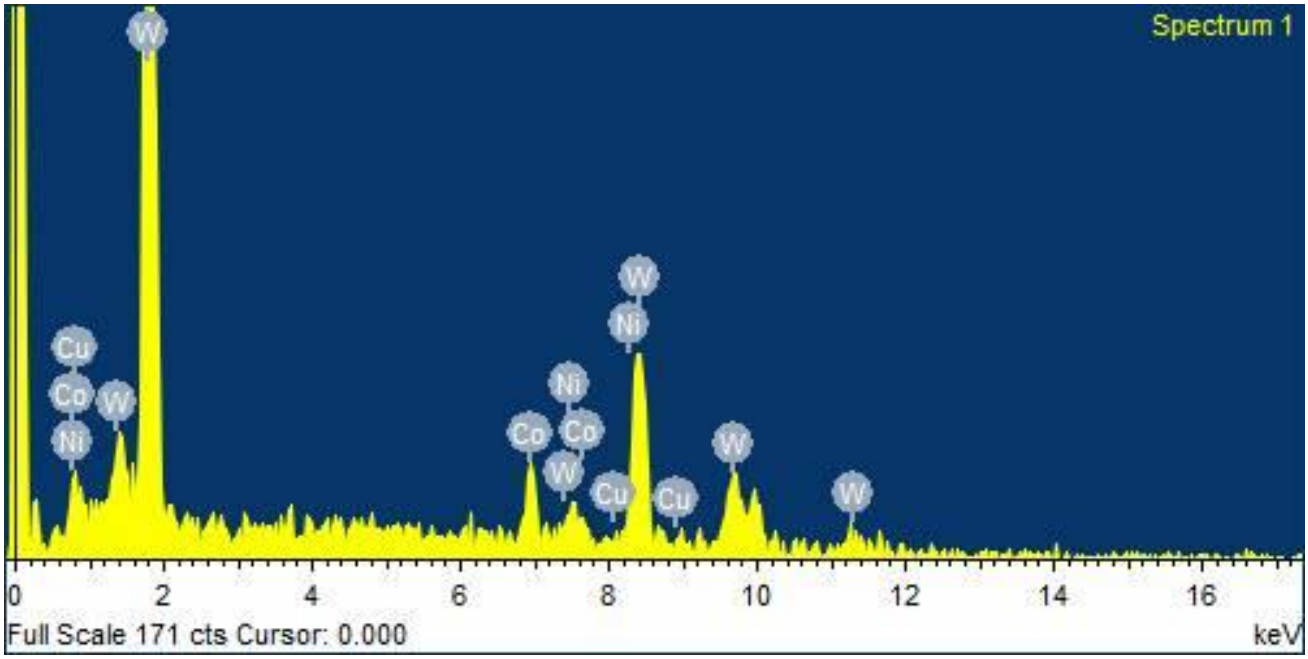
Appendix

EDS analysis

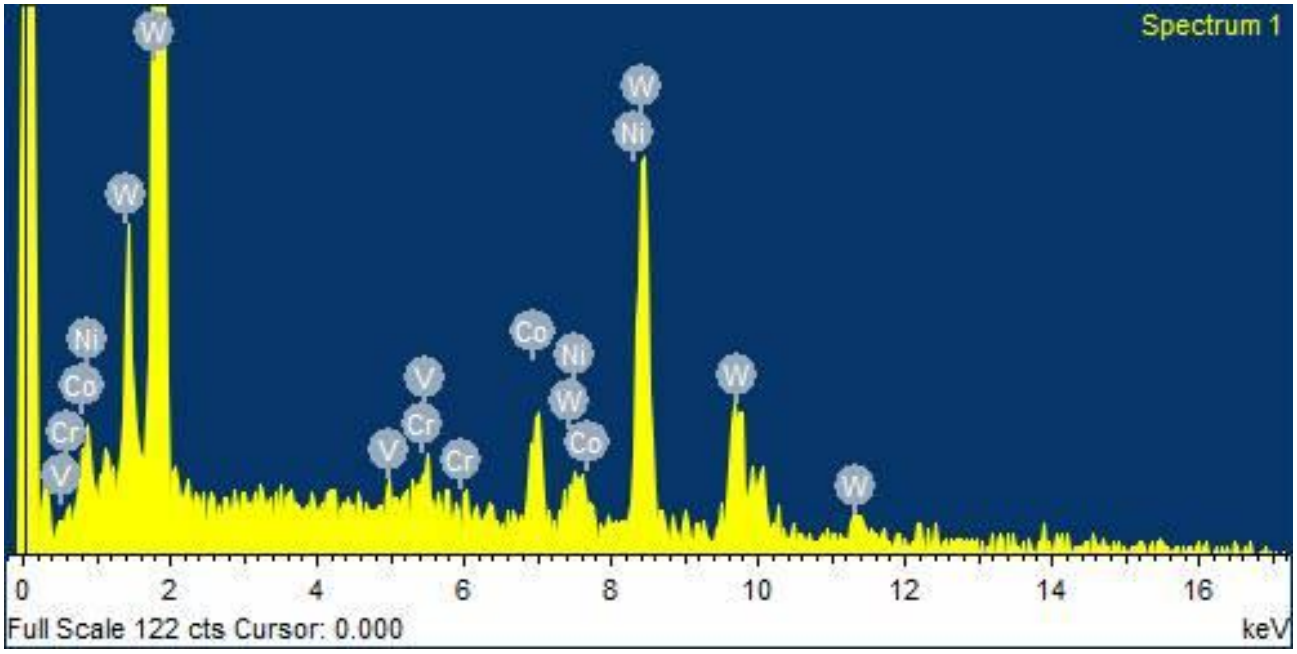
Sample COR



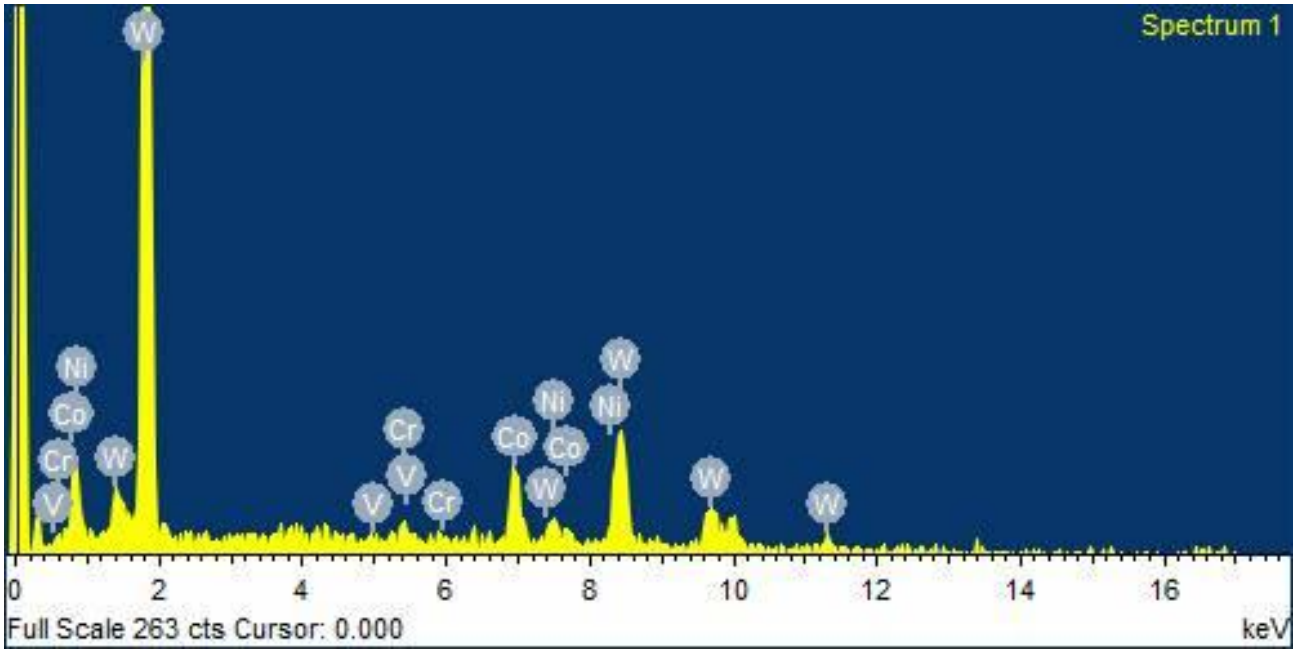
Sample M



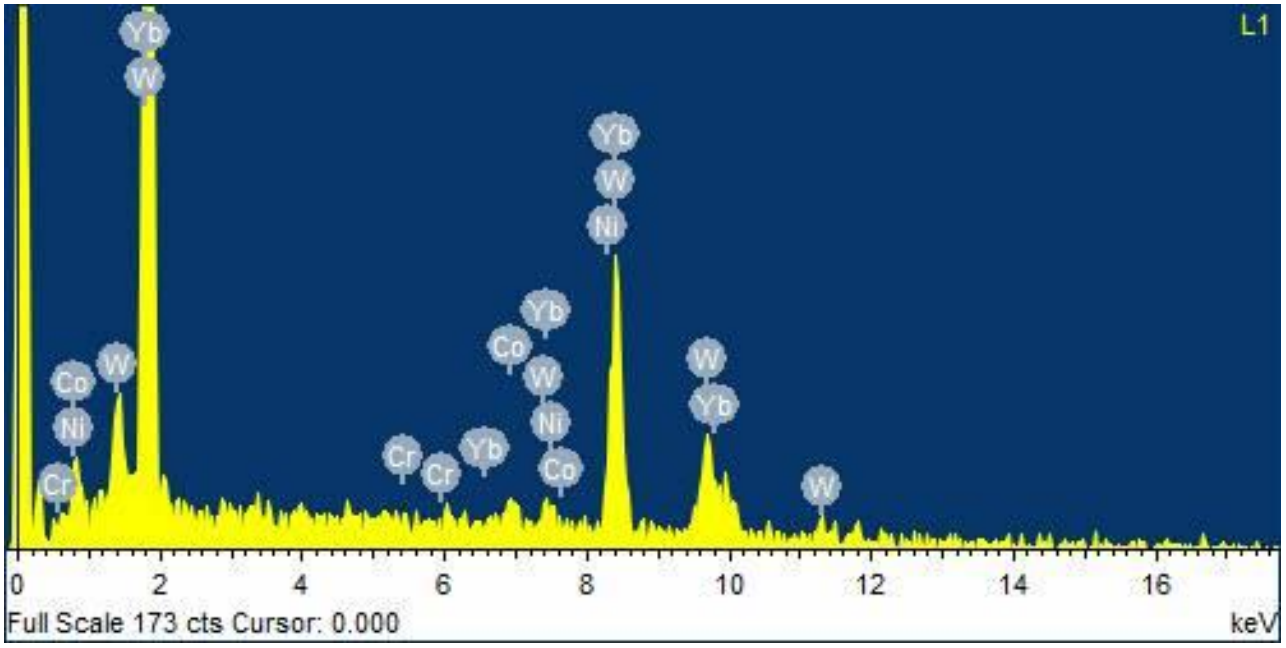
Sample UM



Sample T3



Sample TC


L1
Yb
W
Co
Ni
Cr
Yb
W
Ni
Yb
Co
W
Ni
Co
Cr
Cr
Yb
W
Yb
W
0
2
4
6
8
10
12
14
16
Full Scale 173 cts Cursor: 0.000
keV